Measurement-based Spectrum Database for Spatial Spectrum Sharing

Koya Sato

Department of Communication Engineering and Informatics
The University of Electro-Communications

This dissertation is submitted for the degree of
Doctor of Philosophy

March 2018

Supervisory Committee

Chairperson: Professor Takeo Fujii

1. Member: Professor Yasushi Yamao

2. Member: Professor Jun-ichi Takada

3. Member: Associate Professor Toshiharu Kojima

4. Member: Associate Professor Koji Ishibashi

Day of the Predefense: November 13, 2017.

Day of the Final Defense: February 7, 2018.

Acknowledgements

This thesis is a summary of my doctoral study at the University of Electro-Communications, Tokyo, Japan. I am grateful to a large number of people who have helped me to accomplish my work.

First of all, I would like to express my deepest gratitude to my supervisor, Professor Takeo Fujii, for guiding my throughout my work. His motivations and encouragements immensely helped me throughout my life in the University of Electro-Communications. I also would like to give my special thanks to Professor Yasushi Yamao, Associate Professor Koji ishibashi, and Associate Professor Koichi Adachi for their valuable guidance, instructions and continuous support. I would particularly like to thank Doctor Onur Altintas and Doctor Takayuki Shimizu for the joint research.

I also grateful to all the members of advanced wireless communications and research center (AWCC), especially Assistant Professor Kei Inage, Mr. Masayuki Kitamura, Koji Ichikawa, and Shun Ogata for their discussions and kindness.

Finally, I would like to have my family to thank for their words, attitudes, and every supports.

Abstract

The growth in demand for mobile communication systems has exponentially increased data traffic during the last decade. Because this exponential growth consumes finite spectrum resources, traditional spectrum utilization policies with exclusive resource allocation faces a limit. In order to develop novel spectrum resources, many researchers have shown an interest in spectrum sharing with cognitive radio (CR). This method allows secondary users (SUs) to share spectrum bands with primary users (PUs) under interference constraints for PUs. SUs are required to take into consideration the interference margin to the estimated interference temperature at PUs in order to protect communication quality of PUs. On the other hand, an excess interference margin decreases the spectrum sharing opportunity; therefore, it is important to manage the interference power properly.

Spectrum estimation techniques in spectrum sharing can be categorized into two methods: spectrum sensing and spectrum database. Spectrum sensing uses the detection of PU signals to characterize radio environments. To provide good protection, signal detection must be performed under the (strict) condition that the PU signal strength be below the noise floor, even under low signal-to-noise ratios (SNRs) and fading conditions. These fluctuations make it difficult for the SUs to achieve stable detection; thus, it is very challenging to accurately estimate the actual activity of the PU. The second method is based on storing information about spectrum availabilities of each location in spectrum databases. In this method, after SUs query the database before they utilize the spectrum, the database provides spectrum information to the SUs. Current databases usually evaluate white space (WS) based on empirical propagation models. However, it is well known that empirical propagation models cannot take into account all of the indeterminacies of radio environments, such as shadowing effects. Because SUs must not interfere toward PUs, the conventional database requires the SUs to set large margins to ensure no interference with PUs.

In this dissertation, we propose and comprehensively study a measurement-based spectrum database for highly efficient spectrum management. The proposed database is a hybrid system, combining spectrum sensing and a spectrum database. The spectrum database consists of radio environment information measured by mobile terminals. After enough data are gathered, the database estimates the radio environment characteristics by statistical

processing with the large datasets. Using the accurate knowledge of the received PU signal power, spectrum sharing based on PU signal quality metrics such as the signal-to-interference power ratio (SIR) can be implemented.

We first introduce the proposed database architecture. After we briefly discuss a theoretical performance of the proposed database, we present experimental results for the database construction using actual TV broadcast signals. The experimental results show that the proposed database reduces the estimation error of the radio environment.

Next, we propose a transmission power control method with a radio environment map (REM) for secondary networks. The REM stores the spatial distribution of the average received signal power. We can optimize the accuracy of the measurement-based REM using the Kriging interpolation. Although several researchers have maintained a continuous interest in improving the accuracy of the REM, sufficient study has not been done to actually explore the interference constraint considering the estimation error. The proposed method uses ordinary Kriging for the spectrum cartography. According to the predicted distribution of the estimation error, the allowable interference power to the PU is approximately formulated. Numerical results show that the proposed method can achieve the probabilistic interference constraint asymptotically, and an increase in the number of measurement datasets improves the spectrum sharing capability.

After that, we extend the proposed database to the radio propagation estimation in distributed wireless links in order to accurately estimate interference characteristics from SUs to PUs. Although current wireless distributed networks have to rely on an empirical model to estimate the radio environment, in the spectrum sharing networks, such a path loss-based interference prediction decreases the spectrum sharing opportunity because of the requirement for the interference margin. The proposed method focuses on the spatial-correlation of radio propagation characteristics between different wireless links. Using Kriging-based shadowing estimation, the radio propagation of the wireless link that has arbitrary location relationship can be predicted. Numerical results show that the proposed method achieves higher estimation accuracy than path loss-based estimation methods.

The methods discussed in this thesis can develop more spatial WSs in existing allocated bandwidth such as TVWS, and can provide these WSs to new wireless systems expected to appear in the future. Additionally, these results will contribute not only to such spectrum sharing but also to improvement of the spectrum management in existing systems. For example, in heterogeneous networks (HetNets), a suitable inter-cell interference management enables transmitters to reuse the frequency efficiently and the user equipment can select the optimum base station. We anticipate that this dissertation strongly contributes to improving the spectrum utilization efficiency of the whole wireless systems.

Table of contents

List of figures

List of tables

Nomenclature

Roman Symbols

B	number of iterations in parametric bootstrap
C	channel capacity
G and k	constant factors for aggregate interference
d	distance
e	Napier's constant
f	frequency
h	antenna height
I	interference power
L	propagation loss
l	length
M	number of SUs
N	number of datasets
N_0	noise floor
P	signal power
p	probability
R	radius
W	shadowing factor

Greek Symbols

Δ	difference
ϵ	estimation error
η	path loss index
Γ	SIR
γ	semivariogram
α_n^2, α_s^2, α_r	nugget, sill, and range
λ	wavelength
μ	Lagrange multiplier
ω	weight factor
π	circlar constant
ρ	correlation
σ	standard deviation

Subscripts

b	bootstrap
cor	correlation
d	desired value
err	error
i and j	index
k	Kriging
max	maximum value
mW	value in mW domain
off	offset

out	outage event
P	PU
Rx	receiver
S	SU
sum	summation
Tx	transmitter

Acronyms / Abbreviations

AWGN	Additive White Gaussian Noise
BLUE	Best Linear Unbiased Estimator
CDF	Cumulative Distribution Function
CR	Cognitive Radio
CSI	Channel State Information
EIRP	Equivalent Isotropic Radiated Power
FCC	Federal Communications Commission
FFT	Fast Fourier Transform
GPS	Global Positioning System
HetNet	Heterogeneous Network
IEEE	The Institute of Electrical and Electronics Engineers
i.i.d.	Independent and Identically Distributed
ISDB-T	Integrated Services Digital Broadcasting-Terrestrial
WLAN	Wireless Local Area Network
LOS	Line-of-Sight
M2M	Machine-to-Machine

MAC	Media Access Control
MIC	Ministry of Internal Affairs and Communications
MIMO	Multiple-Input and Multiple Output
ML	Maximum Likelihood
NLOS	Non-Line-of-Sight
NOMA	Non-Orthogonal Multiple Access
Ofcom	Office of Communications
PDF	Probability Density Function
QoS	Quality of Service
REML	Residual Maximum Likelihood
REM	Radio Environment Map
RMSE	Root Mean Squared Error
Rx	Receiver
SDR	Software Defined Radio
SIR	Signal-to-Interference power Ratio
SNR	Signal-to-Noise power Ratio
PU	Primary User
SU	Secondary User
TV	Television
Tx	Transmitter
UE	User Equipment
UK	United Kingdom
USRP	Universal Software Radio Peripheral
US	United States

WDN	Wireless Distributed Network
WS	White Space

Chapter 1

Introduction

This dissertation describes comprehensive studies on the measurement-based spectrum database for highly efficient spectrum utilization. This chapter first introduces the research background and the challenges. After the timeline of the spectrum sharing is summarized, research motivations and contributions are stated. Finally, we give the organization of the thesis.

1.1 Shortage of Spectrum Resources

Because of the growth in demand for mobile communication systems, data traffic has significantly increased during the last decade. Reference [1] predicts an exponential increase in data traffic that corresponds to a 7-fold increase in traffic between 2016-2021, as shown in Fig. 1.1. Similarly, many industries forecast a 1,000-fold increase between 2010 and 2020. In addition, the usage scenes are expanding to many purposes such as cellular, wireless local area network (WLAN), bluetooth, machine-to-machine (M2M) communications. This means wireless communication is an important infrastructure as well as water, energy, and gas; it is not too much to say that we cannot return to the world where has no wireless communications.

However, although the demands for wireless communications are explosively expanding, we face a fundamental, but critical problem: severe shortage of the spectrum resources. In wireless communication systems, because a signal is carried radially from the transmitter, the signal interferes with the other communication systems that share the same spectrum. Therefore, frequencies are exclusively assigned to each system in order to avoid the unanticipated degradation of the communication quality today. Such an exclusive allocation, however, causes the shortage of spectrum resources due to the explosive expansion of the demand for wireless communication systems.

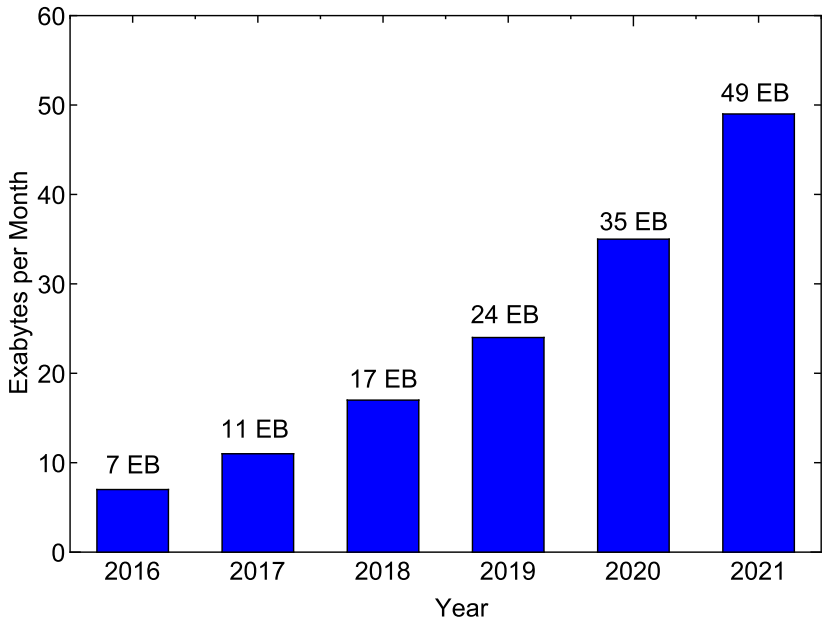

Fig. 1.1 Forecasts by Cisco about global mobile data traffic, 2016 to 2021 [1].

Figure 1.2 summarizes the spectrum allocation in the US [2]. The figure clearly explains that almost all bands from several kHz to several hundred GHz are already allocated to some systems. In particular, several hundred MHz - several GHz bands, which are suitable for mobile communication systems from the viewpoint of antenna design and radio propagation, are in a situation where multiple systems share the same band. Thus, it is too difficult to allocate such a band to new wireless systems appearing in the future.

In addition, paying attention to existing systems such as WLANs and cellular networks, mobile terminals are overcrowded within a given band at the same time. Desired communication quality often cannot be obtained due to densely packing of wireless traffics beyond the limits, thus, the lack of spectrum resources is a fundamental problem that the current wireless communication systems have.

1.2 Countermeasures for Spectrum Shortage and Focus of This Thesis

The shortage of spectrum resources has motivated many researchers to discuss the efficiency of the spectrum use in last decades. Each researcher attacks the problem from different viewpoint, and today's countermeasures for the problem can mainly be classified into three approaches, as follows.

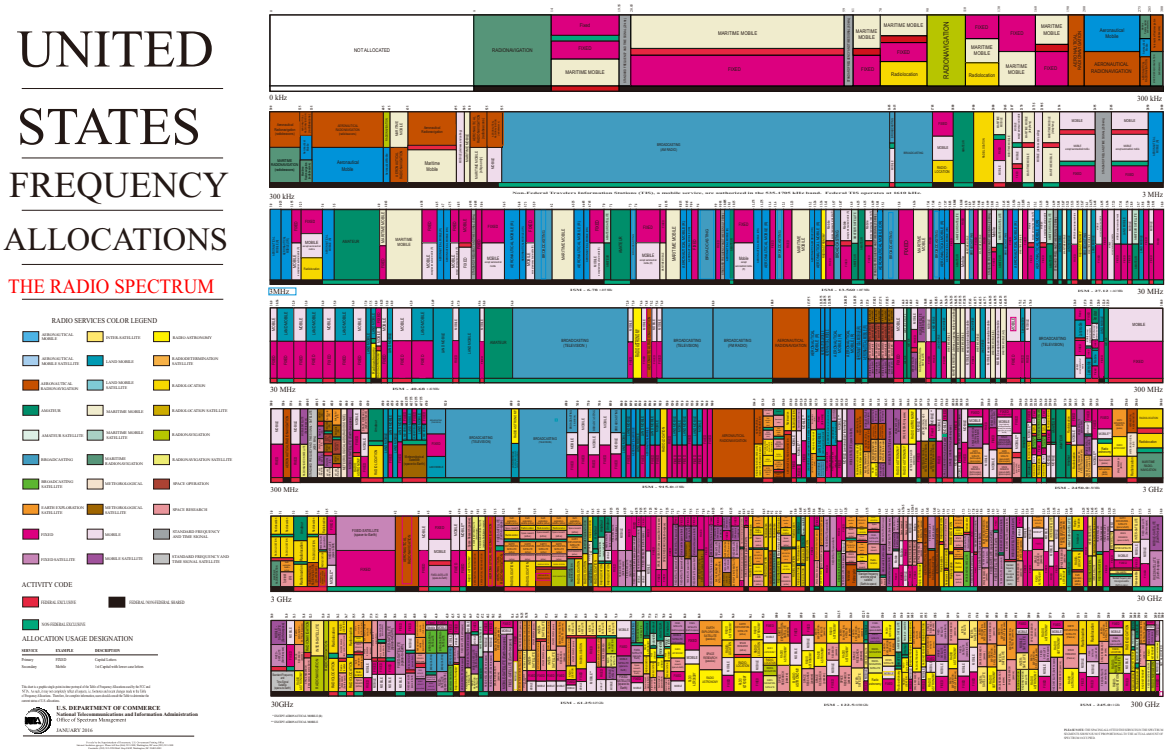

Fig. 1.2 Spectrum allocation in the US [2].

Improvement of Spectrum Utilization Efficiency in Existing System via Sophisticated Low Layer Techniques

A simple direction is to improve the reliability of wireless communication via new low layer technologies in the framework of the current exclusive frequency allocation. The improvement of the reliability enables us to obtain the comparable reliability with lower transmission power than the conventional systems. As a result, the inter-terminal interference can be reduced, and we can improve the efficiency of the spectrum utilization. This direction includes spatial modulation [6][7], full-duplex radio [8][9], non-orthogonal multiple access (NOMA) [10][11], coded MAC [12], and new error correction coding such as polar codes [13].

Development of Ultra High Spectrum

Next direction is to develop a new spectrum resources which are not used in current wireless systems. Many researchers discuss how to communicate over ultra high bands such as millimeter-wave [14] and THz [15], which have been considered difficult to use in wireless communication from the viewpoint of device constraints and radio propagation characteristics. In addition, optical wireless communication [16] might be categorized into this direction.

Spectrum Sharing with Existing Wireless Systems

Most of the frequency bands suitable for mobile communication have already been allocated exclusively to some system as shown above. However, many experimental results show that the spatio-temporal usage rates in these bands are very low, and the other spectra are not used effectively [17][18]. Therefore, spectrum sharing which uses these free bands while guaranteeing the communication quality of existing communication systems is also widely discussed over the last decades.

Of course, the techniques cultivated through these three strategies are not exclusive each other, that is, further improvement in frequency utilization efficiency can be achieved by combining them. The three major approaches are mainly focused for the spectrum shortage today. However, from the viewpoint of fundamental physical characteristics such as antenna size and radio propagation, it is preferable to use a several hundred MHz to several GHz band, and this fact will be no change in the future. If these bands can also be used in the new system, the new system can also intercept all the advantages mentioned above, in addition to ease of hardware design and the development cost. Because only the spectrum sharing enables to allocate such bands to new systems, this thesis mainly focuses on the improvement of the spectrum sharing efficiency.

1.3 Brief Timeline

Spectrum sharing requires tight cooperation among industry, academia and government because secondary users (SUs) opportunistically utilize spectra which are exclusively allocated to primary users (PUs). This feature has caused various works over 20 years including theoretical analysis, experimental verification, and law maintenance. In this section, we summarize the timeline of spectrum sharing.

-Late 1990s: Software Defined Radio as Enabler for Flexible but Low Cost Mobile Terminals

Technical history of the spectrum sharing dates back more than 30 years ago. Since early 1980 an exponential blowup of cellular systems has been observed, which had produced the definition of a plethora of analog and digital standards over the world [19]. This fact required mobile terminals to implement multiple wireless functions such as multiple frequencies and modulations. However, although many functions can be realized by hardware, such an implementation requires the same number of electronic circuits as the wireless communication

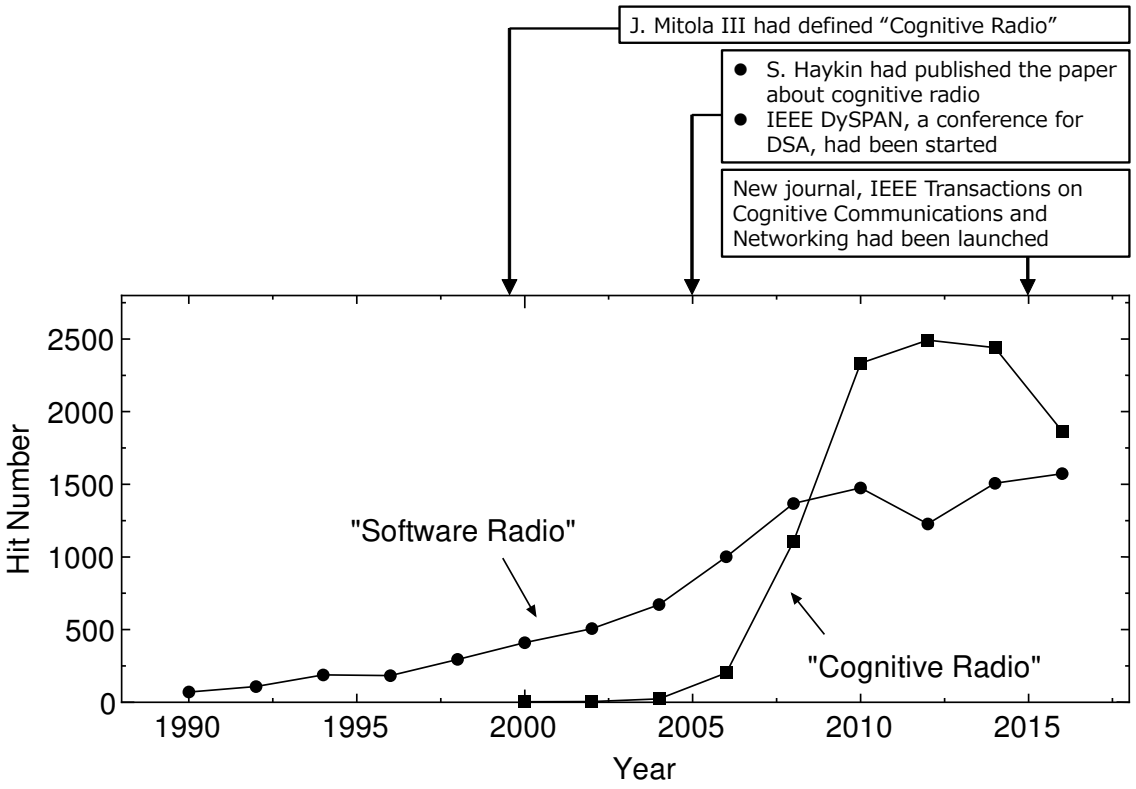

Fig. 1.3 Transition of the number of published articles per year.

method, and has difficulty in miniaturization and cost. This background had motivated the development of software defined radio (SDR) to realize the flexibility of mobile terminals under low cost. SDR is a technology, thought to build flexible radio systems, multiservice, multistandard, multiband, reconfigurable and reprogrammable by software [20–23].

End of 1990s: Proposal of Cognitive Radio

Discussions on SDR had been mainly focused on how the flexibility of hardware can be improved until then, and few works on systems that adaptively control them are under way. In 1999, a new term “cognitive radio” (CR) had been coined by Joseph Mitola as a control model for SDR [24].

In the Mitola’s article, CR is described as follows.

> *Cognitive radio enhances the flexibility of personal services through a Radio Knowledge Representation Language. This language represents knowledge of radio etiquette, devices, software modules, propagation, networks, user needs, and application scenarios in a way that supports automated reasoning about the needs of the user. This empowers software radios to conduct expressive*

> *negotiations among peers about the use of radio spectrum across fluents of space, time, and user context.*

The idea of Radio Knowledge Representation Language was expanded further in his doctoral dissertation in 2000 [25]. This dissertation describes a conceptual overview of CR.

CR had originally been proposed for enhancing the flexibility of personal wireless services. However, because then the depletion of spectrum resources was regarded as a severe problem, CR has attracted attention for improving the spectrum efficiency. In today's wireless communication field, the term "cognitive radio" is generally recognized as a concept that "the terminal that recognizes the surrounding wireless environment and adapts its own communication parameters adaptively".

Figure 1.3 shows the transition of the number of published articles per year. Using "Software Radio" and "Cognitive Radio" as search words, the number of achievements such as conference papers, journal articles, and patents published within the year was searched on the IEEE Xplore, and plotted in this figure. From early 2000 where the shortage of spectrum resources was regarded as a problem, hundreds-thousands articles of CR are published per year. At the same time, the figure shows that articles on SDR are also increasing year by year. SDR and CR have been developed by the two wheels, and even now these continue to evolve.

Early 2000s: Observation of White Spaces and Attention to Cognitive Radio

Since 2000s, the number of wireless devices had explosively increased because of the gain of demands for personal wireless devices such as WLAN, bluetooth, and cellular phone. Many researchers had predicted that the demands will increase exponentially as the year goes on, and these predictions showed a new social problem: severe scarcity of spectrum resources. The US has aggressively discussed the spectrum access and management regimes. In early 2000s, governments in the US centered on FCC had investigated the usage status of existing allocated spectra on time, space, and frequency axes. From the investigation, they reported that the usage rate in the bands is about 20% at the most [26]. The fact sparked the active discussion on the spectrum sharing.

In the spectrum sharing environment, secondary systems have to recognize the surrounding radio environment properly in order to guarantee the own communication opportunity under the interference constraint. Because the strategy of spectrum sharing has to be determined according to multiple information including the usage rate of spectrum, the number of primary and secondary systems, and expected channel capacity in secondary networks, the concept of CR had attracted attention as an application for the spectrum sharing.

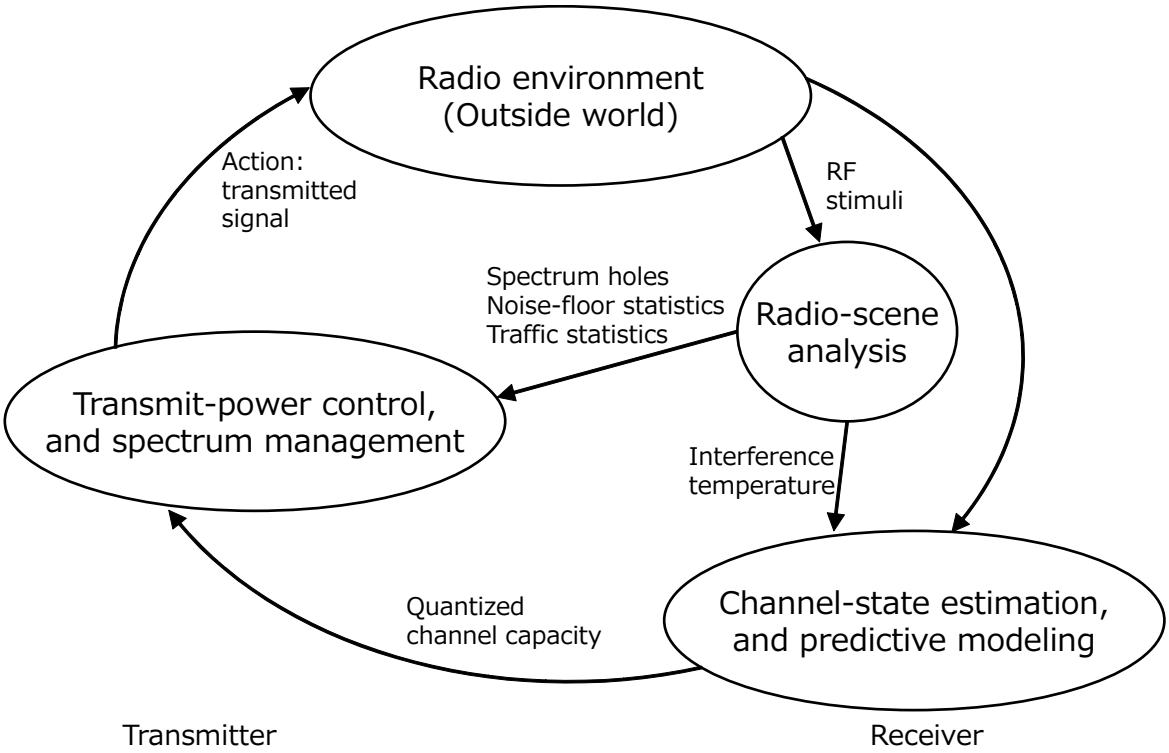

Fig. 1.4 Basic cognitive cycle [3].

Mid 2000s-Early 2010s: Analyses of CR-oriented Spectrum Sharing

After CR-oriented spectrum sharing attracted attention, especially in mid 2000s-early 2010s, many researchers had produced important results on this field. In 2005, Haykin comprehensively discussed the CR focusing on spectrum sharing [3]. In [3], the author simplifies cognitive cycle defined by Mitola as shown in Fig. 1.4. The simplified cycle aims to discuss the CR-oriented spectrum sharing, and mainly consists of following three tasks:

- Radio-scene analysis.
- Channel-state estimation and predictive modeling.
- Transmit-power control and dynamic spectrum management.

By introducing *interference temperature* as a new metric for the spectrum sharing, the author discusses concrete measures and future issues in each task.

Achievable rates of CR channels had been shown by Devroye et al. in 2006 [27]. In the paper, they define the CR channel as a two-sender, two-receiver interference channel in which sender 2 obtains the encoded message sender 1 plans to transmit. By considering additive white Gaussian noise (AWGN), they analyze achievable rates according to the

cooperation states between the senders. The results are compared with inner bound, the interference channel, and an outer bound, a modified Gaussian multiple-input and multiple output (MIMO) broadcast channel.

In addition, other important theoretical results had been shown in 2007 by many researchers such as Gastpar [28], Ghasemi and Sousa [29], and Jafar and Srinivasa [30][31]. As can be seen from the fact that the number of papers about CR dramatically increases after 2007, it is not a overstatement that these theoretical results strongly impact discussions on spectrum sharing after that.

After Late 2000s, many studies mainly focus on the analysis on practical system design. Liang et al. evident a relationship between sensing time and throughput of secondary networks in 2008 [32]. In spectrum sensing, while a long sensing time can accurately acquire the state of surrounding radio environment, excessive sensing time decreases the spectrum sharing opportunity. The authors theoretically show the sensing time-throughput tradeoff in the CR networks, and investigate optimal sensing time in realistic situations. In addition, it is also this time that studies on the transmission power design of the secondary networks, e.g., comparison of peak and average interference power constraints by Zhang [33], was actively performed.

Besides these practical discussions, some researchers have investigated the channel capacity considering realistic scenarios. Especially, there has been a wide discussion about impacts of imperfect channel state information (CSI) on the channel capacity represented by results by Musavian and Aissa [34] and Suraweera et al.[35][36]. For example, in [35], they derive the SU mean capacity in closed form under a peak interference power constraint. In addition, they also discuss the impact of quantizing the imperfect CSI with a finite number of quantization levels. The same authors theoretically claim that secondary networks achieve higher channel capacity by utilizing the estimated instantaneous CSI even in the presence of imperfection, compared to only the use of the mean CSI [36].

Here, it should be noted that theoretical results by Goldsmith and Varaiya in 1997 [37] affects above discussions, although it is *not* the analysis targeting CR. They determine the channel capacity of a fading channel with an average transmission power constraint under different CSI conditions. Although the paper only considers a single peer-to-peer link, we can extend the results to discussions in the channel capacity of secondary network by considering interference constraints at the primary link. Many theoretical results, e.g., Ghasemi and Sousa [29] and Suraweera et al.[35], stand on the system model in [37]; it can be said that this paper has led to many analyzes on later CR.

Early 2010s-: Toward Practical Spectrum Management

After theoretical investigations have been settled, discussions for practical spectrum sharing have become the main field. For example, many countries are rapidly progressing adjustment of law on existing allocated bands toward the spectrum sharing [38]. Some recent trends on spectrum initiatives in the US are summarized as follows (details are well summarized in reference [38]).

- TV Band: In September 2010, the FCC issued final rules to allow low power unlicensed devices to operate on TVWSs in the US [39].
- AWS-3 Band: In January 2015, the FCC completed an auction of Advanced Wireless Services (AWS)-3 licenses in the 1695-1710 MHz, 1755-1780 MHz, and 2155-2180 MHz bands [40]. The incumbents of this band are federal systems including the federal meteorological-satellite systems. The bands will be shared with cellular service providers based on manual coordination of protection zones to protect the federal systems [41].
- 3.5 GHz Band: The FCC has opened up 3550-3700 MHz to SUs [42]. In this band, the SUs will share the spectrum among themselves and PUs under a three-tiered access model composed of the Incumbent Access (IA), Priority Access (PA) and General Authorized Access (GAA) tiers. IA users include authorized satellite users; PA and GAA users must not interfere toward the IA users. The PA tier consists of Priority Access Licensees (PALs) that will be assigned using a competitive bidding process. The GAA tier is licensed-by-rule to enable open, flexible access to the band for the widest possible group of potential users.
- 5 GHz Band: In 2013, the FCC announced that it intends to modify rules that govern the operation of Unlicensed National Information Infrastructure (U-NII) devices and make available an additional 195 MHz in the 5 GHz band [43]. Recently, there is a contention between unlicensed LTE and Wi-Fi stakeholders for access to the band; the LTE-Unlicensed (LTE-U) and Wi-Fi stakeholders held a meeting to discuss these coexistence issues [44].

These political trends have motivated many researchers in both academic and industrial fields to discuss practical applications targeting an explicit spectrum sharing system [45–47]. Especially, because the government obliges SUs to utilize the spectrum database in many cases, there are many discussions on the database-driven spectrum sharing approach [48–51].

In addition, recent rapid densification of terminals in own system, e.g., Wi-Fi and cellular networks, has increased the importance of efficient inter-system spectrum management.

Table 1.1 Typical path loss exponents [4].

Environment	η
Urban macrocells	3.7-6.5
Urban microcells	2.7-3.5
Office building (same floor)	1.6-3.5
Office building (multiple floors)	2-6
Store	1.8-2.2
Factory	1.6-3.3
Home	3

These technologies that have been cultivated through developments for dynamic spectrum access and CR also have attracted attention as enabler for the efficient inter-system spectrum management [52, 53]. Therefore, in recent years, there are not only consideration for spectrum sharing with the explicit term "cognitive radio" but also consideration on efficiency improvement within own system that says "spectrum management" and "interference aware communications" [54–56]. Developments for the CR-oriented communications over the past 20 years have now influenced the spectrum management in the whole wireless communication systems.

1.4 Radio Propagation Issues in Spectrum Sharing

In the spectrum sharing environment, the SUs must satisfy the communication qualities in the PUs because originally the PUs are allowed to occupy the band. For this reason, the SUs need to suppress the interference amount of the signal power to the PUs to a certain level or less: the prediction of the interference amount between the SUs and the PUs becomes a fundamental important technology [57]. However, radio propagation characteristics irregularly fluctuates according to the states of communication environment: e.g., location relationship between the transmitter and the receiver, and heights and density of obstacle structures [4]. The fluctuation factors can be categorized into following three factors.

- Path loss: Path loss shows mean received power variation over long distances (100-1000 m). The attenuation is typically in proportion to

$$10\eta \log_{10} d, \tag{1.1}$$

in decibel domain. Here, d [m] is the link distance, and η is the path loss index that is roughly determined by the obstacle structures and heights of transmitter and receiver.

Table 1.2 Examples of well-known path loss models [5].

Name	Category	Coverage domain	Cite	Year
Friis Freespace	Foundational	$d > 2a^2/\lambda$	[58]	1946
Hata-Okumura	Basic	$1 < d < 10$ km;$150 \leq f \leq 1500$; $30 \leq h_{\mathrm{Tx}} \leq 200$ m; $1 \leq h_{\mathrm{Rx}} \leq 20$ m	[59]	1968
Longley-Rice Irregular Terrain Model	Terrain	$1 < d < 2000$ km $0.02 < f < 20$ GHz	[60]	1982
COST-Hata/COST-231	Basic	$1 < d < 20$ km	[61]	1993
Walfisch-Ikegami	Basic	$0.2 < d < 5$ km; $0.8 < f < 2$ GHz; $4 <$ Tx < 50 m	[61]	1993
Two-Ray	Foundational		[62]	1994
ITU Terrain	Terrain		[63]	2001
IMT-2000	Basic	Urban	[64]	2007

Typical path loss indexes are summarized in Table 1.1. Depending on the environment, η takes various values up from 2 to 6. The path loss is one of the most important factors for efficient wireless communication system design. Many researchers have worked on the path loss modeling because of its strong environmental dependence and difficulty in theoretical modeling. Table 1.2 summarizes examples of well-known path loss models. Many models have been developed from various approaches such as theoretical approaches, measurement-based approaches, and approaches that considers the influence of surrounding structures. In current wireless communication systems, the system design is based on selecting an appropriate path loss model according to the application.

- Shadowing: Variation due to shadowing occurs over distances that are proportional to the length of the obstructing object (10-100m in outdoor environments and less in indoor environments). The well-known statistical model for this attenuation is log-normal shadowing. This model has been empirically confirmed to model accurately the variation in received power in both outdoor and indoor radio propagation environments. The standard deviation differs depending on the communication environment and it is known to take various values from 4 to 13 dB.

- Multipath fading: Due to the sum of multipath components that passed various paths, the instantaneous received power irregularly fluctuates over very short distances, on the order of the signal wavelength. The statistical characteristics are roughly classified according to presence / absence of visibility between the transmitter and the receiver.

Most important models are Nakagami-Rice fading in line-of-sight (LOS) and Rayleigh fading in non-line-of-sight (NLOS).

In the spectrum sharing, it is important to accurately estimate above factors for the suitable communication strategy. However, as mentioned above, statistical characteristics of the radio propagation highly depend on the communication environment. Figure 1.5 shows several simplified path loss models. These curves follow a path loss equation

$$L(d) = 20\log\frac{\lambda}{4\pi d_0} + 10\eta\log\frac{d}{d_0} \ \text{[dB]}, \tag{1.2}$$

where λ is the wavelength [m] calculated by the frequency f, and d_0 is the reference distance [m]. For example, at $d = 1000$ [m], we can confirm a difference of 20 [dB] between $\eta = 2$ and $\eta = 3$ and also between $\eta = 3$ and $\eta = 4$. If we have no information for the path loss, because SUs must not interfere with PUs, their communication parameters are determined based on the worst case scenario. In addition, uncertainties of the shadowing and multipath fading make the spectrum sharing design more difficult. Although many path loss models are established as shown in Table 1.2, the adopted path loss model does not necessarily ensure accuracy in the actual communication environment [5]. Therefore, fundamental issues in the spectrum sharing can be classified into following topics.

- Accurate estimation of radio propagation characteristics in both primary link and interference link.
- Design of the communication parameters of SUs. We need to design the parameters by integrally considering the desired communication qualities in the PUs and the surrounding radio environment.

1.5 Radio Propagation Estimation Techniques in Spectrum Sharing and Motivation of This Dissertation

Spectrum sharing including CR techniques has been widely discussed over the last decades. Today's major cognition techniques can be classified into following two methods.

Spectrum Sensing

Spectrum sensing uses the detection of PU signals to characterize radio environments [65]. To provide good protection, signal detection must be performed under the (strict) condition

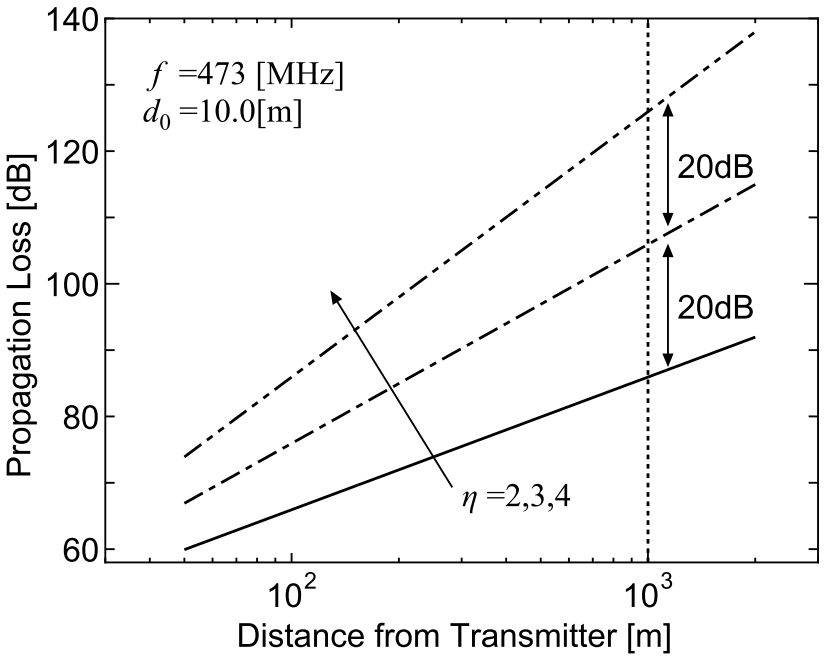

Fig. 1.5 Effect of path loss index η where $f = 473$ [MHz] and $d_0 = 10$ [m].

that the PU signal strength be below the noise floor, even under low signal-to-noise ratios (SNRs) and fading conditions. Fluctuations make it difficult for the SUs to achieve stable detection; thus, although this technique can model the radio environment in real time, it is very challenging to accurately estimate.

Spectrum Database

The second method is based on storing information about spectrum availabilities of each location in spectrum databases [66]. In this method, SUs should query the database before they utilize the spectrum. Then, the database provides spectrum information to the SUs. The spectrum database is especially useful for fixed broadcasting PUs because the spatial distribution of the average signal power does not change. The television (TV) band is a suitable spectrum for database-aided spectrum sharing; its standardization has been discussed in many countries including the US [67], the UK [68], and Singapore [69].

Current databases usually evaluate white space (WS) based on empirical propagation models. For example, *F-Curve*, a propagation model that is utilized in the Federal Communications Commission (FCC)-defined database, estimates the propagation loss based on the percentage of locations, the percentage of time, frequency, and transmitting antenna heights [70]. If the TVWS is exploited in Japan, Notice 640 [71] will be a candidate for the radio propagation estimation. Notice 640 is a propagation model for Japanese TV broadcast

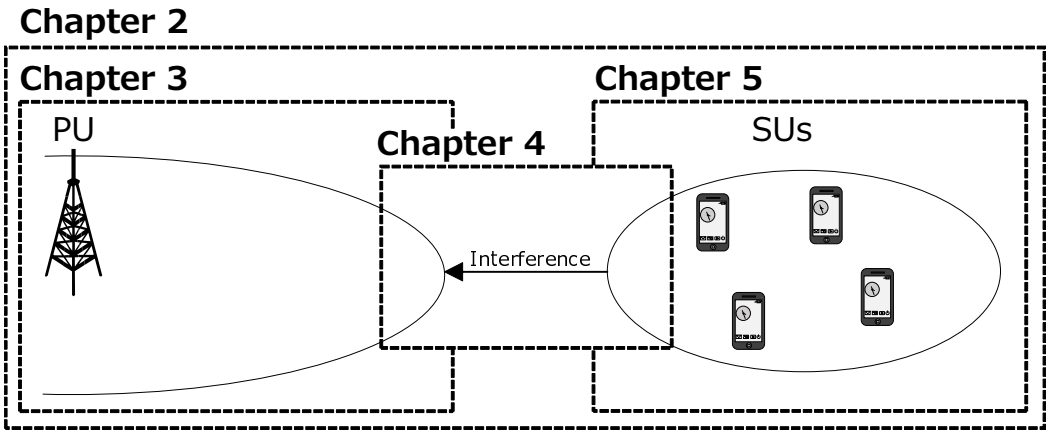

Fig. 1.6 Main focus of each chapter.

systems. This propagation model is defined by the Japanese spectrum regulator, MIC; it is virtually identical to the propagation model defined by the FCC. Japanese TV broadcast operators often use this model to estimate the communication areas of TV transmitters because MIC licenses the use of TV spectrums based on the estimation results for Notice 640. The propagation curve considers multipathing and diffraction due to terrain.

However, it is well known that such propagation models cannot take into account all of the indeterminacies of radio environments. The error characteristics of propagation models have been presented in [72][5]. In [72], the authors measured the field strength of radio waves over TV bands using a highly accurate spectrum analyzer. The statistical results showed that many propagation models perform biased estimation with wide error variances. Phillips et al. [5] analyzed the efficacy of basic path loss models when predicting median path losses in urban environments. By comparing results to those of many other path-loss models, the authors identified the danger of using basic *priori* models to predict the vagaries of the radio environment. It has also been claimed that complex models that consider a larger number of variables (i.e., terrain models) do not necessarily make better predictions. To fit propagation models to the regional radio environment, complex models often require a great deal of information about the radio environment, e.g., terrain, antenna height, antenna pattern, and some measurement data. The fitted curve can achieve near-unbiased estimation over a wide area. However, the information increases the calculation complexities, but cannot improve local accuracy due to shadowing effects.

1.6 Organization

Figure 1.6 shows main focus of each chapter. We describe the detail of the proposed spectrum database and discuss the database-assisted radio propagation estimation in primary networks in chapters 2 and 3. Next, chapter 4 discusses how to manage the interference from SUs to the PU in the presence of imperfect spectrum database. After we propose the database-assisted radio propagation for distributed secondary networks in chapter 5, chapter 6 concludes our works. The detailed organization of this thesis is summarized below.

Chapter 2: Concept of Measurement-based Spectrum Database

In this chapter, we propose a concept of measurement-based spectrum database. After the concept is described, the effect of knowledge of the radio propagation on the spectrum sharing is discussed from a theoretical aspect. Assuming a simple spectrum sharing environment, we show that the uncertainties of the radio propagation notably degrade the average transmission power allowed to the SU. At the same time, it is also shown that the knowledge of shadowing effects can increase the spectrum sharing opportunity.

Chapter 3: Experimental Verification of Measurement-based Spectrum Database over TV Bands

We present experimental results for the database construction using actual TV broadcast signals. In order to evaluate the accuracy of measurement-based spectrum database, two one-week measurement campaigns over TV bands were conducted in Kumagaya city, Saitama, Japan. From the measurement results, we show that the proposed database dramatically reduces the estimation error of the radio environment information.

Chapter 4: Transmission Power Control based on Spectrum Database

In the proposed database, because there are many locations where the measurement nodes cannot enter, the constructed spectrum database has tooth missing information. Although we need to interpolate the tooth missing information from the observed information, the interpolation accuracy strongly depends on the number of measured datasets. This means that SUs will cause a harmful interference if the database determines the transmission power of SUs without considering the quality of the database. This chapter proposes a sophisticated method with the measurement-based spectrum database for designing the appropriate transmission power of the SUs. The proposed method uses ordinary Kriging interpolation for the spectrum cartography. According to the predicted distribution of the estimation error, the

allowable interference power to the PU is approximately formulated. Numerical results show that the proposed method can achieve the probabilistic interference constraint asymptotically. Additionally, it is also shown that the proposed method dramatically improves the outage probability of the interference power compared to the conventional Kriging-based method.

Chapter 5: Database-assisted Radio Propagation Estimation for Wireless Distributed Networks

Above chapters mainly focus on the radio propagation estimation in the primary link, and we assume that SU only knows the path loss in the secondary link for simplicity. On the other hand, if we can improve uncertainties of the interference signal, the spectrum sharing efficiency will be improved further. In this chapter, we propose a spectrum database-assisted radio propagation prediction for distributed SUs. The proposed method focuses on the spatial-correlation of radio propagation characteristics between different wireless links. Using maximum likelihood-based path loss estimation and Kriging-based shadowing estimation, the radio propagation of the wireless link that has arbitrary location relationship can be predicted. From numerical results, it is shown that the proposed method achieves higher estimation accuracy than conventional path loss-based estimation method. After it is shown that the proposed technique can predict the probability density function (PDF) of the estimation error, we evaluate the effect of the proposed radio propagation estimation on the spectrum sharing capability.

Chapter 6: Conclusions and Future Works

We conclude the research contribution of the thesis and discusses future works.

Chapter 2

Concept of Measurement-based Spectrum Database

While the spectrum utilization in whole wireless systems is becoming toward the spectrum database-assisted approach, conventional, path loss-based, database construction has the problem concerning accuracy and is a cause of the degradation of spectrum sharing efficiency. In this chapter, we propose a concept of measurement-based spectrum database. After the concept is described, the effect of knowledge of the radio propagation on the spectrum sharing is discussed from a theoretical aspect.

2.1 Database Architecture

In order to obtain a fully efficient spectrum sharing, we propose a novel concept of a spectrum database that consists of measurement information reported by mobile SUs. Figure 2.1 shows the concept of the proposed spectrum database. The proposed database is a hybrid system, combining spectrum sensing and a spectrum database. The spectrum database consists of radio environment information that is measured by mobile SUs (e.g., vehicles and smartphones). The SUs measure the received signals from the PUs while the SUs move (without transmitting signals). The collected dataset is related to the measurement location, and is reported to the database. After enough data are gathered, the database estimates the radio environment characteristics of the PUs by statistical processing with the large created dataset. Because the data include actual propagation losses and shadowing effects, accurate channel statuses can be determined. SUs can connect the database to a wireless access point such as a cellular network to estimate the radio environment around the SUs, and adjust their own communication parameters, which causes no harmful interference to PUs.

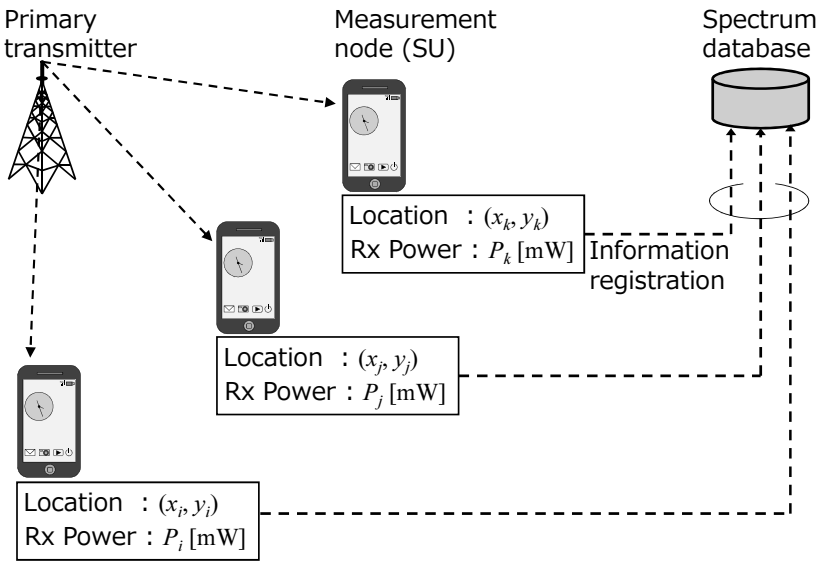

Fig. 2.1 Concept of the measurement-based spectrum database.

Today, there are huge numbers of vehicles and smart phones around the world. Because these mobile terminals have high mobility, we consider them particularly suitable for use as probing sensors. These features of mobile terminals enable the spectrum database to gather measurement data rapidly and over a wide range. Thus, the radio environment can be estimated accurately. In addition, using the accurate knowledge of the received PU signal power, spectrum sharing based on PU signal quality metrics such as the signal-to-interference power ratio (SIR) can be implemented.

Figure 2.2 summarizes the two spectrum database utilization methods: path loss model-based spectrum databases and proposed measurement-based spectrum databases. For the databases populated using propagation modeling, spectrum availability is determined in two steps. First, the service area of a PU is estimated using the propagation model. Second, the expected service area is extended by an additional margin to guarantee interference-free operation for the PUs located at the boundary of the primary coverage area. Because the margin is added without any regard for the actual propagation conditions, the SU transmission power and the SU coverage area are unnecessarily reduced. As a result, the total spectrum sharing performance is degraded. On the other hand, the proposed database can provide accurate propagation information regarding the PU signals to the SUs. Therefore, if the location of the PU receiver is known, aggressive spectrum sharing while controlling the SU transmission power can be realized. This flexible and sophisticated transmission power control method can obtain highly efficient spectrum sharing performance between PUs and SUs because the spectrum database can help to accurately determine the received power of PU signals at any location and any frequency if a perfect spectrum database can be generated.

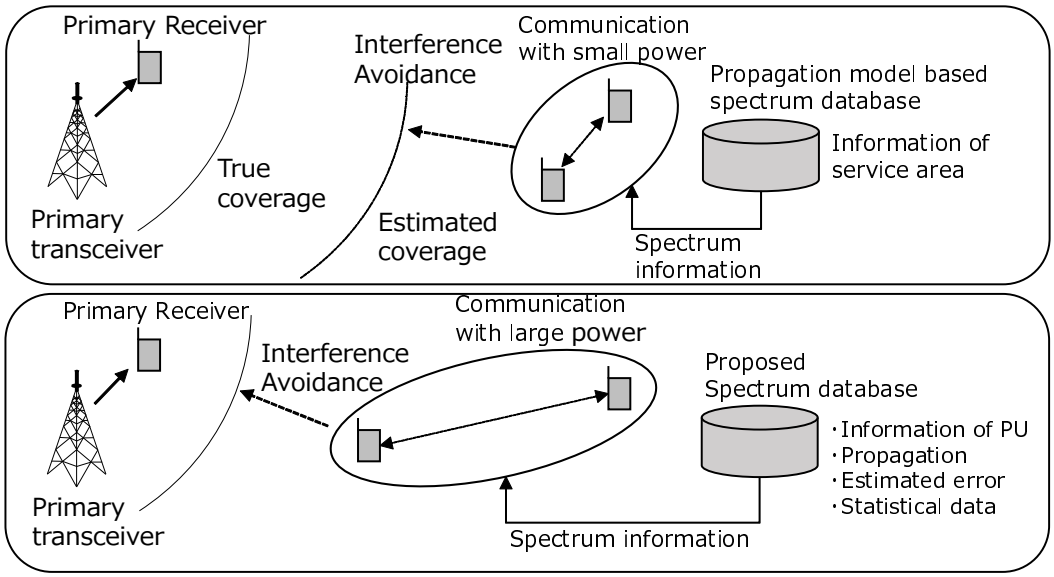

Fig. 2.2 Operation of the spectrum database.

The proposed spectrum database can realize highly efficient spectrum utilization with strict interference management by employing measurement datasets. However, if all of the measurement data are uploaded to the database covering a large area, a large amount of data must be processed to estimate the primary coverage, which makes it difficult to provide spectrum usage information to SUs. Therefore, we consider a hierarchical database structure that supports storing data particles of flexible size in each layer, as shown in Fig. 2.3. In the hierarchical architecture, the size of an area supported by the databases at each layer is different. The databases at the lowest layers operate with high-resolution raw data, but they can only support small areas. Higher layers, with information of lower resolution, are statistically calculated from the lower-layer data. Because of the reduced size of the stored information, the databases on higher layers can support wider areas.

As shown in Fig. 2.3, the lowest-layer database is located at each SU. SUs probe the radio environment during displacement and store the most recent measurement results in these databases at high resolution. However, because an individual local database cannot cover a sufficiently large area, any comprehensive view of the primary signal propagation must be derived from the locally collected data. Hence, a second-layer database is used to store the stochastic information gathered from surrounding SUs. This layer consists of many databases supporting small areas of a few square kilometers in size. SUs upload measurement datasets when the second-layer database requires updates to its own statistical information. After enough data are gathered, SUs can utilize the statistical information provided by the second-layer database. We consider the second-layer database to be fixed

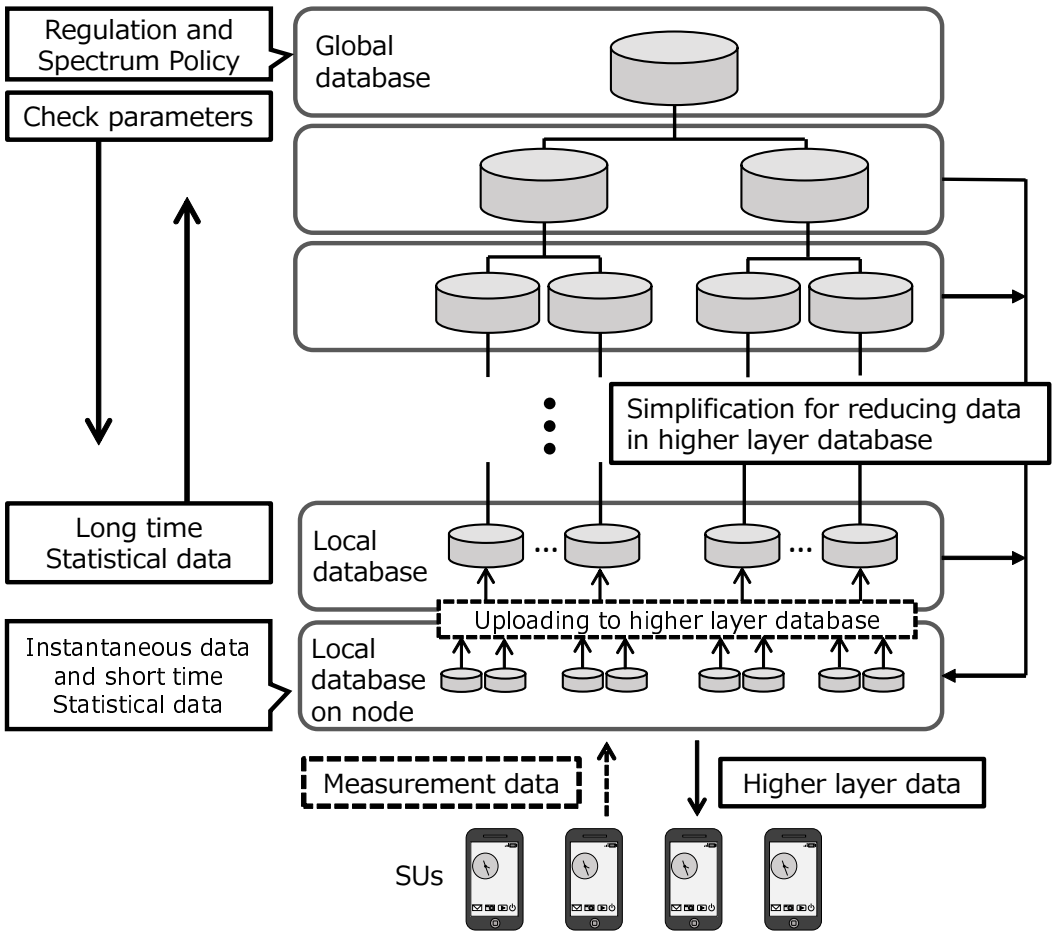

Fig. 2.3 Hierarchical database architecture.

and to be managed by industry, which is permitted to manage the database by governments. If there is an immediate demand for WS utilization, the second-layer database with mobility can be added for the required area. Because it is difficult to store all of the measurement data, stochastic information with lower resolutions is stored according to the location coordinates based on a grid structure. A database of this size can gather information on signal power from surrounding SUs and can store the average power for each frequency and location. This database can support SU interference management so as to achieve strict transmit power control without degradation of PU reception quality. The database at the highest layer implements a spectrum utilization policy provided by the regulatory organization in charge of a region, such as FCC in the US, Ofcom in the UK, or MIC in Japan. As a result, metrological spectrum management can be realized with highly efficient spectrum sharing.

The proposed architecture can be used for various primary systems. Here, various parameters of the database are constructed according to the spectrum characteristics of the primary system. We assume that the frequency of data upload and the spectrum allocation

period are the main parameters used for database construction, and that the database must adjust these parameters based on the spectrum characteristics. In this thesis, we specifically consider the compatibility with the current TVWS spectrum database design. According to the current rules of TVWS utilization, SUs must access the database at intervals of several hours: two hours in the UK and 24 hours in the US. We follow these time frames for the spectrum allocation periods. Because broadcast TV transmitters are fixed, their spectrum occupancies are static in the time domain. Therefore, in terms of TV protection, the importance SUs need to know is the spatial distribution of the average received signal power. Because the variation of the distribution is gradual in the time domain, the frequency of the dataset upload by each measurement terminals is expected to be low. From the practical standpoint of database access cost, frequent dataset uploading is undesirable. Dataset upload should be conducted only when the node can access the wireless networks with sufficient capacity, such as public WLAN, home WLAN, and cellular networks.

Of course the measurement-based database design can be applied to other networks with frequent changes of spectrum usage: unlicensed bands, cellular systems, radar bands, and so on. However, spectrum occupancies of these systems fluctuate drastically in the time domain; thus, other characteristics of WSs, e.g., variance, duty cycle, and transition ratio, are required.

2.2 Low-layer Configuration for Spatial Spectrum Sharing

As already mentioned, the most important spectrum characteristic in TVWS is the average received signal power. To estimate the spatial distribution effectively, we assume that measurement nodes probe signals with short-term averaging. In addition, the second-layer databases collect the datasets and average the data per short-size grid.

2.2.1 Lowest layer: Local database at node

A layer is implemented at each measurement node. Each node probes signals during displacement and stores the signal data in its own database. Because each node moves with the user, the explicit spatial border of this layer is not determined. To remove signal variations due to small-scale fading, each node periodically measure signals (with short-term averaging), as shown in Eq. (2.1).

$$P_i = \frac{1}{N_t} \sum_{t=0}^{N_t-1} |h_i[t]s_i[t] + n_i[t]|^2 , \tag{2.1}$$

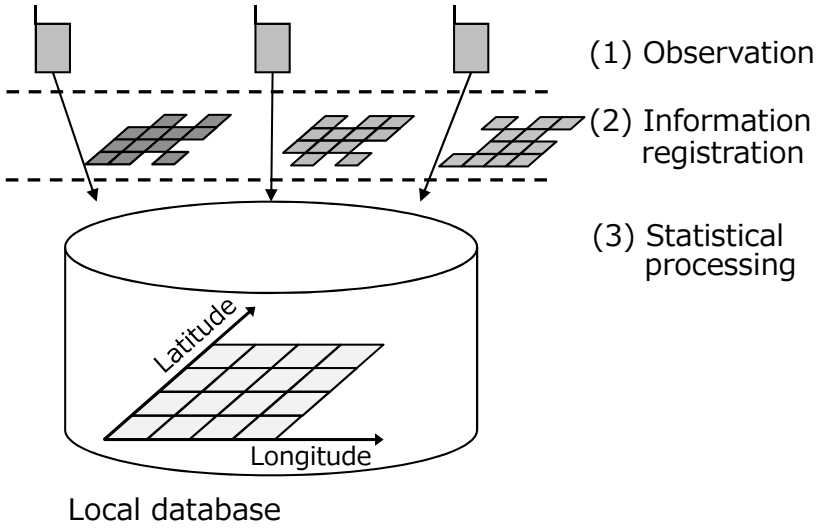

Fig. 2.4 Structure of the local database.

where $h_i[t]$ represents the channel coefficient at the i-th node location, which includes propagation loss, shadowing, and small-scale fading. $s[t]$ is the signal from the primary user. $n_i[t]$ is AWGN. N_t is the number of averaged samples of each sensor. The mobile terminal equipped with a global positioning system (GPS) device stores the value P_i and the current location, time, and observed TV channel in the local database of the node. These values are uploaded to second-layer databases via wireless access networks. After upload, the node can erase the dataset from its own database.

2.2.2 Second layer: Local database

The second layer typically consists of fixed multi-databases managed by industries which are allowed to utilize it by governments. Each database supports a small area of a few kilometers, which matches the typical coverage of TV transmitters. Higher-layer databases divide datasets from mobile nodes into corresponding second-layer databases, based on measurement location and the supported area of the second-layer databases. After the data has been gathered, the spatial distribution of the average received signals can be estimated. In addition to the difficulty of storing a large number of measurements in a single database, another important problem to overcome is the limited accuracy of localization systems in the mobile terminals. A typical GPS device experiences errors on the order of several meters (up to more than 10 meters). For these reasons, we use a grid structure for location indexing, as shown Fig. 2.4. We divide each area of a few square kilometers (which is assigned to a database on the layer immediately above the local databases on the mobile terminals) into a square grid with a side length of l [m]. Each square cell in the grid in the second-layer

databases is represented by the average received signal power of all measurement data that was collected from the cell described with coordinates x and y that satisfy the condition

$$\sqrt{(x-x_c)^2+(y-y_c)^2} \leq \frac{l}{\sqrt{2}}, \tag{2.2}$$

where x_c and y_c represent the coordinates of the grid field's center. In other words, the PU power in a given grid field is estimated as,

$$\frac{1}{N}\sum_{i=1}^{N} P_i, \tag{2.3}$$

where N is the number of observations that satisfy Eq. (2.2).

Note that there are borders of the estimation areas between the databases. Thus, white-space determination methods taking into account the information of databases, which are located on the both ends of the boundary, are required. For example, average of two values which are stored in the both ends of databases is a simple connection method.

2.2.3 Impact of Upload Cost on Existing Networks

When the terminal uploads the observation data to the database, the terminal will upload the data via the existing network such as Wi-Fi or cellular. Thus, an important question that arise here is how the introduce of the measurement-based spectrum database will affect on the existing networks?

Table 2.1 summarizes an example of required data for measurements of an instantaneous signal power. Considering the radio propagation estimation of a broadcast type transmitter such as television broadcasting, an instantaneous measurement requires 52 byte [73]. In the field measurement described in Chapt.3, the number of data observed by one vehicle in a day was about 80,000 records: a terminal will upload about 4MB per day. Note that this file size will be an upper limit because the vehicle measured signals from 9 AM to 7 PM almost all the time except for meals and break time.

In Japan, an user uploads with average 46.6kbps, and files with roughly 500MB are uploaded in a day. Thus, even if all the users upload the measured information everyday, the traffic increase will be less than 1%. Actually, not all users perform mobile observations and observable time zones are limited. Therefore, the effect of the upload on existing networks will be sufficiently ignored. Furthermore, by uploading the observation results of one day at the same time during low traffic such as midnight, further mitigation of the influence on existing networks will be excepted.

Table 2.1 Required data for measurements of an instantaneous signal power. Right two columns are based on MySQL 5.7.

Name	Data type	Data size[byte]
Measurement time	datetime	8
Latitude	double	8
Longitude	double	8
Measurement frequency [Hz]	double	8
Number of Samples	int	4
Sampling rate [sec]	double	8
Received signal power [mW]	double	8

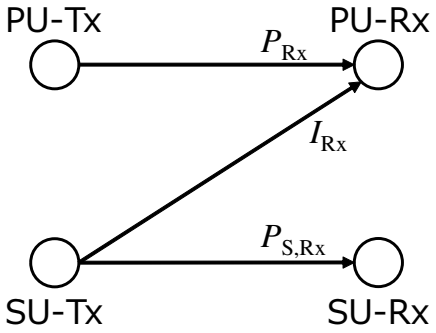

Fig. 2.5 Spectrum sharing model.

2.3 Analysis of Channel Capacity in Proposed Database-aided Spectrum Sharing

Let us discuss the effect of knowledge of radio propagation information on spectrum sharing from a theoretical perspective. We consider a typical spectrum sharing environment shown in Fig. 2.5 where a secondary transmitter SU-Tx share a spectrum with a primary link. To evaluate the spectrum sharing efficiency, we calculate the allowable transmission power at SU-Tx under a given channel information. Note that following discussion does not consider the knowledge of instantaneous multipath fading gain: SU-Tx only knows path loss gain and shadowing gain. This is because the acquisition of the instantaneous factor requires some feedbacks from PU-Rx generally In the spectrum sharing with legacy wireless systems, such feedbacks are *not* realistic assumption. Aiming for the improvement of spectrum sharing efficiency in the legacy systems, this thesis consider no instantaneous feedbacks from the PUs. If the PU feedbacks such information to the SU, it is possible to further improve the spectrum sharing efficiency [29].

2.3.1 Spectrum Sharing Model

First, P_{Rx} [dBm] is defined as the received signal power at the primary receiver PU-Rx from the primary transmitter PU-Tx. We assume the value fluctuates according to the path loss and the log-normal shadowing, as follows:

$$P_{\mathrm{Rx}} = P_{\mathrm{P,Tx}} - L_{\mathrm{P}} + W_{\mathrm{P}} \quad [\mathrm{dBm}] \tag{2.4}$$

$$\triangleq \overline{P}_{\mathrm{Rx}} + W_{\mathrm{P}}, \tag{2.5}$$

where $P_{\mathrm{P,Tx}}$ [dBm] is the transmission power at PU-Tx, L_{P} [dB] is the path loss in the primary link, and W_{P} [dBm] is the shadowing gain following i.i.d. log-normal distribution with zero mean and standard deviation σ_{P} [dB].

Next, we assume that SU-Tx interferes to PU-Rx with the following power:

$$I_{\mathrm{Rx}} = P_{\mathrm{S,Tx}} - L_{\mathrm{S}} + W_{\mathrm{S}} \quad [\mathrm{dBm}] \tag{2.6}$$

$$\triangleq \overline{I}_{\mathrm{Rx}} + W_{\mathrm{S}}, \tag{2.7}$$

where $P_{\mathrm{S,Tx}}$ is the transmission power at SU-Tx, L_{S} is the path loss in the interference link, and W_{S} is the shadowing gain. W_{S} follows i.i.d. log-normal distribution with zero mean and standard deviation σ_{S} [dB], and is statistically independent from W_{P}. In addition, SU-Rx receives the signal from SU-Tx with following received signal power,

$$P_{\mathrm{S,Rx}} = P_{\mathrm{S,Tx}} - L_{\text{SU-SU}} + W_{\text{SU-SU}}, \tag{2.8}$$

where $L_{\mathrm{SU-SU}}$ is the constant path loss between SU-Tx and SU-Rx, and $W_{\text{SU-SU}}$ is the shadowing effect between SU-Tx and SU-Rx that follows i.i.d.log-normal distribution with zero mean and standard deviation σ_{S}. According to Shannon-Hartley theorem, channel capacity at SU-Rx can be derived as,

$$C_{\text{SU-Rx}} = \log_2\left(1 + 10^{\frac{P_{\mathrm{S,Rx}} - N_0}{10}}\right) \text{[bps/Hz]}, \tag{2.9}$$

where N_0 [dBm] is the average AWGN at SU-Rx. Note that we do not consider the effect of the interference from PU-Tx to SU-Rx.

Under the above condition, we utilize the signal-to-interference power ratio (SIR) as the protection criterion for the primary communication according to a typical rule of spectrum sharing over TVWS [74]. Here, the SIR at PU-Rx can be written as

$$\Gamma = P_{\mathrm{Rx}} - I_{\mathrm{Rx}} \ \ [\mathrm{dB}]. \tag{2.10}$$

If the PU determines the desired SIR as Γ_{d} [dB], the outage event can be formulated as $\Gamma_{\mathrm{d}} > \Gamma$. Thus, considering the desired protection probability $1 - p_{\mathrm{out}}$, the SU must satisfy the protection probability at PU-Rx, given by the following equation

$$\Pr[\Gamma \geq \Gamma_{\mathrm{d}}] \geq 1 - p_{\mathrm{out}}. \tag{2.11}$$

Using the channel information in both the primary and secondary links, SU-Tx estimates the maximum transmission power

$$\max P_{\mathrm{S,Tx}} \triangleq P_{\mathrm{S,max}} \quad [\mathrm{dBm}], \tag{2.12}$$

that is subject to Eq. (2.11). An example of this situation is spectrum sharing between a TV transmitter and a white space device over TVWS.

2.3.2 Comparison Methods

According to the above model, we analyze the performances of the maximum allowed transmission power at SU-Tx under following three conditions.

- Method 1: both P_{Rx} and $L_{\mathrm{S}} + W_{\mathrm{S}}$ are estimated via the measurement-based spectrum database (PU: path loss + shadowing, SU: path loss + shadowing). This can be achieved by the method proposed in Chapt. 5.
- Method 2: in the primary channel, P_{Rx} is estimated via the measurement-based spectrum database. On the other hand, in the interference channel, L_{S} and σ_{S} are estimated via the conventional spectrum database (PU: path loss + shadowing, SU: path loss). This can be achieved by the method proposed in Chapt. 4.
- Method 3: $\overline{P}_{\mathrm{Rx}}$, σ_{P}, L_{S} and σ_{S} are estimated via the conventional spectrum database (PU: path loss, SU: path loss).

Let us define $\hat{P}_{\mathrm{Rx}}$ and $\hat{L}_{\mathrm{S,sum}}$ as estimated P_{Rx} and $L_{\mathrm{S}} + W_{\mathrm{S}}$, respectively. In order to discuss the effect of imperfection of the measurement-based spectrum database on the spectrum sharing, we assume that both $\hat{P}_{\mathrm{Rx}}$ and $\hat{L}_{\mathrm{S,sum}}$ have estimation error. These estimation error factors are modeled as,

$$\begin{aligned} \epsilon_{\mathrm{P}} &= P_{\mathrm{Rx}} - \hat{P}_{\mathrm{Rx}} \\ \epsilon_{\mathrm{S}} &= (L_{\mathrm{S}} + W_{\mathrm{S}}) - \hat{L}_{\mathrm{S,sum}}. \end{aligned} \tag{2.13}$$

If the measurement-based spectrum database is utilized for the radio propagation estimation, we can predict the variances of error factors, $\mathrm{Var}[\epsilon_\mathrm{P}] \triangleq \sigma^2_{\epsilon_\mathrm{P}}$ and $\mathrm{Var}[\epsilon_\mathrm{S}] \triangleq \sigma^2_{\epsilon_\mathrm{S}}$, by considering a characteristic of *Kriging interpolation* (see Chapt. 4.4 and Chapt. 5.4.3). Therefore, it is also assumed that $\sigma^2_{\epsilon_\mathrm{P}}$ and $\sigma^2_{\epsilon_\mathrm{S}}$ can be predicted perfectly when the measurement-based spectrum database is used.

In the situation where we use the conventional spectrum database, we assume that estimated $\overline{P}_\mathrm{Rx}$, σ_P, L_S and σ_S have no error.

2.3.3 Modeling Error Characteristics of Measurement-based Spectrum Database

Before the performance comparison, we model the error characteristics of measurement-based spectrum database. We assume that both $\hat{P}_\mathrm{Rx}$ and $\hat{L}_\mathrm{S,sum}$ are estimated by the Kriging-based database construction proposed in Chapt. 4 and Chapt. 5, respectively. As can be seen from some results in Sect. 4.4 and Sect. 5.4, these estimation error factors follow a log-normal distribution with median zero [dB], and estimated and true values are highly correlated each other in the log domain. Thus, P_Rx and $\hat{P}_\mathrm{Rx}$, and $(L_\mathrm{S} - W_\mathrm{S})$ and $\hat{L}_\mathrm{S,sum}$ follow a bivariate log-normal distribution respectively. Namely, P_Rx and $\hat{P}_\mathrm{Rx}$ follow the bivariate log-normal distribution with median $\overline{P}_\mathrm{Rx}$ and the covariance matrix,

$$\begin{pmatrix} \sigma^2_\mathrm{P} & \rho_\mathrm{P}\sigma_\mathrm{P}\sigma_{\hat{P}_\mathrm{Rx}} \\ \rho_\mathrm{P}\sigma_{\hat{P}_\mathrm{Rx}}\sigma_\mathrm{P} & \sigma^2_{\hat{P}_\mathrm{Rx}} \end{pmatrix}, \tag{2.14}$$

where σ_P [dB] is the standard deviation of W_P, $\sigma_{\hat{P}_\mathrm{Rx}}$ is the standard deviation of $\hat{P}_\mathrm{Rx}$, and ρ_P is the correlation coefficient between P_Rx and $\hat{P}_\mathrm{Rx}$. The PDF of $\epsilon_\mathrm{P} = P_\mathrm{Rx} - \hat{P}_\mathrm{Rx}$ can be derived from the bivariate log-normal distribution. Because ϵ_P consists of the different of two variables following a bivariate log-normal distribution and Kriging can perform unbiased estimation, ϵ_P also follows a log-normal distribution with median zero (this also can be seen from Fig. 4.3). In addition, its variance can be calculated by,

$$\sigma^2_{\epsilon_\mathrm{P}} = \sigma^2_\mathrm{P} + \sigma^2_{\hat{P}_\mathrm{Rx}} - 2\rho_\mathrm{P}\sigma_\mathrm{P}\sigma_{\hat{P}_\mathrm{Rx}}. \tag{2.15}$$

For simplicity, we approximate $\sigma_{\hat{P}_\mathrm{Rx}}$ by σ_P. From this relationship, $\sigma^2_{\epsilon_\mathrm{P}}$ can be derived as,

$$\sigma^2_{\epsilon_\mathrm{P}} \approx 2\sigma^2_\mathrm{P}(1 - \rho_\mathrm{P}). \tag{2.16}$$

Using these characteristics, we can easily emulate the Kriging-based radio propagation estimation by σ_{P} and ρ_{P}. Note that ρ_{P} strongly depends on the estimation condition such as the number of datasets and the size of measurement circle, as mentioned in Sect. 5.4.

Similarly, $(L_{\mathrm{S}} - W_{\mathrm{S}})$ and $\hat{L}_{\mathrm{S,sum}}$ follow the bivariate log-normal distribution with median L_{S} and the covariance matrix,

$$\begin{pmatrix} \sigma_{\mathrm{S}}^2 & \rho_{\mathrm{S}}\sigma_{\mathrm{S}}\sigma_{\hat{L}_{\mathrm{S,sum}}} \\ \rho_{\mathrm{S}}\sigma_{\hat{L}_{\mathrm{S,sum}}}\sigma_{\mathrm{S}} & \sigma_{\hat{L}_{\mathrm{S,sum}}}^2 \end{pmatrix}, \tag{2.17}$$

where σ_{S} is the standard deviation of W_{S}, $\sigma_{\hat{L}_{\mathrm{S,sum}}}$ is the standard deviation of $\hat{L}_{\mathrm{S,sum}}$, and ρ_{S} is the correlation coefficient between $(L_{\mathrm{S}} - W_{\mathrm{S}})$ and $\hat{L}_{\mathrm{S,sum}}$. In addition, the PDF of $\epsilon_{\mathrm{S}} = I_{\mathrm{Rx}} - \left(P_{\mathrm{S,Tx}} - \hat{L}_{\mathrm{S,sum}}\right)$ can be derived by the log-normal distribution with median zero. Then, the variance can be calculated by,

$$\sigma_{\epsilon_{\mathrm{S}}}^2 = \sigma_{\mathrm{S}}^2 + \sigma_{\hat{L}_{\mathrm{S,sum}}}^2 - 2\rho_{\mathrm{S}}\sigma_{\mathrm{S}}\sigma_{\hat{L}_{\mathrm{S,sum}}}. \tag{2.18}$$

Finally, by approximating $\sigma_{\hat{L}_{\mathrm{S,sum}}}$ as σ_{S}, $\sigma_{\epsilon_{\mathrm{S}}}^2$ can be written as,

$$\sigma_{\epsilon_{\mathrm{S}}}^2 \approx 2\sigma_{\mathrm{S}}^2(1 - \rho_{\mathrm{S}}). \tag{2.19}$$

Here, it should be note that both $\sigma_{\epsilon_{\mathrm{P}}}^2$ and $\sigma_{\epsilon_{\mathrm{S}}}^2$ can be directly estimated with the Kriging variance (see Sect. 4.4 and Sect. 5.4).

2.3.4 Allowed Transmission Power

We derive the allowable transmission power of SU-Tx $P_{\mathrm{S,max}}$ that satisfies the interference constraint defined in Eq. (2.11).

Method 1 (PU: Path Loss + Shadowing, SU: Path Loss + Shadowing)

In this situation, both P_{Rx} and $L_{\mathrm{S}} + W_{\mathrm{S}}$ are estimated by the measurement-based spectrum database. When we estimate both P_{Rx} and I_{Rx} by the Kriging interpolation, the SIR Γ follows a log-normal distribution with median $\hat{P}_{\mathrm{Rx}} - \left(P_{\mathrm{S,Tx}} - \hat{L}_{\mathrm{S,sum}}\right)$ and variance $\sigma_{\epsilon_{\mathrm{P}}}^2 + \sigma_{\epsilon_{\mathrm{S}}}^2$. Thus, the maximum allowed transmission power at SU-Tx can be written as,

$$P_{\mathrm{S,max}} = \hat{P}_{\mathrm{Rx}} + \hat{L}_{\mathrm{S,sum}} - \Gamma_{\mathrm{d}} - \sqrt{2\left(\sigma_{\epsilon_{\mathrm{P}}}^2 + \sigma_{\epsilon_{\mathrm{S}}}^2\right)}\mathrm{erf}^{-1}(1 - 2p_{\mathrm{out}}). \tag{2.20}$$

Method 2 (PU: Path Loss + Shadowing, SU: Path Loss)

In this situation, only P_{Rx} is estimated by the measurement-based spectrum database, and $L_{\mathrm{S}} + W_{\mathrm{S}}$ is estimated by the conventional spectrum database. In this situation, the allowable transmission power can be derived by,

$$P_{\mathrm{S,max}} = \hat{P}_{\mathrm{Rx}} + L_{\mathrm{S}} - \Gamma_{\mathrm{d}} - \sqrt{2\left(\sigma_{\epsilon_{\mathrm{P}}}^2 + \sigma_{\mathrm{S}}^2\right)}\mathrm{erf}^{-1}(1-2p_{\mathrm{out}}). \tag{2.21}$$

Method 3 (PU: Path Loss, SU: Path Loss)

This situation means that both P_{Rx} and $L_{\mathrm{S}} + W_{\mathrm{S}}$ are estimated by the conventional spectrum database: SU-Tx only knows $\overline{P}_{\mathrm{Rx}}$, σ_{P}, L_{S} and σ_{S}. Thus, the SIR follows a log-normal distribution with a median $\overline{P}_{\mathrm{Rx}} - \overline{I}_{\mathrm{Rx}}$ and a standard deviation $\sqrt{\sigma_{\mathrm{P}}^2 + \sigma_{\mathrm{S}}^2}$. Therefore, its CDF can be formulated as

$$F_{\Gamma}(\Gamma_{\mathrm{d}}|\overline{P}_{\mathrm{Rx}}, L_{\mathrm{S}}) = \frac{1}{2}\left\{1 + \mathrm{erf}\left(\frac{\Gamma_{\mathrm{d}} - \left(\overline{P}_{\mathrm{Rx}} - \overline{I}_{\mathrm{max}}\right)}{\sqrt{2\left(\sigma_{\mathrm{P}}^2 + \sigma_{\mathrm{S}}^2\right)}}\right)\right\} \tag{2.22}$$

$$= p_{\mathrm{out}}. \tag{2.23}$$

Therefore, the allowed transmission power can be calculated by,

$$P_{\mathrm{S,max}} = L_{\mathrm{S}} + \overline{P}_{\mathrm{Rx}} - \Gamma_{\mathrm{d}} - \sqrt{2(\sigma_{\mathrm{P}}^2 + \sigma_{\mathrm{S}}^2)}\mathrm{erf}^{-1}(1-2p_{\mathrm{out}}). \tag{2.24}$$

2.3.5 Theoretical Analysis of Average Channel Capacity

According to the allowed transmission power, we analyze the theoretical average channel capacity $\mathrm{E}[C_{\text{SU-Rx}}]$. Here, $P_{\mathrm{S,Rx}}$ in all the methods follows the log-normal distribution because $\hat{P}_{\mathrm{Rx}}$ and $\hat{I}_{\mathrm{Rx}}$ with the proposed spectrum database follow the log-normal distribution, and the method 3 designs a constant transmission power according to Eq. (2.24). In addition, because the channel capacity can be approximated as $C_{\text{SU-Rx}} \approx \log_2\left(10^{\frac{P_{\mathrm{S,Rx}} - N_0}{10}}\right)$ in high-SNR region, $C_{\text{SU-Rx}}$ nearly follows a normal distribution. Thus, considering these characteristics, we can approximately model the average channel capacity in all the methods as,

$$\mathrm{E}[C_{\text{SU-Rx}}] \approx \frac{\log_2 10}{10}\left(L_{\mathrm{S}} - \overline{P}_{\mathrm{Rx}} - \Gamma_{\mathrm{d}} - A\mathrm{erf}^{-1}(1-2p_{\mathrm{out}}) - L_{\text{SU-SU}} - N_0\right), \tag{2.25}$$

where A is the constant factor that depends on the method, and is derived as,

$$A = \begin{cases} \sqrt{2(\sigma_{\epsilon_{\mathrm{P}}}^2 + \sigma_{\epsilon_{\mathrm{S}}}^2)} & \text{(PU:path loss+shadowing, SU: path loss+shadowing)} \\ \sqrt{2(\sigma_{\epsilon_{\mathrm{P}}}^2 + \sigma_{\mathrm{S}}^2)} & \text{(PU:path loss+shadowing, SU: path loss)} \\ \sqrt{2(\sigma_{\mathrm{P}}^2 + \sigma_{\mathrm{S}}^2)} & \text{(PU:path loss, SU: path loss).} \end{cases} \tag{2.26}$$

Finally, by concatenating and summarizing the above equations with inequalities, we can derive the conditions that the proposed database outperforms the path loss-based radio propagation estimation from the view point of average channel capacity $\mathrm{E}[C_{\text{SU-Rx}}]$. Each condition is shown below.

- Method 1 outperforms method 2 when,

$$\rho_{\mathrm{S}} \geq \frac{1}{2}. \tag{2.27}$$

  Note that we assume that both two methods take the same ρ_{P}.

- Method 2 outperforms method 3 when,

$$\rho_{\mathrm{P}} \geq \frac{1}{2}. \tag{2.28}$$

- Method 1 outperforms method 3 when,

$$\rho_{\mathrm{S}} - \frac{\sigma_{\mathrm{P}}^2}{2\sigma_{\mathrm{S}}^2}(1 - 2\rho_{\mathrm{P}}) \geq \frac{1}{2}. \tag{2.29}$$

  If $\sigma_{\mathrm{P}} = \sigma_{\mathrm{S}}$, this condition can be simplified as,

$$\rho_{\mathrm{P}} + \rho_{\mathrm{S}} \geq 1. \tag{2.30}$$

These conditions show that the proposed database can outperform the path loss-based estimation if we can estimate with 0.5 or more correlation between estimated and true received signal powers.

Performances of the estimation accuracy with practical techniques for the radio propagation estimation are evaluated in Sect. 4.4 and Sect. 5.4. In these sections, we show that such an accuracy is realistically achievable value.

2.3.6 Performance Comparison

We evaluate the effect of the proposed radio propagation estimation on the spectrum sharing capability via Monte Carlo simulation. Figure 2.6 shows the average capacity where $p_{\text{out}} = 0.10$, $\Gamma_{\text{d}} = 10$ [dB], $L_{\text{S}} = 100.0$ [dB], $\overline{P}_{\text{Rx}} = -90.0$ [dBm], $L_{\text{SU-SU}} = 20.0$ [dB], and $N_0 = -100.0$ [dBm]. Although the theoretical values are calculated with the approximation, theoretical curves agree well with simulation values. In addition, comparing three methods each other, the magnitude relation of each capacity satisfies the conditions shown in Sect. 2.3.5.

The characteristic of average transmission power at SU-Tx is shown in Fig. 2.7. We can confirm that the measurement-based spectrum database can enhance the average transmission power of SU-Tx, and the difference between the other methods increases according to the increase of σ_{P} and σ_{S}, even if ρ_{S} is low. For example, in $\sigma_{\text{P}} = \sigma_{\text{S}} = 8.0$ [dB], the proposed method can improve roughly 17.8 [dB] at maximum. Here, comparing Figs.2.6 and 2.7, we can confirm that the magnitude relation of each curve is reversed in the region where ρ_{P} is low. This is because the allowed transmission power $P_{\text{S,max}}$ follows a log-normal distribution. In a log-normal distribution, the average value strongly depends on the value in the right tail of the PDF. On the other hand, as Eq.(2.9) shows, the effect of the increase of $P_{\text{S,max}}$ decreases as $P_{\text{S,max}}$ increases.

When evaluating spectrum sharing efficiency using average transmission power at the SU, it is necessary to pay attention to the magnitude relation of channel capacity between curves. On the other hand, because a correlation of 0.5 or more can be realistically achieved as shown in Sect. 4.4 and Sect. 5.4, the average transmission power can sufficiently evaluate the spectrum sharing efficiency. Therefore, for simplicity, we use the average transmission power at the SU as the criterion for the spectrum sharing opportunity in the following chapters.

2.4 Chapter Summary

In this chapter, we have proposed the concept of the measurement-based spectrum database. The spectrum database consists of radio environment information measured by mobile terminals. After enough data are gathered, the database estimates the radio environment characteristics by statistical processing with the large datasets.

Additionally, we have analyzed the channel capacity of the proposed database-aided spatial spectrum sharing. It has been shown that the proposed spectrum database can outperform the path loss-based spectrum database from the viewpoint of channel capacity.

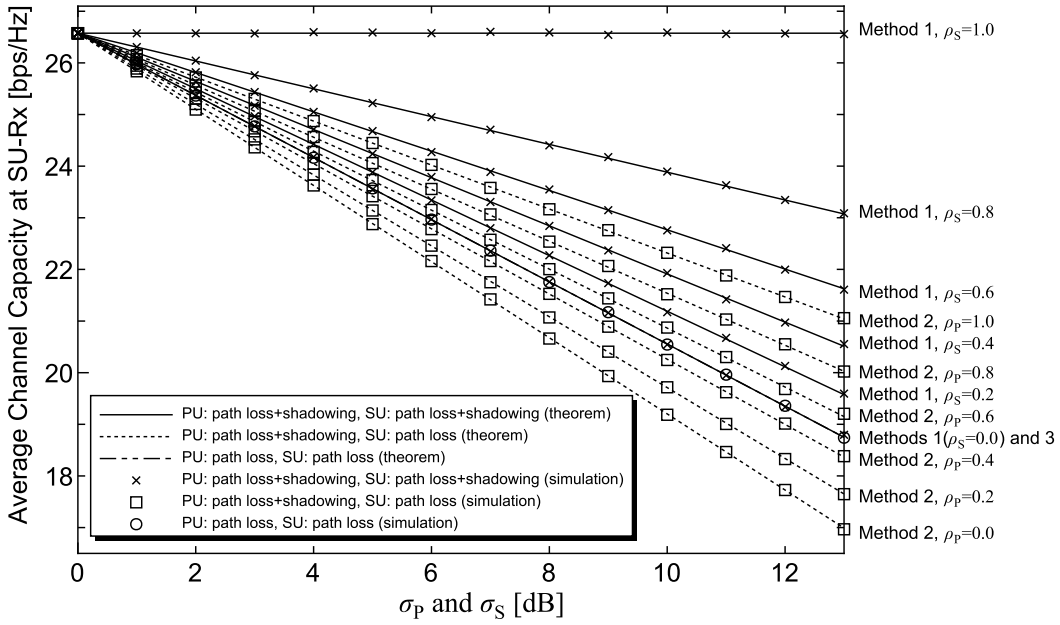

Fig. 2.6 Simulation and theoretical results of average capacity where $p_{\text{out}} = 0.10$, $\Gamma_{\text{d}} = 10$ [dB], $L_{\text{S}} = 100.0$ [dB], $\overline{P}_{\text{Rx}} = -90.0$ [dBm], $L_{\text{SU-SU}} = 20.0$ [dB], and $N_0 = -100.0$ [dBm]. Method 1 assumes $\rho_{\text{P}} = 1.0$.

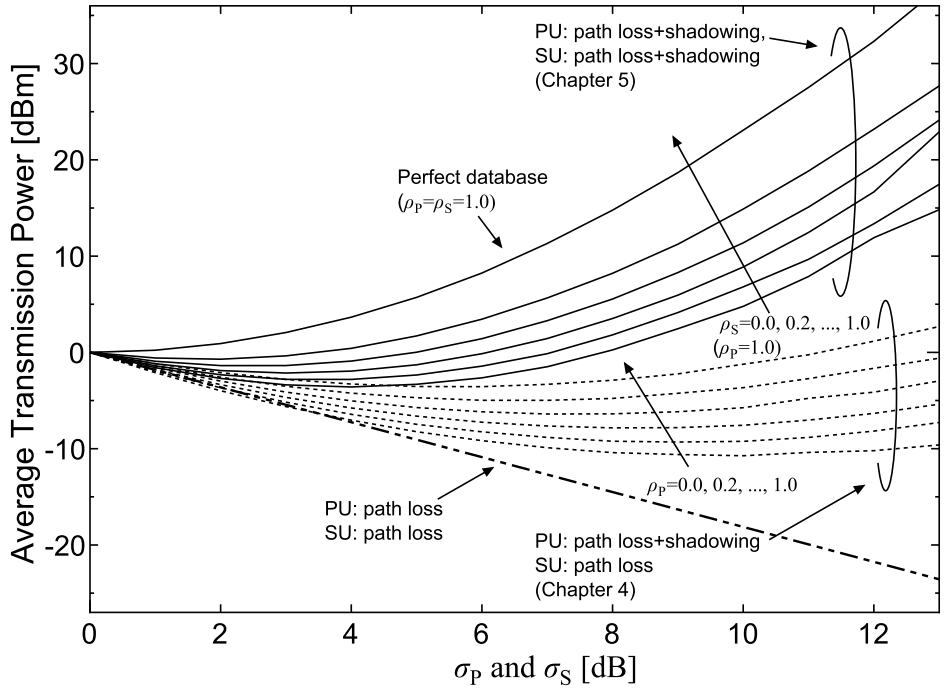

Fig. 2.7 Simulation results of average allowed transmission power at SU-Tx where $p_{\text{out}} = 0.10$, $\Gamma_{\text{d}} = 10$ [dB], $L_{\text{S}} = 100.0$ [dB], and $\overline{P}_{\text{Rx}} = -90.0$ [dBm].

Chapter 3

Experimental Verification of Measurement-based Spectrum Database over TV Bands

We conducted a large-scale measurement campaign to evaluate the performance of the local database in the proposed architecture. We used five vehicles with spectrum sensors. A TV transmitter was treated as the primary system, and measured the signal power from the transmitter. Two one-week measurement campaigns were conducted, in October 2013 and in February 2014. The prior measurement datasets were stored in the spectrum database. On the other hand, the posterior measurement datasets were treated as instantaneous measurement data and were used for strict evaluation of the statistical estimation error characteristics.

3.1 Measurement Setup

3.1.1 Measurement Object and Measurement Area

Figure 3.1 shows the measurement area and the object of measurement. This figure describes a 40 [km]$\times$ 45 [km] square area. In this experiment, Kumagaya relay station was treated as the PU transmitter. This station is located in Kumagaya city, Saitama, Japan, which is a suburban area near metropolitan Tokyo. We mainly measured the signal of 13CH (center frequency of 473.14 MHz and bandwidth of 6 MHz). The signal is a vertical polarized signal with an equivalent isotropic radiated power (EIRP) at 31 W.

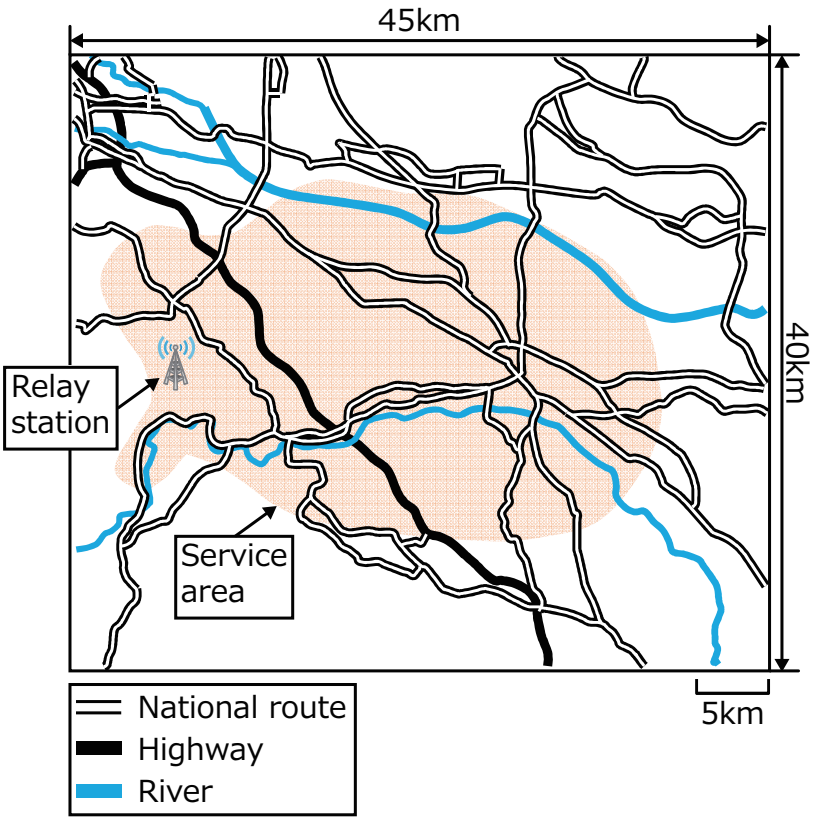

Fig. 3.1 Measurement area.

3.1.2 Experimental Structure

Figure 3.2 shows the sensing equipment used. The spectrum sensing function was implemented on a software-defined radio platform, Universal Software Radio Peripheral (USRP) N210, using GNU Radio software, and run on a laptop computer. The TV signal was sampled using a fast Fourier transform (FFT) with a 200-kHz sampling rate; the number of samples M was set to 2,048. Five vehicles measured the signal while driving on roads. The observation results were stored on the laptop, together with location information collected using a Garmin GPS18xUSB GPS unit. To allow data collection in a short time, we had two sensing devices in each vehicle, as shown in Fig. 3.3. We used five vehicles in total; thus, ten measurement units were utilized. Each USRP has individual (linear) differences in measurement values. Therefore, we had to offset the difference by employing tone signals in the TV band, provided by a signal generator (Rohde-Schwarz, SMU200A).

Here, the measurement parameters dictate that the measurement system probes only a 200-kHz wide band within the (total) 6-MHz bandwidth. Therefore, we need to understand the relationship between the measured signal power and the full-band signal power to allow calibration. To investigate this relationship, we measured the signal based on Integrated

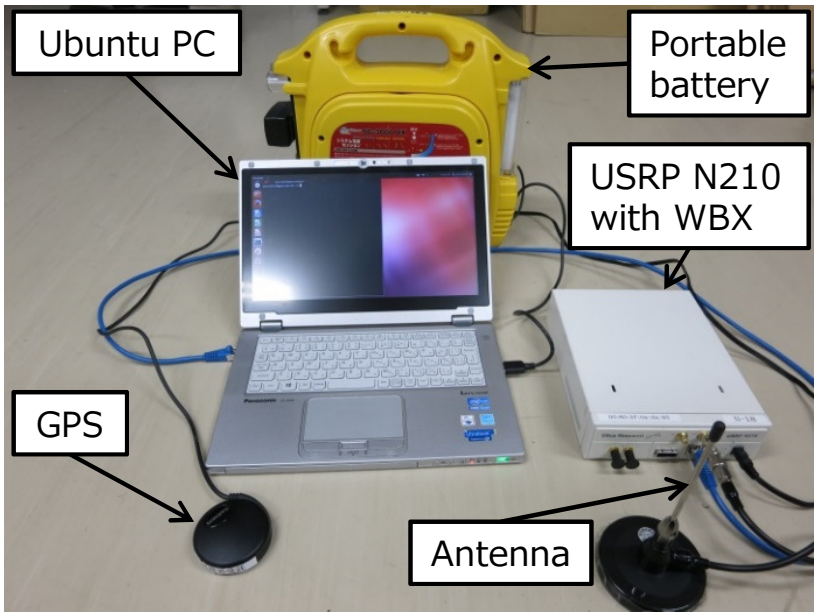

Fig. 3.2 Measurement equipment.

Services Digital Broadcasting-Terrestrial (ISDB-T). Figure 3.4 presents the experimental system. The ISDB-T signals in 13CH were generated by the signal generator. After the signals were attenuated, the USRP measured the signal with the parameters presented above. The measurement result is shown in Fig. 3.5. In this figure, input power is defined as $P_{\mathrm{Tx}} - \Gamma$ [dBm], where P_{Tx} is the transmission power of the signal generator in full band [dBm], and Γ is the attenuated value at the output of the attenuator [dB]. The measurement value shows the received signal power averaged over a sufficiently large set of FFT signals. In the linear region, the difference between the full band signal and the measured signal is roughly -16.7 dB. Because of the 2.0-dB attenuation due to the two SMA cables, the measurement signal power is 14.7 dB lower than that of the full-band signal power. Because the ratio of the bandwidth between full band and limited band is $10\log\{(6.0\times10^6)/(2.0\times10^3)\} \simeq 14.77$ [dB], the experimental result is considered to have the proper attenuation ratio.

3.1.3 Spectrum Database Construction

For statistical processing of the measurement dataset, we prepared a MySQL database server at our university. The database server has two tables: a raw data table and a statistical data table. The raw data table stores the large measurement dataset with no changes. Each measurement datum is associated with measurement parameters: location, frequency, power, and so on. The statistical data table has the average received signal power for each spatial grid cell containing raw data. In addition, the database uses statistical processing functions

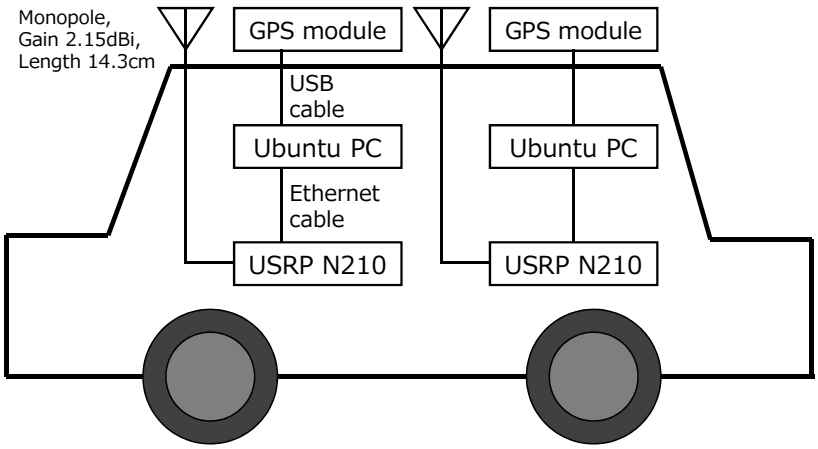

Fig. 3.3 Experimental configuration in a vehicle.

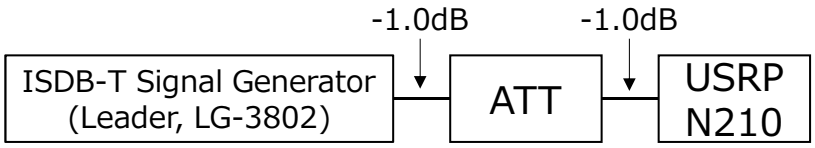

Fig. 3.4 Calibration equipment for investing the difference between the band-limited measurement power and the full band signal power.

that generate the statistical data table from the raw data table. These functions produce spatially-distributed average received signal information when the appropriate queries are made.

After the field test, all measurement data were recorded on the MySQL database server. To estimate the spatially-distributed average received signal information, the prior measurement datasets were averaged over spatial grids with a 10-m side length.

3.2 Measurement Results

Figure 3.6 shows an average received signal map at 473.14 MHz. This map consists of datasets measured in a prior measurement campaign and stored in the MySQL database server. The strong trend of path loss increasing with increased distance from the transmitter is clearly visible. The map also indicates that some regions have a received power value significantly different from the received power value measured in adjacent cells. Because of time variation factors, which include AWGN, are averaged out using long-term measurement, these variations are attributed to shadowing effects.

In this section, we evaluate the estimation error performance of the constructed spectrum database. The generated map is an instance of the proposed spectrum database. The dataset

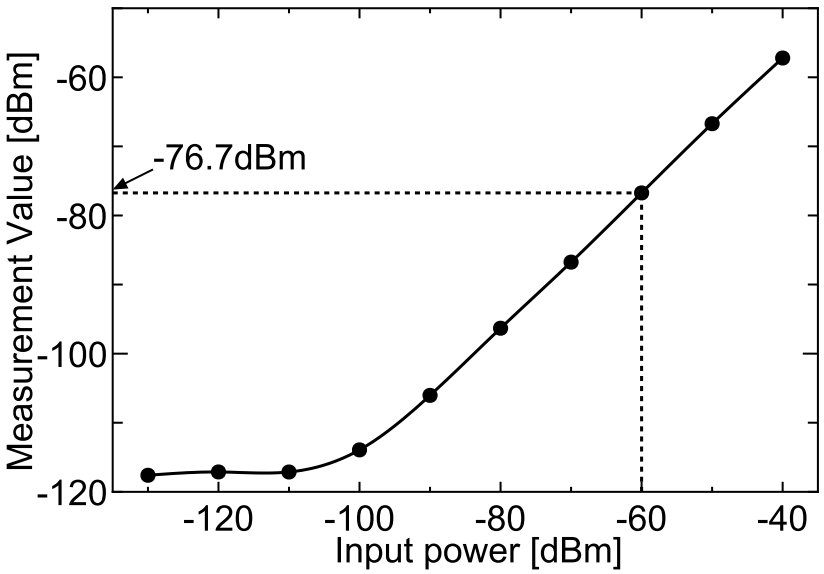

Fig. 3.5 Measurement power of USRP N210: Measurement of 6-MHz ISDB-T signal using FFT with 200-kHz sampling rate.

that is measured *a posteriori* is used to obtain the most probable value and is compared with both the map and a propagation model.

3.2.1 Comparison with a Propagation Model

To clarify the probabilistic error performances, we evaluated the CDF of the radio environment estimation error. As a comparison method, we used Notice 640, which is a propagation model for Japanese TV broadcast systems. This propagation model is defined by the Japanese spectrum regulator, MIC; it is virtually identical to the propagation model defined by the FCC. Japanese TV broadcast operators often use this model to estimate the communication areas of TV transmitters because MIC licenses the use of TV spectrums based on the estimation results for Notice 640. According to MIC, the propagation curve considers multipathing and diffraction due to terrain; however, the theoretical rationale is unclear. To estimate the radio environment based on Notice 640, we used a radio propagation simulator called *area kakube* [75]. This software was made for Japanese TV broadcast operators. Notice 640 based electrical field strength can be calculated using stored Japanese terrain information. Note that the measurement signal power is attenuated because of the band limit on the measurement. Therefore, we subtracted 14.7 dB from the calculation results taken from *area kakube*.

Figure 3.7 shows a statistical comparison of residual-error performance. The first curve indicates the CDF of differences between average values in the constructed radio environment map and the dataset of instantaneous received signals, which are collected in the second

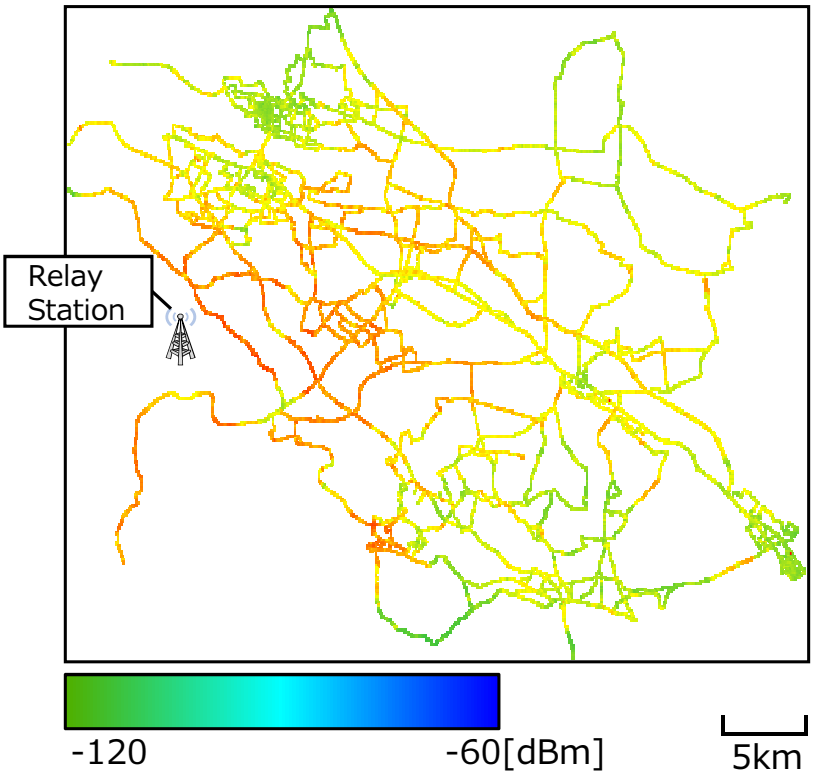

Fig. 3.6 Generated radio environment map at 473.14 MHz.

measurement campaign. The second curve shows the residual error performance of Notice 640. This figure confirms that the curve of the proposed database rises rapidly from −10 dB. On the other hand, the curve of Notice 640 rises slowly from −80dB to +80dB. Note that the root mean squared errors (RMSEs) of these methods are 4.27dB in the proposed database and 26.7dB in Notice 640, respectively. In the proposed method, the influence of instantaneous fluctuation is removed with the averaging process. This means that the influence of multipath fading eventually remains as an error term even if the number of dataset is increased. For example, in Rayleigh fading environment, the limit of the estimation of received signal power can be derived as

$$RMSE = \lim_{N\to\infty} \sqrt{\frac{1}{N}\sum_{i=1}^{N}(10\log_{10}x_i)^2} \approx 6.13 \ \ [\mathrm{dB}], \tag{3.1}$$

where N is the number of compared instantaneous received signal power and x_i is the channel gain that follows the exponential distribution with mean 1.0. In the evaluation described in Fig. 3.7, because the true value was obtained via the FFT-based analysis, the limit of accuracy

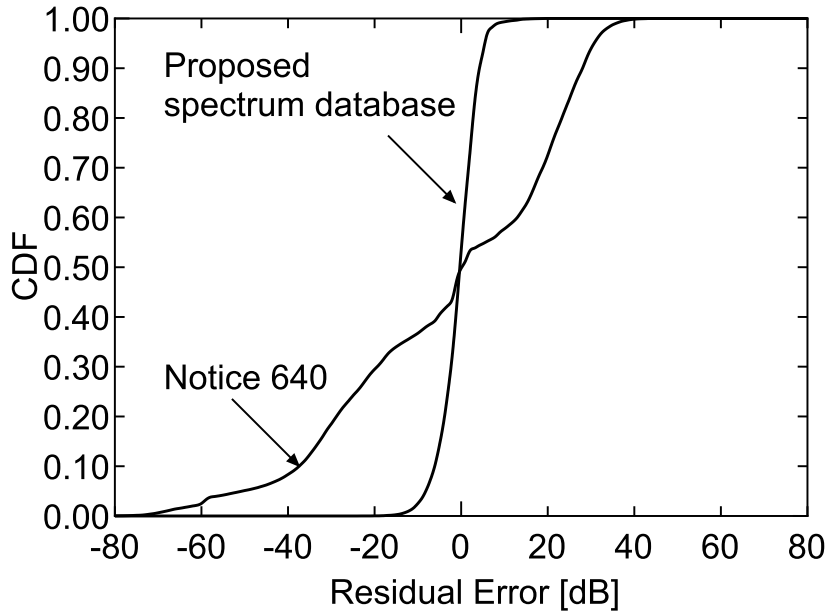

Fig. 3.7 CDF of estimation error: Comparison with a propagation model, Notice 640.

in this experiment will be lower than Eq.(3.1). These facts explain that the estimation accuracy of the proposed database is close to the limit.

Here, we show the CDF of the absolute error to confirm the residual error level, as shown in Fig. 3.8. In the 90th percentile, the proposed database has a residual error of roughly 7.0 dB, and the propagation model has a residual error of roughly 37.0 dB. This figure shows the poor accuracy of the propagation model. On the other hand, the proposed database is shown to achieve high estimation accuracy.

3.2.2 Comparison between First and Second Measurement Results

Because the changes of building structure affect the radio propagation characteristics, it is important to discuss the update frequency of the constructed spectrum database.

Figure 3.10 shows a comparison between averaged received signal powers obtained in first and second measurement campaigns. Although three months have passed, The results have a high, roughly 0.94, correlation. Therefore, in such a suburban area, the constructed database will be able to perform a highly accurate radio propagation estimation without any updates for several months.

On the other hand, the accuracy of the constructed database may be extremely deteriorated if there is an extreme change in structure environment. To deal with such a problem, the following process can be considered as a countermeasure.

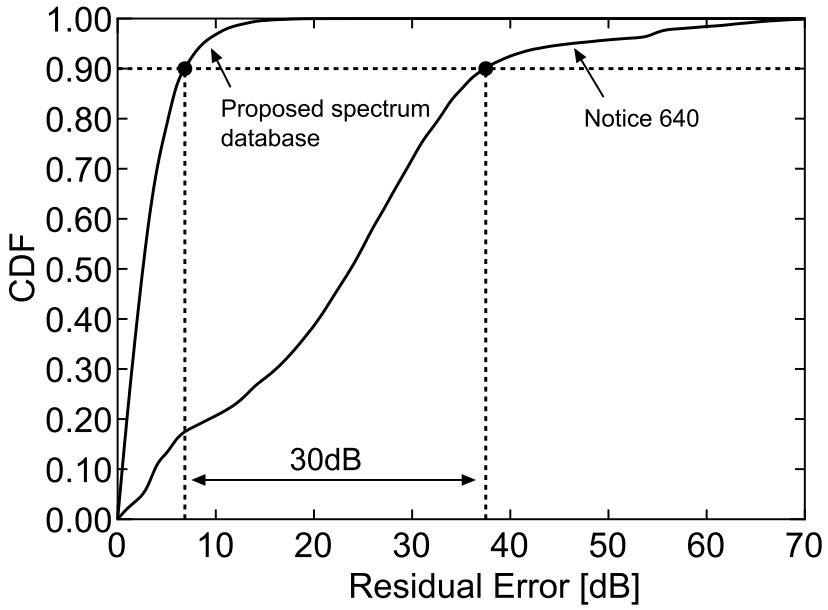

Fig. 3.8 CDF of absolute estimation error.

Fig. 3.9 Comparison between first and second measurement results where the mesh size is 10m.

1. The database compares the most recent dataset in the mesh with the probability distribution of the past data set.

2. If a significant difference can be obtained, the database updates the average received signal power by averaging only the recent dataset or by taking the weighted average with forgetting factor.

3.2.3 Impact of the Database on Reduction of the Excess Interference Margin

When SUs share a spectrum, they must set an interference margin after due consideration of the probabilistic error performances based on the radio environment estimation. If SUs estimate the radio environment with a low-precision method, SUs need to set exceed margin. This means that SUs lose opportunities for spectrum sharing so as to protect primary communications. Thus, the estimation error in cumulative probability indicates the extent to which SUs determine the interference margin directly. For example, considering the guarantee of SIR in PU-Rx as discussed in Chapt. 2, SU-Tx should satisfy the condition $\Pr[(P_{\mathrm{Rx}} - I_{\mathrm{Rx}}) \geq \Gamma_{\mathrm{d}}] \geq 1 - p_{\mathrm{out}}$. Here, when the database estimates P_{Rx}, the estimated value

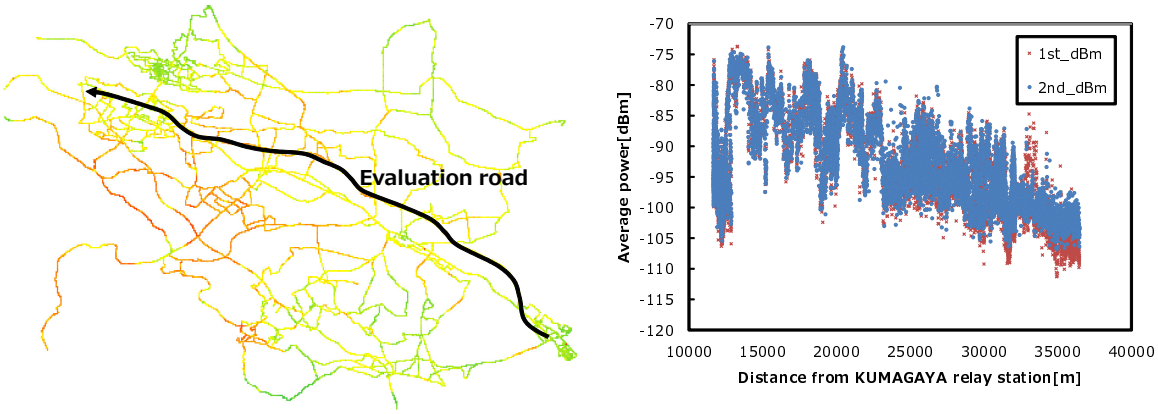

(a) Evaluation road. (b) Comparison result.

Fig. 3.10 Comparison between first and second measurement results where the mesh size is 10m.

can be expressed as $\hat{P}_{\mathrm{Rx}} = P_{\mathrm{Rx}} + \epsilon_{\mathrm{P}}$, where ϵ_{P} [dB] is the error factor. Therefore, if I_{Rx} and P_{Rx} are given, the above condition can be re-written as

$$\Pr\left[I_{\mathrm{Rx}} + \Gamma_{\mathrm{d}} - \hat{P}_{\mathrm{Rx}} \leq \epsilon_{\mathrm{P}}\right] \leq 1 - p_{\mathrm{out}}. \tag{3.2}$$

This equation explains that the CDF of estimation factor can express the required interference margin directly. This section evaluates the extent to which the proposed spectrum database can improve the error performance in terms of cumulative probability. Figure 3.11 presents the upside cumulative probability performance and downside cumulative probability performance; the former shows underestimation characteristics, and the latter shows overestimation characteristics. Each value is plotted with reference to Fig. 3.7. In the evaluation results, the proposed database achieves more than 20 dB performance improvement, for both the upside performance and the downside performance. The improvement in the estimation error is shown in Fig. 3.12; this figure shows the difference between the proposed spectrum database and Notice 640. This figure clarifies that the proposed spectrum database can mitigate the excess interference margin by more than 20 dB.

3.3 Chapter Summary

In this chapter, to evaluate the estimation error characteristics of the local layer in the measurement-based spectrum database, the field experiment for radio environment probing over TV bands was presented. From the spectrum database construction results, we confirmed

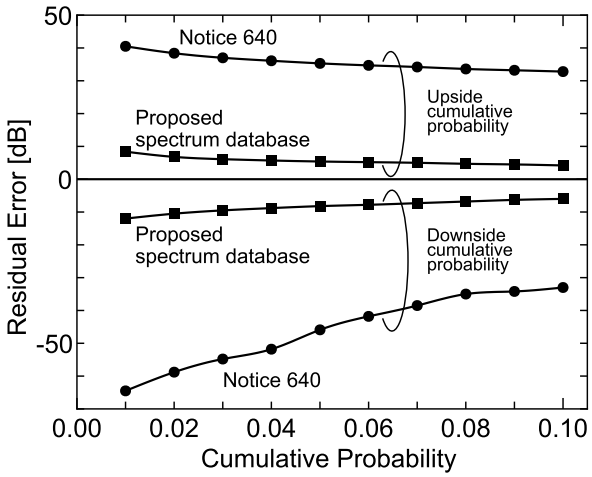

Fig. 3.11 Comparison of the residual error in cumulative probability.

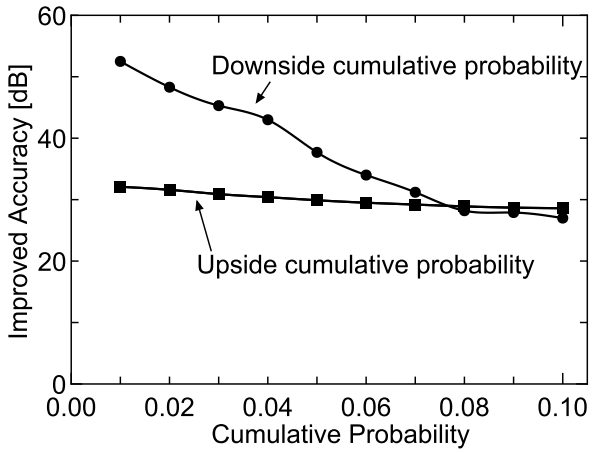

Fig. 3.12 Impact of the proposed spectrum database on the improvement of estimation error.

that the proposed database dramatically reduces the estimation error of the radio environment information. In addition, we showed that the proposed database can reduce the interference margin.

Chapter 4

Transmission Power Control based on Spectrum Database

Chapter 3 has shown that the local database in the proposed database architecture can achieve the highly accurate radio propagation estimation. On the other hand, some important questions may arise here:

- There are many locations where the SUs cannot enter: the generated local database has tooth missing information. Therefore, after the reported signals are averaged, we need to interpolate the tooth missing information.
- We need to discuss how the higher-layer database should perform, that is, how the communication parameters of the SUs should be determined towards the efficient spectrum sharing.

In this chapter, we consider these two problems together. In the spectrum sharing, the SUs must not cause a harmful interference power at the PUs. However, because a low-accurate spectrum database tends to overestimate the communication opportunity at the SUs, it is important to design their communication parameters considering the accuracy of the database.

This chapter particularly discusses how the higher-layer database should design the transmission power of the SUs so that the interference power at the PU belows a given threshold.

4.1 Background

The interference power constraint between transmitters is a critical issue for spatial spectrum sharing. A typical situation that requires strict interference management is spectrum sharing

over TVWS. In a spectrum sharing environment, SUs must not interfere with the PUs. On the other hand, an excess interference margin decreases the spectrum sharing opportunity; therefore, it is important to manage the interference power properly [36]. Additionally, HetNets need to efficiently manage inter-cell interference [76]. A suitable interference management method enables transmitters to reuse the frequency efficiently and the UE can select the optimum base station.

There has been a wide range of discussion concerning the interference power constraint in the spectrum sharing environment. The channel capacity of spectrum sharing where a primary link and a secondary link share the same spectrum is discussed in [29, 33, 77]. Based on the theoretical analyses, several researchers have discussed the power control of multiple SUs. References [78] and [79] discuss the power control method where the information of SU-to-PU channels is limited to signal distribution. It is also assumed that the SUs know the allowable interference power of each primary receiver, and each SU determines its own transmission power based on the allowable interference power and the distribution of the aggregate interference. However, these studies hardly give adequate accounts for the estimation of the *maximum* allowable interference power for the PU. Although the maximum allowable interference power strongly depends on the channel state in the primary link and the desired QoS, these works assume that the PU determines a constant allowable interference power. From the theoretical perspective, the allowable interference power needed to achieve the desired QoS can be reduced if the primary link has a good channel state, and the SUs can increase its own transmission power in this instance [36]. On the other hand, the transmission power with a constant allowable interference power is limited to a constant value. These facts motivate us to discuss the estimation of the *maximum* allowable interference power in the spectrum sharing environment.

The REM is a tool for managing inter-transmitter interference. The REM stores the spatial distribution of the average signal power received which is estimated by a path-loss model or by a measurement dataset. For example, in TVWS systems, SUs usually estimate white spaces and the allowable interference power based on the REM stored in a spectrum database [67][68]. Using the REM, we can improve the efficiency of spectrum sharing [80][81]. Because the estimation accuracy of the REM directly affects the spectral efficiency, several researchers focus on building an accurate REM construction [5][72]. This has led to the creation of various techniques for spectrum cartography. In particular, it is well known that the measurement-based REM using Kriging interpolation, a geostatistical technique [82], can achieve a highly accurate estimation [72][83][84]. In [72], the authors have measured the field strength of radio waves over TV bands to improve the accuracy for spectrum databases. Statistical results have demonstrated that several propagation models perform a

biased estimation with a wide error variance. It is also shown that measurements with the Kriging interpolation dramatically improve this estimation error.

However, although many researchers have maintained a continuous interest in improving the accuracy of the measurement-based methods, sufficient study has not been done to actually explore the transmitter parameter adaption methods based on the estimation results. The estimation error is inseparable from the estimation methods, even if a measurement-based method is utilized. The error depends upon the measurement methods such as the quantity of the measurement data and the statistical conversion method. Therefore, we need to consider the error characteristics when designing the transmission parameters. In [85], the authors propose a REM-based downlink power allocation algorithm using Kriging interpolation and compressive sensing. The proposed method determines the allowable transmission power for the SU according to the constructed REM. However, because the estimated transmission power ignores the estimation error of the REM, the interference property highly depends on the number of measurement sensors. Reference [86] developed a distributed Kriging-based spectrum cartography. In this method, distributed cognitive radio terminals preliminarily collect radio environment information by exchanging training symbols with each other. The time-varying shadowing is then tracked by utilizing Kriged Kalman filtering. The method was applied to a cognitive radio resource allocation by considering a maximum interference free power level [87] as the spectrum sharing criterion. However, the proposed resource allocation also does not consider any estimation errors of the REM construction. Because the authors have only provided an estimated map and an interference map to discuss the spectrum sharing efficiency, whether or not the probabilistic interference constraint can be achieved still remains unclear.

In this chapter, we propose a probabilistic interference power constraint method using Kriging-based REM with the error distribution prediction. Kriging interpolation optimizes the interpolation value by minimizing the error variance. The estimation error approximately follows a log-normal distribution within a correlated shadowing environment; therefore, the error distribution can be predicted using the minimized variance called the *Kriging variance*. The proposed method estimates the maximum allowable interference power at the PU using predicted error distribution. A suitable transmission power for the interference sources is then designed by combining the allowable interference power with the interference channel distribution. We compare the performance of the proposed scheme with three methods: the perfect estimation, the path loss-based method, and Kriging-based method without the error prediction. Comparison results show that the proposed method achieves a higher transmission power for the interference source than the path loss-based method, even if only a small amount of measurement data is available. It is also shown that the proposed method

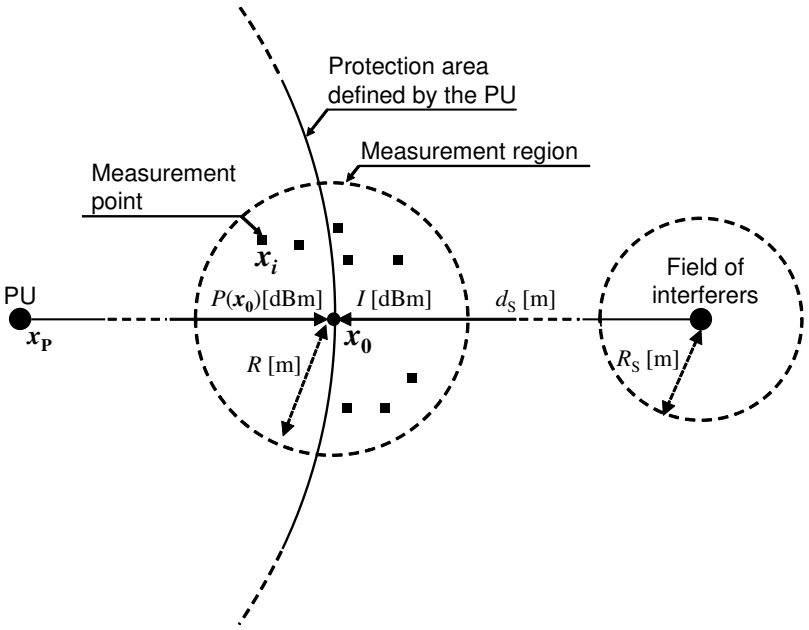

Fig. 4.1 Spectrum sharing model.

dramatically improves the primary protection performance compared with the conventional Kriging-based method.

4.2 System Model

Figure 4.1 shows the spectrum sharing environment under consideration. Here, we consider a situation where a cluster of SUs spatially share a spectrum with a fixed PU. The SUs can connect to the spectrum database that stores the radio environment information, and the spectrum database reads the allowable transmission power to the SUs based on a measurement-based REM. The spectrum database only knows the number of SUs but has no knowledge of the detailed location of the SUs. In addition, it is also assumed that the primary transmitter preliminarily gives its own location and the communication protection area to the spectrum database. An example of this situation is spectrum sharing between a TV transmitter and Wi-Fi devices over TVWS. Note that the location of the primary transmitter can be obtained from the measurement datasets, even if the PU gives no information about the location. This can be achieved by utilizing received signal power-based localization methods such as [88].

We discuss the interference power constraint at the communication protection area defined by the PU. The SUs transmit the secondary signal while considering the aggregate interference power at the location $\boldsymbol{x}_0$, which is the closest edge of the protection area from the interference cluster.

4.2.1 Radio Propagation Model of Primary Signal

Let $\boldsymbol{x}_{\mathrm{P}}$ denote the location of the PU. We assume a received signal power in location $\boldsymbol{x}$ given by the following equation:

$$P(\boldsymbol{x}) = P_{\mathrm{Tx}} - L(\|\boldsymbol{x}_{\mathrm{P}} - \boldsymbol{x}\|) + W_{\mathrm{P}}(\boldsymbol{x}), \tag{4.1}$$

where P_{Tx} is the primary transmission power [dBm] and $W_{\mathrm{P}}(\boldsymbol{x})$ [dB] is the shadowing loss at $\boldsymbol{x}$. The shadowing loss $W_{\mathrm{P}}(\boldsymbol{x})$ follows a log-normal distribution with a standard deviation σ_{P} [dB]. $L(d)$ [dB] is defined as the propagation loss with distance d [m] between the PU and the receiver. We assume the propagation loss as,

$$L(d) = 10\eta_{\mathrm{P}}\log_{10}d, \tag{4.2}$$

where η_{P} is the path loss index. According to the experimental result discussed in Sect. 3.2, we do not consider effects of multipath fading on the measurement In this chapter, we assume a spatially correlated shadowing. When two the locations $\boldsymbol{x}_i$ and $\boldsymbol{x}_j$ are exposed to the shadowing values $W_{\mathrm{P}}(\boldsymbol{x}_i)$ and $W_{\mathrm{P}}(\boldsymbol{x}_j)$, the correlation coefficient $\rho_{i,j}$ can be expressed by the following equation:

$$\rho_{i,j} = \frac{\mathrm{E}[W_{\mathrm{P}}(\boldsymbol{x}_i)W_{\mathrm{P}}(\boldsymbol{x}_j)]}{\sigma_{\mathrm{P}}^2} \tag{4.3}$$

$$= \exp\left(-\frac{\|\boldsymbol{x}_i - \boldsymbol{x}_j\|}{d_{\mathrm{cor,P}}}\ln 2\right), \tag{4.4}$$

where $d_{\mathrm{cor,P}}$ is the correlation distance [m] which is defined as the distance satisfying $\rho_{i,j} = 0.50$. It is well known that the distance depends on the surrounding structures [89]. To simulate the correlated shadowing environment, the *Monte Carlo Method* [90] is used.

According to [72], we assume that small-scale fading and additive white Gaussian noise (AWGN) are eliminated owing to long-term measurement. In [72], the authors measured the field strength of the radio wave from TV transmitters to verify the improvement of the TVWS prediction. Samples were created repeatedly with the smallest possible resolution of the spectrum analyzer in order to average over the effects of small-scale fading and the noise floor of the device. They observed that the datasets with this setup follows the Gaussian process, and it was shown that ordinary Kriging can generate accurate REM.

4.2.2 Radio Environment Map Construction

The measurement environment is also shown in Fig. 4.1. The area consists of a circle with radius R [m] where the center point is located at $\boldsymbol{x}_0$. For the REM construction, N nodes measure signals from the PU within the circle. Here, the measurement locations $\{\boldsymbol{x}_i | i = 1, \cdots, N\}$ are selected randomly, and each node is measured in each location.

In this chapter, the REM is defined as a map that has two-dimensional information of the average received signal power. The task for the REM is to provide accurate $P(\boldsymbol{x})$. The REM is typically divided into a square grid in order to remove the effects of small-scale fading and to reduce the quantity of information [80]. However, if the REM consists of larger grids compared to the correlation distance $d_{\mathrm{cor,P}}$, the average received signal power $P(\boldsymbol{x})$ obviously fluctuates in the grid [91]. For simplicity, we assume that the grid is sufficiently small enough that the shadowing correlation in the grid can be regarded as $\rho_{i,j} \approx 1$. Using the measurement datasets $\boldsymbol{y} = (P(\boldsymbol{x}_1), P(\boldsymbol{x}_2), \cdots, P(\boldsymbol{x}_N))^{\mathrm{T}}$, the database interpolates $P(\boldsymbol{x}_0)$.

4.2.3 Interference Model

We consider that an interference cluster with M SUs is located d_{S} [m] away from $\boldsymbol{x}_0$. Each SU is randomly distributed in the circle with radius, R_{S} [m] according to the two-dimensional uniform distribution. In addition, we assume that each SU transmits with a given power P_{S} [dBm].

As with the primary signal, each interference power at $\boldsymbol{x}_0$ transmitted by a SU i is described by the path loss and the spatially correlated shadowing[1]:

$$I_{\mathrm{mW},i} = 10^{\frac{P_{\mathrm{S}}}{10}} d_{\mathrm{S},i}^{-\eta_{\mathrm{S}}} 10^{\frac{W_{\mathrm{S},i}}{10}} \quad [\mathrm{mW}], \tag{4.5}$$

where η_{S} is the path loss index $d_{\mathrm{S},i} \triangleq \|\boldsymbol{x}_0 - \boldsymbol{x}_{\mathrm{S},i}\|$ [m], and $W_{\mathrm{S},i}$ [dB] is the shadowing loss that fluctuates according to a log-normal distribution with standard deviation σ_{S} [dB] and correlation distance $d_{\mathrm{cor,S}}$ [m]. We assume that $W_{\mathrm{S},i}$ is statistically independent from $W_{\mathrm{P}}(\boldsymbol{x}_i)$.

[1] There is room for a consideration on whether or not it is better to assume such a generalized model rather than a site-specific model as the propagation model for the interference power. However, the distance between the transmitter and receiver will be on the order of several hundred meters to several kilometers because the PU-Rx located in the edge of the coverage only accepts a very low interference power. In such an environment, the interference signal is influenced by a myriad of structures. Therefore, the central limit theorem works for the propagation attenuation, and this interference model will make sense.

The total interference power at $\boldsymbol{x}_0$ is then given by,

$$\begin{aligned} I_{\mathrm{mW}} &= \sum_{i=1}^{M} I_{\mathrm{mW},i} \quad [\mathrm{mW}], \\ I &= 10\log_{10} I_{\mathrm{mW}} \quad [\mathrm{dBm}] \\ &= P_{\mathrm{S}} + 10\log_{10} \sum_{i=1}^{M} d_{\mathrm{S},i}^{-\eta_{\mathrm{S}}} 10^{\frac{W_{\mathrm{S},i}}{10}}. \end{aligned} \tag{4.6}$$

The main focus of this chapter is the attainment of the protection criterion based on the measurement-based REM. Therefore, we assume that the spectrum database can estimate σ_{S}, η_{S}, $d_{\mathrm{cor,S}}$, and M perfectly. These values can be obtained by utilizing an empirical formula [92] or measurement-based parameter estimation [93][94].

4.2.4 Spectrum Sharing Criterion

We utilize the SIR as the protection criterion for the primary communication. Here, the SIR at $\boldsymbol{x}_0$ can be written as,

$$\Gamma(\boldsymbol{x}_0) = P(\boldsymbol{x}_0) - I \ \ [\mathrm{dB}]. \tag{4.7}$$

If the PU determines the desired SIR as Γ_{d} [dB], the outage event can be formulated as $\Gamma_{\mathrm{d}} > \Gamma(\boldsymbol{x}_0)$. Thus, considering the desired protection probability $1 - p_{\mathrm{out}}$, the SU must satisfy the protection probability at $\boldsymbol{x}_0$, given by the following equation,

$$\Pr[\Gamma(\boldsymbol{x}_0) \geq \Gamma_{\mathrm{d}}] \geq 1 - p_{\mathrm{out}}. \tag{4.8}$$

Using the generated REM and channel information of the SUs, the spectrum database estimates the maximum median value of the interference signal max $P_{\mathrm{S}} \triangleq P_{\mathrm{S,max}}$ [dBm] that is subject to Eq. (4.8).

4.3 Kriging Interpolation

We estimate $P_{\mathrm{S,max}}$ according to the Kriging-based REM. Kriging interpolation is a minimum mean squared error method of spatial prediction that depends upon the second order properties of the process [82]. The goal is to estimate the unknown value at an arbitrary location $\boldsymbol{x}_0$ from the measurement datasets. This is achieved by assigning a weight factor ω_i $(i = 1, \cdots, N)$

to each value measured by the N nodes, as follows:

$$\hat{P}(\boldsymbol{x}_0) = \sum_{i=1}^{N} \omega_i P(\boldsymbol{x}_i), \tag{4.9}$$

where $\hat{P}(\boldsymbol{x}_0)$ is the interpolated value; the true value is $P(\boldsymbol{x}_0)$. Further, to achieve the best linear unbiased estimator (BLUE), the Kriging methods set a constraint,

$$\sum_{i=1}^{N} \omega_i = 1. \tag{4.10}$$

Kriging methods are subdivided on the basis of the decision rule of ω_i, but all the methods preliminarily estimate the spatial-covariance structure of the random process from the datasets. In this chapter, the residual maximum likelihood (REML) method [95] is utilized for estimating the spatial-covariance structure. Additionally, to determine ω_i, we apply ordinary Kriging that does not require a knowledge of the mean average of the field.

4.3.1 Residual Maximum Likelihood Method

This method assumes that the measurement vector $\boldsymbol{y}$ follows a Gaussian process described as $\boldsymbol{y} \sim N(\boldsymbol{X\beta}, \boldsymbol{M})$. In the channel model defined in Eq. (4.1), $\boldsymbol{X}$ and $\boldsymbol{\beta}$ can be defined as follows:

$$\boldsymbol{X} = \begin{pmatrix} 1 & -10\log_{10}(d_1) \\ 1 & -10\log_{10}(d_2) \\ \vdots & \vdots \\ 1 & -10\log_{10}(d_N) \end{pmatrix}, \boldsymbol{\beta} = \begin{pmatrix} P_{\mathrm{Tx}} \\ \eta_{\mathrm{P}} \end{pmatrix}. \tag{4.11}$$

$\boldsymbol{M}$ is the variance-covariance matrix defined as $\boldsymbol{M} = \alpha_n^2 \boldsymbol{I} + \alpha_s^2 \boldsymbol{H}(\alpha_r)$; its elements consist of several covariance functions. α_n^2, α_s^2, α_r, the parameters of the covariance function, are called *nugget*, *sill*, *range*, and the parameter vector $\boldsymbol{\theta}$ consists of these parameters. $\boldsymbol{I}$ is the $N \times N$ identity matrix, and $\boldsymbol{H}(\alpha_r)$ is a $N \times N$ correlation matrix that follows a theoretical correlation function. From the assumption in Eq. (4.4), each correlation can be written as,

$$H_{i,j} = \exp\left(-\frac{\|d_{i,j}\|}{\alpha_r}\right). \tag{4.12}$$

Then, the log-likelihood function of the measurement datasets can be formulated as,

$$l(\boldsymbol{y}|\boldsymbol{\beta},\boldsymbol{\theta}) = -\frac{N}{2}\ln 2\pi - \frac{1}{2}\ln|\boldsymbol{M}| - \frac{1}{2}(\boldsymbol{y}-\boldsymbol{X}\boldsymbol{\beta})^{\mathrm{T}}\boldsymbol{M}^{-1}(\boldsymbol{y}-\boldsymbol{X}\boldsymbol{\beta}). \tag{4.13}$$

Although ML estimation can be achieved by maximizing Eq. (4.13), the estimators are biased as a consequence of the loss in the degree of freedom from estimating $\boldsymbol{\beta}$ [95]. This bias is substantial even for moderately sized datasets if either the spatial correlation is strong or q, the dimensionality of $\boldsymbol{\beta}$, is large.

The bias can be reduced by employing a variant of the maximum likelihood estimation known as the REML estimation. The REML method linearly transforms Eq. (4.13) in order to remove the dependence property between $\boldsymbol{\theta}$ and $\boldsymbol{\beta}$. Namely, the log-likelihood function associated with $N-q$ linearly independent linear combinations of the observations, rather than the log-likelihood function associated with the observations, is maximized. Because only $\boldsymbol{\theta}$ is estimated, the bias due to estimating $\boldsymbol{\beta}$ can be mitigated.

In this method, $\boldsymbol{y}$ is multiplied by an idempotent matrix $\boldsymbol{M}_{\boldsymbol{X}} = [\boldsymbol{I} - \boldsymbol{X}(\boldsymbol{X}^{\mathrm{T}}\boldsymbol{X})^{-1}\boldsymbol{X}^{\mathrm{T}}]$. This procedure removes $\boldsymbol{\beta}$ from Eq. (4.13) and generates the residual error vector. Then, the log-likelihood function of the residual error can be written as,

$$l_R(\boldsymbol{y}|\boldsymbol{\theta}) = const. - \frac{1}{2}\ln|\boldsymbol{M}| - \frac{1}{2}\ln|\boldsymbol{X}^{\mathrm{T}}\boldsymbol{M}^{-1}\boldsymbol{X}| - \frac{1}{2}\boldsymbol{y}^{\mathrm{T}}\boldsymbol{P}(\boldsymbol{\theta})\boldsymbol{y}, \tag{4.14}$$

where

$$\boldsymbol{P}(\boldsymbol{\theta}) = \boldsymbol{M}^{-1} - \boldsymbol{M}^{-1}\boldsymbol{X}[\boldsymbol{X}^{\mathrm{T}}\boldsymbol{M}^{-1}\boldsymbol{X}]^{-1}\boldsymbol{X}^{\mathrm{T}}\boldsymbol{M}^{-1}. \tag{4.15}$$

The maximization of Eq. (4.14) can determine $\boldsymbol{\theta}$.

Note that the method can easily be extended to a more complex path loss model. Several researchers have proposed complex path loss models that have more than one parameter for more accurate path loss estimation [92]. However, we can apply REML for such models because most of the path loss models can be written as the vector $\boldsymbol{X}\boldsymbol{\beta}$. For example, reference [96] proposes a path loss model that consists of four parameters:

$$L(d,\beta_0,\beta_1,\beta_2,\beta_3) = \beta_0 + \beta_1\log_{10}d + \beta_2 d + \beta_3\log_{10}h, \tag{4.16}$$

where h is the relative humidity percentage. In this case, $\boldsymbol{X}$ and $\boldsymbol{\beta}$ can be written as,

$$\boldsymbol{X} = \begin{pmatrix} 1 & -1 & -\log_{10}(d_1) & -d_1 & -\log_{10}h_1 \\ 1 & -1 & -\log_{10}(d_2) & -d_2 & -\log_{10}h_2 \\ \vdots & \vdots & \vdots & \vdots & \vdots \\ 1 & -1 & -\log_{10}(d_N) & -d_N & -\log_{10}h_N \end{pmatrix},$$
$$\boldsymbol{\beta} = \begin{pmatrix} P_{\mathrm{Tx}} \\ \beta_0 \\ \beta_1 \\ \beta_2 \\ \beta_3 \end{pmatrix}. \tag{4.17}$$

Using Eq. (4.17), REML can be applied to Eq. (4.16).

4.3.2 Ordinary Kriging

Ordinary Kriging assumes to be constrained in the local neighborhood of each estimation point, i.e. $\mathrm{E}[P(\boldsymbol{x})] = \mu$ for each nearby data value [97]. This method determines the weights that minimize the variance of the estimation error $\sigma_k^2 = \mathrm{E}[\{\hat{P}(\boldsymbol{x}_0) - P(\boldsymbol{x}_0)\}^2]$ under the condition Eq. (4.10). Using the method of the Lagrange multiplier, the objective function $\phi(\omega_i, \mu)$ can be written as,

$$\phi(\omega_i, \mu) = \sigma_k^2 - 2\mu\left(\sum_{i=1}^{N}\omega_i - 1\right), \tag{4.18}$$

where μ is the Lagrange multiplier. Here, σ_k^2 can be written as the following equation:

$$\sigma_k^2 = -\gamma(d_{0,0}) - \sum_{i=1}^{N}\sum_{j=1}^{N}\omega_i\omega_j\gamma(d_{i,j}) + 2\sum_{i=1}^{N}\omega_i\gamma(d_{i,0}), \tag{4.19}$$

where $d_{i,j} \triangleq \|\boldsymbol{x}_i - \boldsymbol{x}_j\|$. Note that $\gamma(d_{i,j})$ is a semivariogram. Because of the assumption of correlated shadowing expressed in Eq. (4.4), we assume an exponential semivariogram model:

$$\gamma(d_{i,j}) = \frac{1}{2}\mathrm{E}[\left(P(\boldsymbol{x}_i) - P(\boldsymbol{x}_j)\right)^2] \tag{4.20}$$
$$= \alpha_n^2 + \alpha_s^2\left\{1 - \exp\left(-\frac{d_{i,j}}{\alpha_r}\right)\right\}. \tag{4.21}$$

From the partial derivatives in Eq. (4.19), we can obtain $N+1$ simultaneous equations,

$$\begin{pmatrix} \gamma(d_{1,1}) & \cdots & \gamma(d_{1,N}) & 1 \\ \gamma(d_{2,1}) & \cdots & \gamma(d_{2,N}) & 1 \\ \vdots & \vdots & \vdots & \vdots \\ \gamma(d_{N,1}) & \cdots & \gamma(d_{N,N}) & 1 \\ 1 & \cdots & 1 & 0 \end{pmatrix} \begin{pmatrix} \omega_1 \\ \omega_2 \\ \vdots \\ \omega_N \\ \mu \end{pmatrix} = \begin{pmatrix} \gamma(d_{1,0}) \\ \gamma(d_{2,0}) \\ \vdots \\ \gamma(d_{N,0}) \\ 1 \end{pmatrix}. \tag{4.22}$$

From the above simultaneous equations, the weights that minimize σ_k^2 can be derived. Here, the minimized σ_k^2 is called the *Kriging variance*, and σ_k is called the *Kriging standard deviation*.

Note that the Kriging interpolation assumes that the semivariogram only depends on $d_{i,j}$. The spatial correlation and the standard deviation of the aggregate received signal power from multiple PUs fluctuate spatially; therefore, the number of PUs is implicitly limited to one.

Here, we evaluate the semivariogram in the real environment by using the experiment result obtained in Chapter 3. Figure 4.2a shows the evaluation area. The evaluation was performed at Area A, Area B, and the entire area surrounded by the red line. To obtain the semivariogram, the squared difference of all the pairs between average received powers within the mesh was calculated and plotted for each distance between samples. After the values were averaged every 5m, the averaged semivariograms were fitted to the theoretical semivariogram defined in Eq. (4.21) via the non-linear least squares. The calculated semivariograms are summarized in Fig.4.2b. The semivariogram well fits the exponential semivariogram in all areas, and we can confirm that the semivariogram can be derived as a function of the distance.

On the other hand, these fitted curves have difference each other because of the difference of surrounding obstacle structures. Since the accuracy of the semivariogram directly influences the accuracy of the spatial interpolation, it is preferable to model the semivariogram using only the dataset around the area to be interpolated each time when the interpolation is performed, rather than modeling in bulk for a wide area.

4.4 Kriging-based Interference Power Constraint

The ordinary Kriging can achieve the optimal interpolation of $P(\boldsymbol{x}_0)$. On the other hand, because the estimated value includes some estimation errors, the transmission power control of the SUs without consideration for the error will generate a harmful interference for the PU. The proposed method predicts the probabilistic distribution of the estimation error to

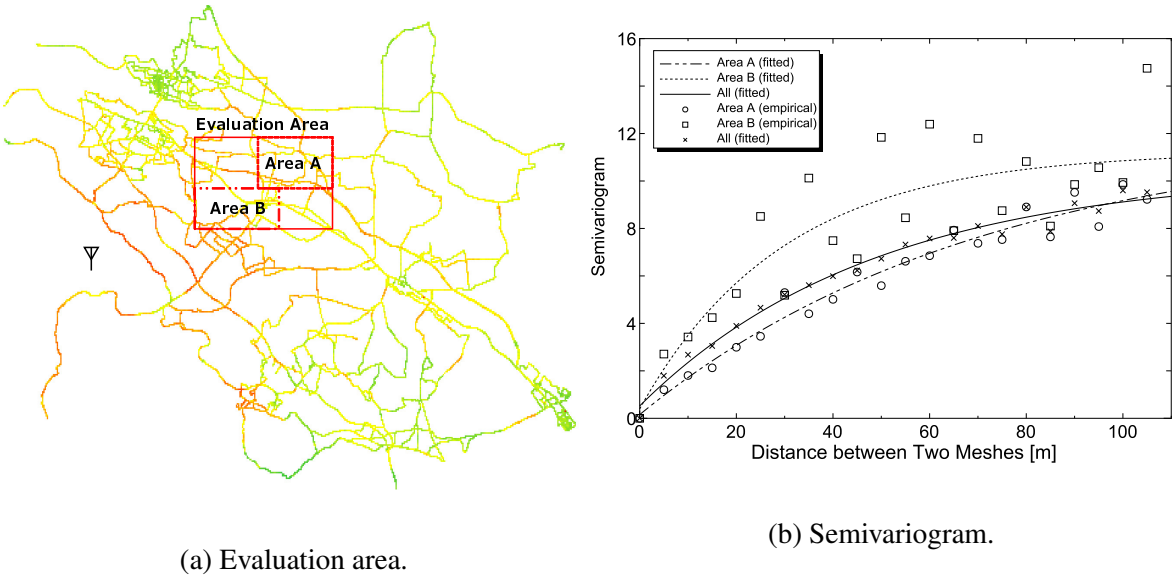

(a) Evaluation area.

(b) Semivariogram.

Fig. 4.2 Semivariogram in Kumagaya city where the mesh size is 10m.

determine the suitable transmission power for the SUs that satisfy the spectrum sharing criterion defined in Eq. (4.8).

4.4.1 Statistical Property of Estimation Error

In the ordinary Kriging method, the estimation error follows a Gaussian distribution if the samples spatially fluctuate with a Gaussian process [82]. This behavior can be applied to typical radio propagation because the variations in the radio signal follow a logarithmic Gaussian process. Figure 4.3 shows three examples of the estimation error distribution: $N = 10, 50, 90$. Each distribution indicates the estimation error $\epsilon \triangleq P(\boldsymbol{x}_0) - \hat{P}(\boldsymbol{x}_0)$ [dB]. The simulation parameters are described in Table 4.1.

Note that this chapter defines a trial of the evaluation in the following procedure.

1. The PU is deployed at $\boldsymbol{x}_\mathrm{P}$. Here, we determine the distance between $\boldsymbol{x}_\mathrm{P}$ and $\boldsymbol{x}_0$ so that $\overline{P}(\boldsymbol{x}_0)$ is equal to the simulation parameter. This is achieved by the following.

$$\|\boldsymbol{x}_\mathrm{P} - \boldsymbol{x}_0\| = 10^{\frac{P_\mathrm{Tx} - \overline{P}(\boldsymbol{x}_0)}{10\eta_\mathrm{P}}} \quad [\mathrm{m}]. \tag{4.23}$$

   In the simulation parameters, the distance is $\|\boldsymbol{x}_\mathrm{P} - \boldsymbol{x}_0\| \fallingdotseq 3727.6$ [m].

2. N terminals are randomly deployed in the measurement circle without $\boldsymbol{x}_0$. Each measurement location $\boldsymbol{x}_i$ is selected according to a two-dimensional uniform distribution.

Table 4.1 Simulation parameters.

Desired SIR Γ_{d} [dB]	20.0
Desired outage probability p_{out}	0.10
Transmission power P_{Tx} [dBm]	30.0
Correlation distance $d_{\mathrm{cor,P}}$ and $d_{\mathrm{cor,S}}$ [m]	20.0
Shadowing σ_{P} and σ_{S} [dB]	8.0
Path loss index η_{P} and η_{S}	3.5
Median $\overline{P}(\boldsymbol{x}_0)$ [dBm]	-95.0
Measurement radius R [m]	50, 100, 200
Number of SUs M	1,000
Radius of interference cluster R_{S} [m]	1,000
Distance d_{S} [m]	3,000
Number of trials	100,000

3. Each terminal measures the received signal power $P(\boldsymbol{x}_i)$ according to Eq. (4.1) and reports the value to the spectrum database.

4. $P(\boldsymbol{x}_0)$ is estimated with the ordinary Kriging. ϵ is then calculated.

5. The spectrum database estimates $P_{\mathrm{S,max}}$ based on the proposed method.

6. M SUs are deployed in the interference cluster and transmit interference signals.

7. The SIR at $\boldsymbol{x}_0$ is calculated.

The detailed procedure of estimating $P_{\mathrm{S,max}}$ is presented in 4.4.3.

In Fig. 4.3, each curve clearly plots the log-normal distribution, and the variance becomes narrow if the number of measurement points N are increased. Correlation and covariance between $\hat{P}(\boldsymbol{x}_0)$ and $P(\boldsymbol{x}_0)$ are summarized in Fig. 4.4. Because $\hat{P}(\boldsymbol{x}_0)$ and $P(\boldsymbol{x}_0)$ are highly correlated each other, we can model the PDF of $\hat{P}(\boldsymbol{x}_0)$ and $P(\boldsymbol{x}_0)$ as a bivariate log-normal distribution. In Sect. 2.3, we have shown that the measurement-based spectrum database can outperform the path loss-based spectrum database from the view point of the channel capacity if the correlation is more than 0.5. Because many numerical results in this figure take 0.5 or more, such an advantageous region can be achieved realistically.

Here, the variance can be predicted by considering the property of the Kriging interpolation. If the semivariogram can be estimated accurately, the minimized Kriging standard deviation σ_k is approximately equal to the standard deviation of the estimation error. Figure 4.5 indicates $\mathrm{E}[\sigma_k]$ and the standard deviation of ϵ. Note that $\mathrm{E}[\sigma_k]$ is the expectation of σ_k obtained from the Monte Carlo simulation. In this figure, as the number of measurement points N increases, the Kriging standard deviation converges to the standard deviation of the

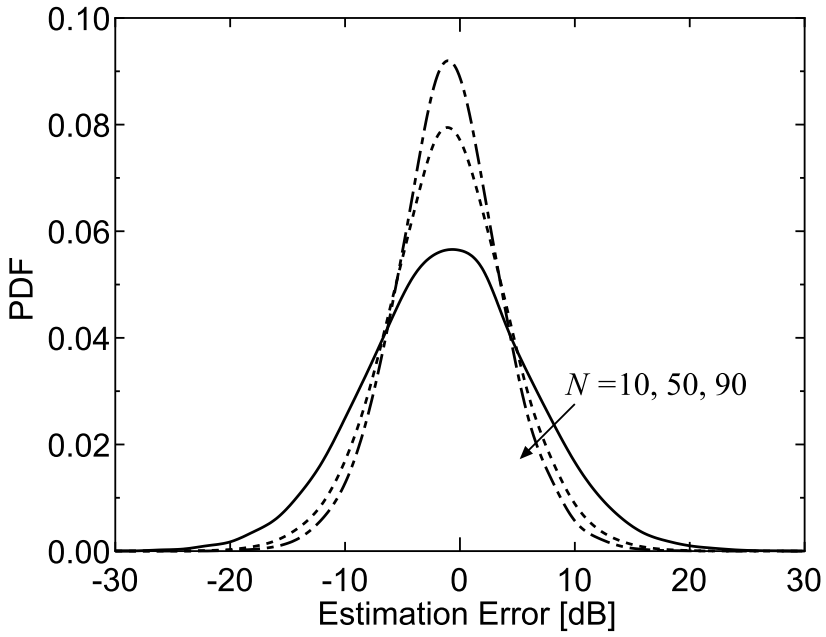

Fig. 4.3 PDF of the estimation error ϵ where $\sigma_{\mathrm{P}} = 8.0$, $\eta_{\mathrm{P}} = 3.5$, $P_{\mathrm{Tx}} = 30.0$ [dBm], $\overline{P}(\boldsymbol{x}_0) = -95.0$ [dBm], and $R = 100.0$ [m]. Each error follows a log-normal distribution.

estimation error. Therefore, if N is large enough, ϵ nearly follows a log-normal distribution with a median value of zero and a standard deviation of σ_k. These characteristics permit the prediction of the probabilistic distribution of the estimation error ϵ. Utilizing these behaviors, we can estimate the maximum allowed transmission power based on the predicted error characteristics.

Here, the reason the standard deviation of ϵ exceeds σ_k is that σ_k is the standard deviation of the estimation error under a perfect semivariogram estimation. The Kriging method initially applies a theoretical semivariogram model to the datasets; it is clear that this procedure has an estimation error. Thus, the upper bound of $\mathrm{E}[\sigma_k]$ is equal to the standard deviation of ϵ [82].

4.4.2 Statistical Property of Aggregate Interference

Next, we describe the statistical property of the aggregate interference I to estimate the allowable transmission power. In large scale wireless networks, it is too difficult to find the distribution of the aggregate interference in a closed form, and some researchers have discussed the approximation method. Reference [98] shows that the sum of many signals with correlated log-normal shadowing approximately follows log-normal distribution. In addition, a simple calculation method for moments of the distribution is proposed in [99]. According to [99], we approximate I as the log-normal distribution and calculate the moments.

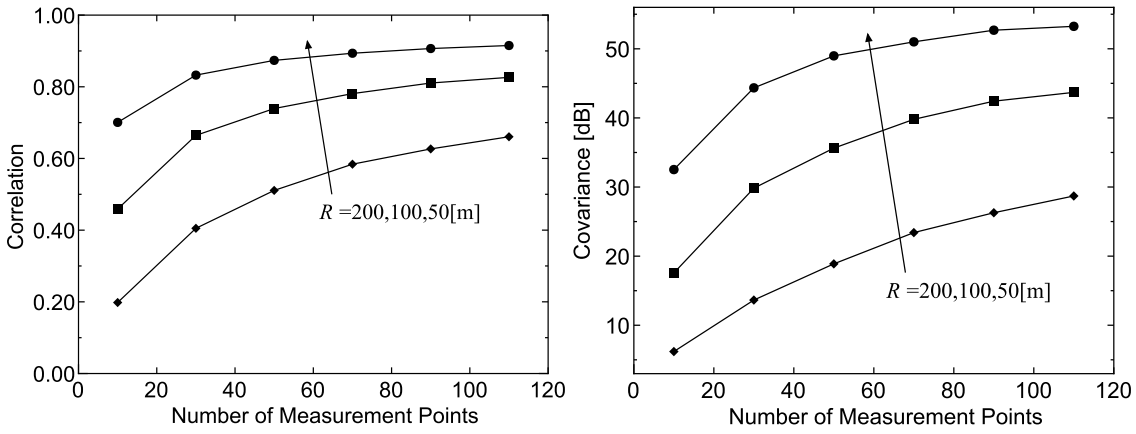

(a) Correlation.

(b) Covariance.

Fig. 4.4 Correlation and covariance between $\hat{P}(\boldsymbol{x}_0)$ and $P(\boldsymbol{x}_0)$ where $\sigma_{\mathrm{P}} = 8.0$, $\eta_{\mathrm{P}} = 3.5$, $P_{\mathrm{Tx}} = 30.0$ [dBm], $\overline{P}(\boldsymbol{x}_0) = -95.0$ [dBm], and $R = 100.0$ [m].

First, the logarithmic mean of the aggregate interference $\mathrm{E}[\ln I_{\mathrm{mW}}]$ and the variance $\mathrm{Var}[\ln I_{\mathrm{mW}}]$ can be written as

$$\mathrm{E}[\ln I_{\mathrm{mW}}] = \frac{3}{2}\ln M + (0.1\ln 10)P_{\mathrm{S}} - \eta_{\mathrm{S}}G_1 - \frac{1}{2}k, \tag{4.24}$$

$$\mathrm{Var}[\ln I_{\mathrm{mW}}] = (0.1\ln 10)^2\sigma_{\mathrm{S}}^2 - \ln M + \eta_{\mathrm{S}}^2(G_2 - G_1^2) + k, \tag{4.25}$$

where

$$k = \ln\left(1 + (M-1)e^{\left((0.1\ln 10)^2\sigma_{\mathrm{S}}^2(G_{\mathrm{cor}}-1) - \eta_{\mathrm{S}}^2(G_2-G_1^2)\right)}\right). \tag{4.26}$$

G_n and G_{cor} are to be found by numerical integration:

$$\begin{aligned} G_n &= \mathrm{E}[\ln^n d_{\mathrm{S},i}] \\ &= \iint_{\mathcal{A}_g} \ln^n(d_{\mathrm{S}})\mathrm{d}\boldsymbol{x}_{\mathrm{S}}, \end{aligned} \tag{4.27}$$

$$\begin{aligned} G_{\mathrm{cor}} &= \frac{\mathrm{E}[W_{\mathrm{S},i}W_{\mathrm{S},j}]}{\sigma_{\mathrm{S}}^2}(i \neq j) \\ &= \iint_{\mathcal{A}_g}\iint_{\mathcal{A}_g} h(\boldsymbol{x}_{\mathrm{S},i}, \boldsymbol{x}_{\mathrm{S},j})g(\boldsymbol{x}_{\mathrm{S},i})g(\boldsymbol{x}_{\mathrm{S},j})\mathrm{d}\boldsymbol{x}_{\mathrm{S},i}\mathrm{d}\boldsymbol{x}_{\mathrm{S},j}, \end{aligned} \tag{4.28}$$

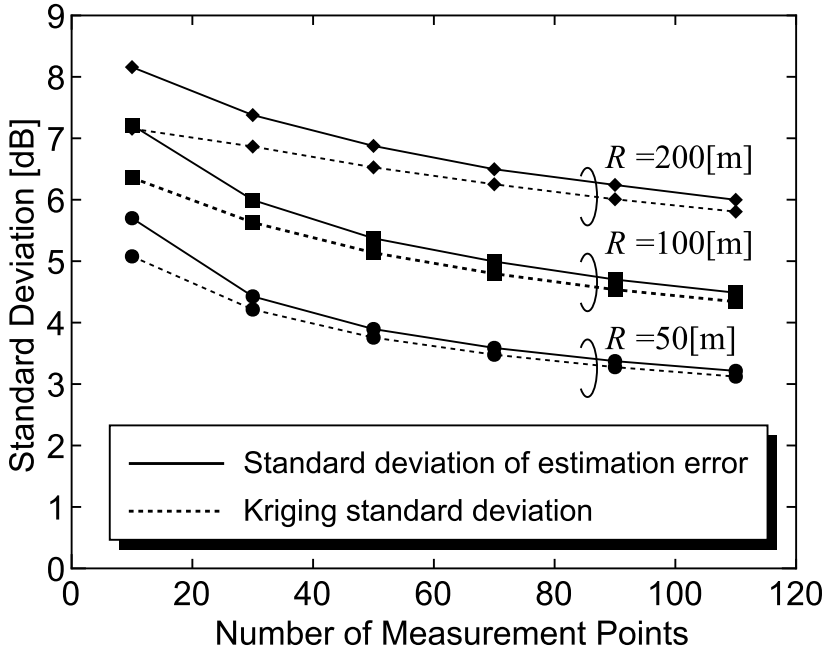

Fig. 4.5 Standard deviations where $\sigma_{\mathrm{P}} = 8.0$, $\eta_{\mathrm{P}} = 3.5$, $P_{\mathrm{Tx}} = 30.0$ [dBm], and $\overline{P}(\boldsymbol{x}_0) = -95.0$ [dBm]. As the number of measurement points N increases, the Kriging standard deviation converges to the standard deviation of the estimation error.

where $g(\boldsymbol{x}_{\mathrm{S},j})$ is the interferer density, $h(\boldsymbol{x}_{\mathrm{S},i}, \boldsymbol{x}_{\mathrm{S},j})$ is the shadowing correlation, and $\mathcal{A}_g$ is the area over which $g(\boldsymbol{x}_{\mathrm{S},j})$ is non-zero. Finally, the mean and the variance of I can be written as

$$\begin{aligned}
\mathrm{E}[I] &= \frac{\mathrm{E}[\ln I_{\mathrm{mW}}]}{0.1\ln 10} \\
&= P_{\mathrm{S}} + 15\log_{10} M - \frac{1}{0.1\ln 10}\left(\eta_{\mathrm{S}} G_1 + \frac{1}{2}k\right) \\
&\triangleq \overline{I}, \qquad (4.29) \\
\mathrm{Var}[I] &= \frac{\mathrm{Var}[\ln I_{\mathrm{mW}}]}{(0.1\ln 10)^2} \\
&\triangleq \sigma^2_{\mathrm{sum}}. \qquad (4.30)
\end{aligned}$$

4.4.3 Allowed Transmission Power

Using both distributions of the primary signal and the interference signal, we determine the allowable transmission power $P_{\mathrm{S,max}}$. First, we define $\overline{I}_{\max}$ [dBm] as the maximum allowable value of $\overline{I}$ that satisfies $\Pr[\Gamma(\boldsymbol{x}_0) \geq \Gamma_{\mathrm{d}}] = 1 - p_{\mathrm{out}}$. After $\overline{I}_{\max}$ is calculated, using Eq. (4.29),

$P_{\mathrm{S,max}}$ can be written as follows:

$$P_{\mathrm{S,max}} = \bar{I}_{\max} - \left(15\log_{10}M - \frac{1}{0.1\ln 10}\left(\eta_{\mathrm{S}}G_1 + \frac{1}{2}k\right)\right). \tag{4.31}$$

When the number of measurement points N is sufficiently large, the SIR at $\boldsymbol{x}_0$ can be formulated as $\Gamma(\boldsymbol{x}_0) = \left\{\hat{P}(\boldsymbol{x}_0) + \epsilon\right\} - I$ [dB]. Thus, the distribution of the SIR approximately follows a log-normal distribution with a median value $\hat{P}(\boldsymbol{x}_0) - \bar{I}$ and a standard deviation $\sqrt{\sigma_k^2 + \sigma_{\mathrm{sum}}^2}$. Using the cumulative distribution function (CDF) of the SIR $F_\Gamma(t)$, we estimate $\bar{I}_{\max}$ that satisfies $F_\Gamma(\Gamma_{\mathrm{d}}) = p_{\mathrm{out}}$. Under the condition, $F_\Gamma(\Gamma_{\mathrm{d}})$ can be written as follows:

$$\begin{aligned} F_\Gamma(\Gamma_{\mathrm{d}}) &\approx \frac{1}{2}\left\{1 + \mathrm{erf}\left(\frac{\Gamma_{\mathrm{d}} - \left(\hat{P}(\boldsymbol{x}_0) - \bar{I}_{\max}\right)}{\sqrt{2(\sigma_k^2 + \sigma_{\mathrm{sum}}^2)}}\right)\right\} \\ &= p_{\mathrm{out}}, \end{aligned} \tag{4.32}$$

where $\mathrm{erf}(\cdot)$ is the error function. By solving Eq. (4.32), $\bar{I}_{\max}$ can be determined as

$$\bar{I}_{\max} \approx \hat{P}(\boldsymbol{x}_0) - \Gamma_{\mathrm{d}} + \sqrt{2(\sigma_k^2 + \sigma_{\mathrm{sum}}^2)}\mathrm{erf}^{-1}(2p_{\mathrm{out}} - 1). \tag{4.33}$$

Then, we can determine $P_{\mathrm{S,max}}$ by substituting Eq. (4.33) for Eq. (4.31).

4.5 Comparison of Different Estimation Methods

We compare the performances of the proposed method with three other methods: the perfect estimation, the path loss-based interference power constraint without Kriging, and the Kriging-based interference power constraint without consideration of the estimation error. The first method assumes that the SU can perfectly estimate the signal power $P(\boldsymbol{x}_0)$. This situation implies that a measurement node directly probes the signal at $\boldsymbol{x}_0$. In the second method, we assume that the SU only knows the median $\overline{P}(\boldsymbol{x}_0) \triangleq P_{\mathrm{Tx}} - L(\|\boldsymbol{x}_{\mathrm{P}} - \boldsymbol{x}_0\|)$ and σ_{P} of the PU link. The third method estimates $P(\boldsymbol{x}_0)$ using the ordinary Kriging, but neglects the estimation error. For simplicity, we assume that all methods know σ_{S}, η_{S}, and $d_{\mathrm{cor,S}}$ perfectly.

Note that this section only describes the estimation method of $\bar{I}_{\max}$. As with the proposed method, all compared methods can obtain $P_{\mathrm{S,max}}$ by assigning $\bar{I}_{\max}$ to Eq. (4.31).

4.5.1 Perfect Estimation

This situation is equal to method 2 defined in Sect. 2.3 with $\rho_{\mathrm{P}} = 1.0$. In this situation, because the SUs know the $P(\boldsymbol{x}_0)$ and $\overline{I}$, the SIR $\Gamma_{\mathrm{d}}(\boldsymbol{x}_0)$ follows a log-normal distribution with a median $P(\boldsymbol{x}_0) - \overline{I}$ and a variance σ^2_{sum}. Thus, based on the condition of $\overline{I}_{\max}$, we can formulate $F_{\Gamma}(\Gamma_{\mathrm{d}})$ as

$$\begin{aligned} F_{\Gamma}(\Gamma_{\mathrm{d}}) &= \frac{1}{2}\left\{1 + \mathrm{erf}\left(\frac{\Gamma_{\mathrm{d}} - (P(\boldsymbol{x}_0) - \overline{I}_{\max})}{\sqrt{2}\sigma_{\mathrm{sum}}}\right)\right\} \\ &= p_{\mathrm{out}}. \end{aligned} \tag{4.34}$$

Therefore, $\overline{I}_{\max}$ can be formulated as

$$\overline{I}_{\max} = \left\{\overline{P}(\boldsymbol{x}_0) + W_{\mathrm{P}}(\boldsymbol{x}_0)\right\} - \Gamma_{\mathrm{d}} - \sqrt{2}\sigma_{\mathrm{sum}}\mathrm{erf}^{-1}(1 - 2p_{\mathrm{out}}). \tag{4.35}$$

Here, in order to evaluate the spectrum sharing efficiency, we analyze the expected value of the transmission power $10\log_{10}\mathrm{E}\left[10^{\frac{P_{\mathrm{S,max}}}{10}}\right]$. Let us rewrite $\overline{I}_{\max}$ as a function of $w_{\mathrm{P}} \triangleq 10^{W_{\mathrm{P}}/10}$, $\overline{I}_{\max}(w_{\mathrm{P}})$. From its PDF $f_{w_{\mathrm{P}}}(y)$, the expected value is shown as

$$\begin{aligned} \mathrm{E}\left[10^{\frac{\overline{I}_{\max}(w_{\mathrm{P}})}{10}}\right] &= \int_0^{\infty} 10^{\frac{\overline{I}_{\max}(y)}{10}} f_{w_{\mathrm{P}}}(y)dy \\ &= \int_0^{\infty} Cy\frac{10/\ln 10}{\sqrt{2\pi}\sigma_{\mathrm{P}}y}\exp\left[-\frac{(10\log_{10}y)^2}{2\sigma_{\mathrm{P}}^2}\right]dy, \end{aligned} \tag{4.36}$$

where

$$C = 10^{\frac{\overline{P}(\boldsymbol{x}_0) - \Gamma_{\mathrm{d}} + \sqrt{2}\sigma_{\mathrm{sum}}\mathrm{erf}^{-1}(2p_{\mathrm{out}}-1)}{10}}. \tag{4.37}$$

Solving the integration, we can formulate the allowable interference power as

$$10\log_{10}\mathrm{E}\left[10^{\frac{\overline{I}_{\max}}{10}}\right] = \overline{P}(\boldsymbol{x}_0) - \Gamma_{\mathrm{d}} + \sqrt{2}\sigma_{\mathrm{sum}}\mathrm{erf}^{-1}(2p_{\mathrm{out}} - 1) + \frac{\sigma_{\mathrm{P}}^2}{20}(\ln 10)^2\log_{10}e. \tag{4.38}$$

Thus, from Eq. (4.31) and Eq. (4.38), the mean of $P_{\mathrm{S,max}}$ can be written as

$$\begin{aligned} 10\log_{10}\mathrm{E}\left[10^{\frac{P_{\mathrm{S,max}}}{10}}\right] =& \overline{P}(\boldsymbol{x}_0) - \Gamma_{\mathrm{d}} + \sqrt{2}\sigma_{\mathrm{sum}}\mathrm{erf}^{-1}(2p_{\mathrm{out}} - 1) + \frac{\sigma_{\mathrm{P}}^2}{20}(\ln 10)^2\log_{10}e \\ &- \left(15\log_{10}M - \frac{1}{0.1\ln 10}\left(\eta_{\mathrm{S}}G_1 + \frac{1}{2}k\right)\right). \end{aligned} \tag{4.39}$$

The equation implies that the intensity of the shadowing variation in the primary channel increases the transmission power in proportion to σ_{P}^2 in the log space. On the other hand, in the secondary channel, the value decreases in proportion to $-\sigma_{\mathrm{sum}}$.

4.5.2 Path Loss-based Interference Power Constraint without Kriging Interpolation

This situation is equal to method 3 defined in Sect. 2.3. This method only knows $\overline{P}(\boldsymbol{x}_0)$, σ_{P}, and $\overline{I}$. Thus, the SIR follows a log-normal distribution with a median $\overline{P}(\boldsymbol{x}_0) - \overline{I}$ and a variance $\sigma_{\mathrm{P}}^2 + \sigma_{\mathrm{sum}}^2$. Therefore, its CDF can be formulated as

$$\begin{aligned} F_{\Gamma}(\Gamma_{\mathrm{d}}) &= \frac{1}{2}\left\{1 + \mathrm{erf}\left(\frac{\Gamma_{\mathrm{d}} - \left(\overline{P}(\boldsymbol{x}_0) - \overline{I}_{\max}\right)}{\sqrt{2\left(\sigma_{\mathrm{P}}^2 + \sigma_{\mathrm{sum}}^2\right)}}\right)\right\} \\ &= p_{\mathrm{out}}. \end{aligned} \tag{4.40}$$

Because $\overline{I}_{\max}$ depends only on the channel distribution information, the median and the variance are $10\log_{10}\mathrm{E}\left[10^{\frac{\overline{I}_{\max}}{10}}\right] = \overline{I}_{\max}$. Thus,

$$10\log_{10}\mathrm{E}\left[10^{\frac{\overline{I}_{\max}}{10}}\right] = \overline{P}(\boldsymbol{x}_0) - \Gamma_{\mathrm{d}} - \sqrt{2(\sigma_{\mathrm{P}}^2 + \sigma_{\mathrm{sum}}^2)}\mathrm{erf}^{-1}(1 - 2p_{\mathrm{out}}). \tag{4.41}$$

Using Eq. (4.31) and Eq. (4.41), the mean of $P_{\mathrm{S,max}}$ can be written as

$$\begin{aligned} 10\log_{10}\mathrm{E}\left[10^{\frac{P_{\mathrm{S,max}}}{10}}\right] =& \overline{P}(\boldsymbol{x}_0) - \Gamma_{\mathrm{d}} - \sqrt{2(\sigma_{\mathrm{P}}^2 + \sigma_{\mathrm{sum}}^2)}\mathrm{erf}^{-1}(1 - 2p_{\mathrm{out}}) \\ &- \left(15\log_{10}M - \frac{1}{0.1\ln 10}\left(\eta_{\mathrm{S}}G_1 + \frac{1}{2}k\right)\right). \end{aligned} \tag{4.42}$$

Unlike the perfect estimation, the intensity of the shadowing variation in the primary channel also decreases the average transmission power. This phenomenon corresponds to the perception that indeterminacies in the radio environment require SUs to set considerable interference margins.

4.5.3 Kriging-based Interference Power Constraint without Error Distribution Prediction

For the comparison of the outage probability performance, the performance of the Kriging-based interference power constraint without error distribution prediction is evaluated. In this

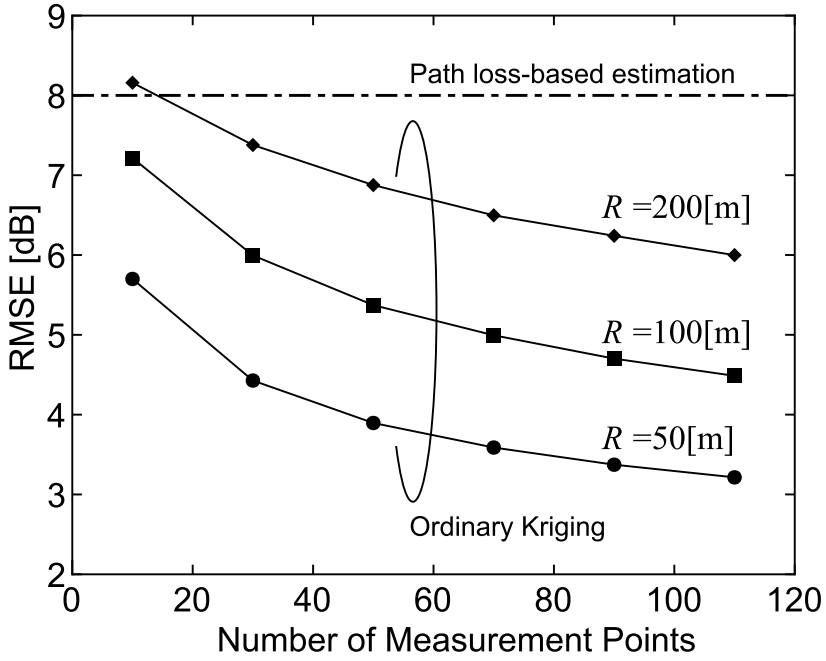

Fig. 4.6 RMSE vs the number of measurement points.

method, the SU treats $\hat{P}(\boldsymbol{x}_0)$ as the true received signal power $P(\boldsymbol{x}_0)$. Thus, the estimation of $\overline{I}_{\max}$ can be achieved by assigning $\hat{P}(\boldsymbol{x}_0)$ to $\left\{\overline{P}(\boldsymbol{x}_0) + W_{\mathrm{P}}(\boldsymbol{x}_0)\right\}$ in Eq. (4.35), as follows:

$$\overline{I}_{\max} \approx \hat{P}(\boldsymbol{x}_0) - \Gamma_{\mathrm{d}} - \sqrt{2}\sigma_{\mathrm{sum}}\mathrm{erf}^{-1}(1-2p_{\mathrm{out}}). \tag{4.43}$$

However, because Eq. (4.43) neglects the estimation error of $\hat{P}(\boldsymbol{x}_0)$, it can be presumed that the outage probability performance of the method is inferior to the proposed method.

4.6 Performance Evaluation

In this section, the performance evaluation of the interference constraint is presented. The simulation procedure is the same as in Sec. 4.4 and the simulation parameters are defined in Table 5.1.

4.6.1 Radio Propagation Estimation Accuracy

First, the root mean squared error (RMSE) of the estimation of $P(\boldsymbol{x}_0)$ with the ordinary Kriging is shown in Fig. 4.6. The path loss-based estimation cannot estimate the shadowing factor $W_{\mathrm{P}}(\boldsymbol{x}_0)$. Therefore, its RMSE is equal to the shadowing standard deviation σ_{P}. On the other hand, the ordinary Kriging can provide a more accurate estimation than the path loss-

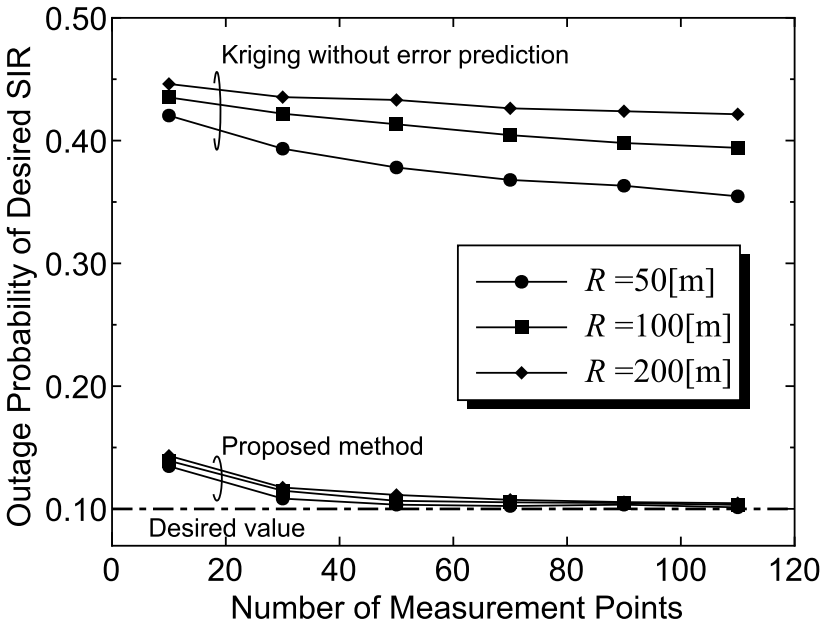

Fig. 4.7 Outage probability of the desired SIR vs the number of measurement points N. The proposed method almost achieves the desired protection criteria $p_{\text{out}} = 0.10$.

based method because the interpolation utilizes the spatial correlation for estimating $W_{\text{P}}(\boldsymbol{x}_0)$. Additionally, this figure indicates that measurements in a small circle can estimate the radio propagation with a high accuracy; this is because the neighboring measurements can acquire an accurate spatial correlation structure. The accurate structure provides a suitable weight factor for the Kriging interpolation. Therefore, the neighboring measurements improve the estimation accuracy.

Note that these results are nearly equal to the error standard deviation shown in Fig. 4.5 because the Kriging interpolation achieves an unbiased estimation in the dB domain.

4.6.2 Outage Probability of the Desired SIR

The outage probability of the desired SIR $\Pr[\Gamma_{\text{d}} > \Gamma(\boldsymbol{x}_0)]$ is shown in Fig. 4.7. In order to confirm the impact of the radio propagation estimation error, the simulation was conducted in three environments: R = 50, 100, 200 [m]. First, the Kriging-based method without error distribution prediction obviously generates harmful interference with the PU. On the other hand, each curve of the proposed method approximately satisfies the desired outage probability and converges to the value. Additionally, the small measurement circle and the highly accurate propagation estimation improve the outage probability. However, all the curves of the proposed method cause some harmful interference, particularly in regions with few measurement points. The cause of the harmful interference is the underestimation of the

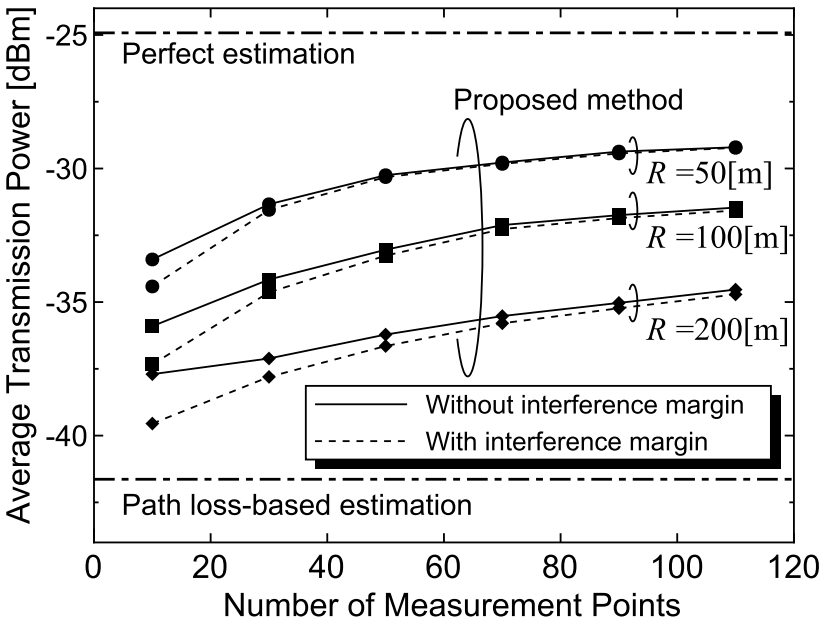

Fig. 4.8 Average transmission power vs the number of measurement points N. Each dot-curve includes the interference margin that satisfies the strict desired protection criteria $p_{\text{out}} = 0.10$.

estimation error that is shown in Fig. 4.5. In the proposed method, the estimation error ϵ is predicted based on the Kriging standard deviation σ_k. However, the standard deviation of the estimation error exceeds σ_k even if there are several measurement points as mentioned in 4.4.1. Considering this behavior, the proposed method should set a very slight interference margin.

Note that the underestimation can be improved using a *parametric bootstrap method*. The method predicts the distribution of the estimator by conducting repeated resampling and estimations from the measurement data. In [100], it is shown that the method can reduce the difference between the Kriging variance and the variance of the error. The implementation procedure is summarized in appendix A.

4.6.3 Average Transmission Power

Under a peak interference power constrained spectrum sharing environment, it is important to increase the average transmission power of the interference source with the interference constraint in order to improve the spectrum usage efficiency. From this perspective, we have evaluated the average transmission power characteristics.

The characteristics of the average transmission power are shown in Fig. 4.8. Note that the Kriging-based interference power constraint without the error distribution prediction obviously interferes with the PU, as shown in Fig. 4.7. Thus, the performance of the

conventional Kriging-based method is not included in the figure in order to compare the transmission capability. Because of the demand of the interference margin for a strict interference constraint, we have evaluated the required margin using numerical simulations. Here, each outage probability of the SIR is associated with Fig. 4.7. This figure shows that an increase in the number of measurement points N improves the capability of the spectrum sharing and reduces the required margin.

Additionally, the proposed method can achieve a higher spectrum sharing capability than the path loss-based method even if there are only a few datasets. Note that achieving the limit of the path loss-based method is difficult because the SUs cannot estimate the actual path loss parameters and σ_{P} without the measurements. Model-tuning is an estimation method for improving the accuracy of the path loss models [92]. Fitting several parameters of a path loss model with the measurement data, the radio environment estimation accuracy can be improved. However, because the limit of the model-tuning is equal to that of the path loss-based method, the advantage is inferior to the Kriging-based method.

4.6.4 Effects of Radio Environment Parameters

Next, we show effects of the radio environment parameters on the spectrum sharing performances. Figure 4.9 shows the effects of the standard deviation σ_{P} and σ_{S}. In the simulation, both σ_{P} and σ_{S} are changed simultaneously. Figure 4.9a shows the standard deviation of the estimation error and the Kriging standard deviation. First, it can be seen from Fig. 4.9b that the outage probability with the conventional Kriging-based approach is clearly degraded as the standard deviation increases. This is because such deep shadowing decreases the estimation accuracy of $P(\boldsymbol{x}_0)$ as shown in Fig. 4.9a. On the other hand, the proposed method can almost achieve the desired outage probability even if the standard deviation becomes large owing to the error prediction.

The average transmission power of the SUs is shown in Fig. 4.9c. In the figure, two dot-curves, perfect estimation and path loss-based estimation, are plotted with Eq. (4.39) and Eq. (4.42). Because the transmission power with the path loss-based method decreases in direct proportion to $\sqrt{2(\sigma_{\mathrm{P}}^2+\sigma_{\mathrm{sum}}^2)}$, the curve is a monotonically decreasing function. On the other hand, the curve of the perfect estimation increases in proportion to σ_{P}^2 because of the knowledge of the shadowing variation in the primary signal W_{P}. The proposed method also has a similar property. Therefore, these results imply that the more the standard deviation of the shadowing grows, the more the SUs can gain their own transmission capability using the proposed method.

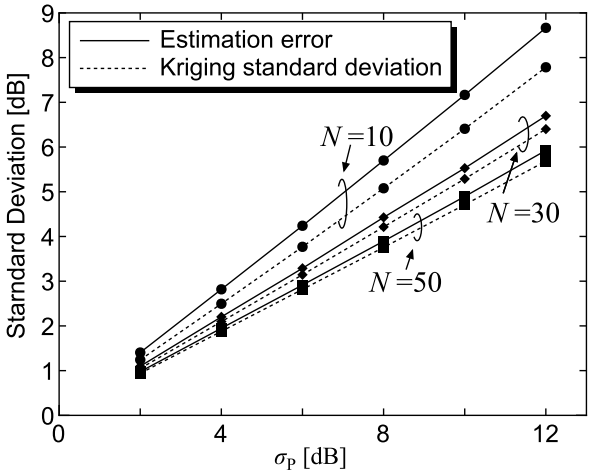

(a) Standard deviation.

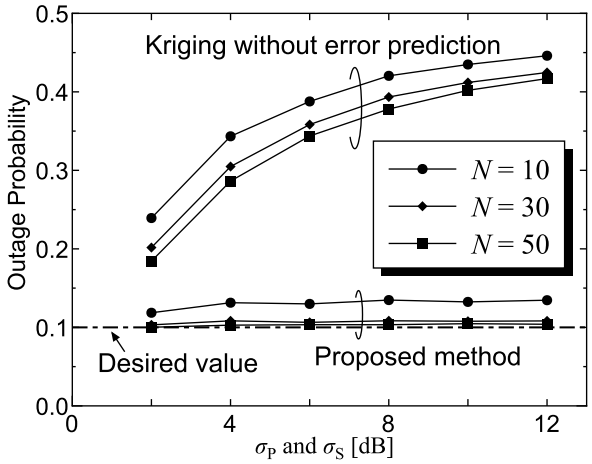

(b) Outage probability.

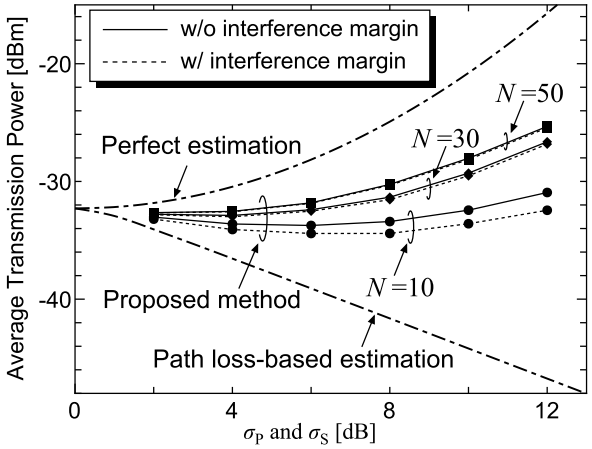

(c) Average transmission power.

Fig. 4.9 Effects of shadowing standard deviations, where $d_{\mathrm{cor,P}} = 20$ [m], $\eta_{\mathrm{P}} = 3.5$, and $R = 50$ [m]. Even though the standard deviation of the estimation error has a high value, the proposed method can almost achieve the desired outage probability.

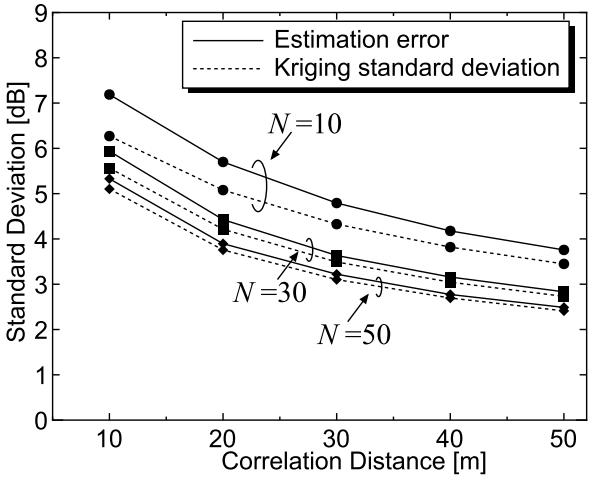

(a) Standard deviation.

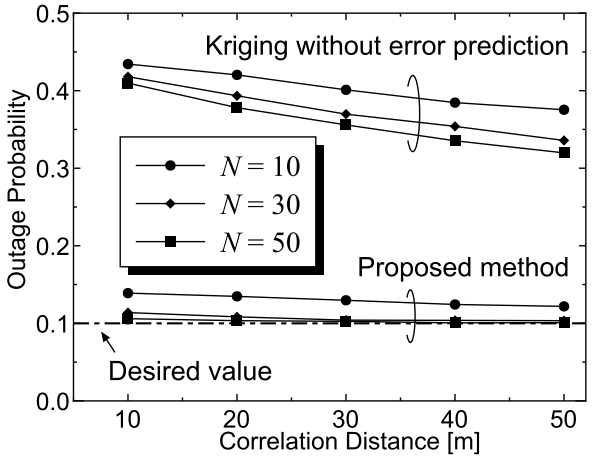

(b) Outage probability.

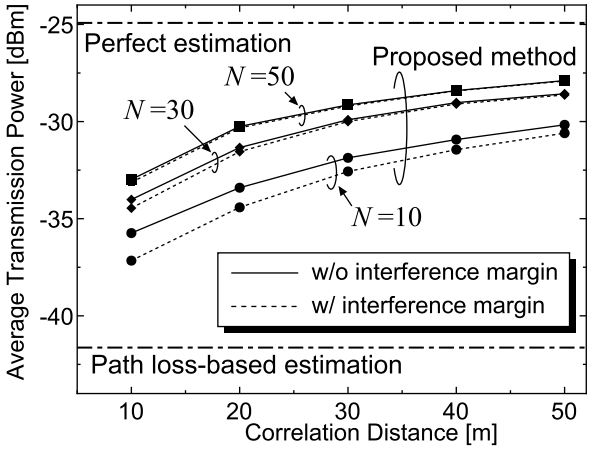

(c) Average transmission power.

Fig. 4.10 Effects of correlation distance, where $\sigma_{\mathrm{P}} = \sigma_{\mathrm{S}} = 8.0$ [dB], $\eta_{\mathrm{P}} = 3.5$, and $R = 50$ [m].

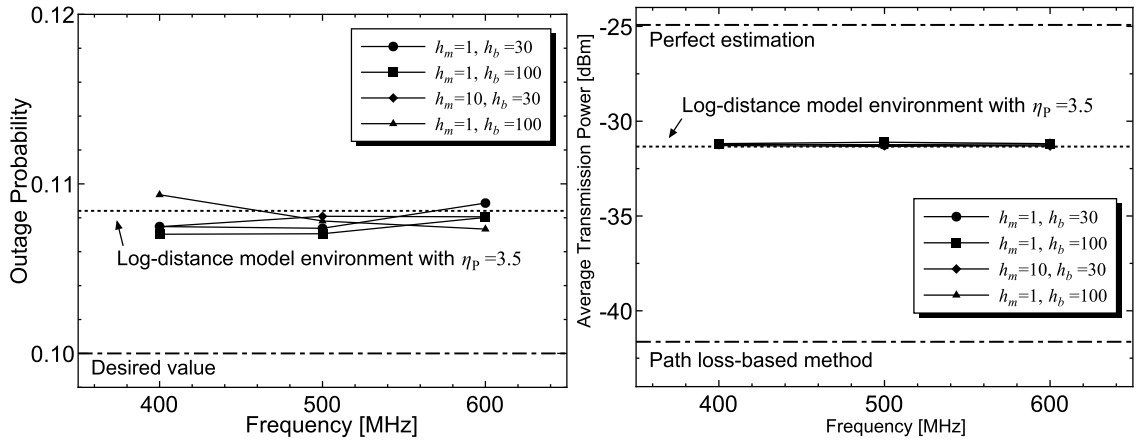

(a) Outage probability. (b) Average transmission power.

Fig. 4.11 Spectrum sharing performances in Hata model environment, where $\sigma_P = \sigma_S =$ 8.0 [dB], $N = 30$, and $R = 50$ [m].

Figure 4.10 illustrates the effects of the correlation distance. In Fig. 4.7 and Fig. 4.8, we confirmed that the small measurement radius R improves both the radio environment estimation accuracy and the spectrum sharing capability under a given correlation distance. This is because the measurement in the small area strengthens the correlation among the datasets. The behavior can also be seen in Fig. 4.10; Fig. 4.10b and Fig. 4.10c show that the proposed method performs well under a high correlation distance environment.

Next, we show the effects of the path loss environment. The above simulations generate the path loss model according to Eq. (4.2) with the same path loss index. On the other hand, in realistic situations, the path loss characteristics highly depend on the communication environment such as antenna height and frequency. We evaluate the performance of the proposed method under the Hata model environment in order to confirm the applicability in realistic situations.

In the simulation, the path loss of the primary signal follows the Hata model for urban areas [101]. Although the primary signal follows the Hata model, the proposed method assumes Eq. (4.2). This model can be written as

$$L(d,h_M,h_B,f) = 69.55 + 26.16\log_{10}f - 13.82\log 10h_B - C_H + (44.9 - 6.55\log_{10}h_B)\log_{10}d, \tag{4.44}$$

where h_b [m] is the height of the transmitter, h_m [m] is the height of the receiver, and f [MHz] is the signal frequency. C_H is the antenna height correlation factor. In large cities, C_H can be

written as

$$C_H = \begin{cases} 8.29(\log_{10}(1.54h_M))^2 - 1.1 & (150 \le f \le 200), \\ 3.2(\log_{10}(11.75h_M))^2 - 4.97 & (200 < f \le 1500). \end{cases} \tag{4.45}$$

Figure 4.11 shows the outage probability and the average transmission power. We also plot the results, where $\eta_{\mathrm{P}} = 3.5$ represents the reference value. It can be confirmed that the spectrum sharing performances are independent of each parameter h_m, h_b, and f; the proposed method has the robustness for the path loss environment.

4.6.5 Effects of Imperfect Channel Information

We show the effects of imperfect channel information on the spectrum sharing performances. The above results assume that the spectrum database has perfect information of the interference distribution. On the other hand, we should consider the imperfection of this information when setting communication parameters because such information also has some estimation errors. In the simulation, we consider the estimation error of both the path loss index in secondary channel η_{S}, and the shadowing standard deviation σ_{S}.

According to some results for the maximum likelihood-based path loss estimation [93][94], we assume that the spectrum database has the following imperfect path loss information:

$$\hat{\eta_{\mathrm{S}}} = \eta_{\mathrm{S}} + \eta_{\mathrm{err}}, \tag{4.46}$$

where η_{err} is the estimation error component that follows the Gaussian distribution with zero-mean and standard deviation $\sigma_{\eta_{\mathrm{S}}}$. Next, we assume that the spectrum database has the following imperfect information of the shadowing standard deviation σ_{S}:

$$\hat{\sigma}_{\mathrm{S}} = \sigma_{\mathrm{S}} + \sigma_{\mathrm{off}}, \tag{4.47}$$

where σ_{off} [dB] is the constant offset value.

Using Eq. (4.25), (4.26), (4.30), $\hat{\eta}_{\mathrm{S}}$, and $\hat{\sigma}_{\mathrm{S}}$, we can write the imperfect variance of the aggregate interference $\hat{\sigma}^2_{\mathrm{sum}}$ as follows:

$$\hat{\sigma}^2_{\mathrm{sum}} = \hat{\sigma}^2_{\mathrm{S}} + \frac{1}{(0.1\ln 10)^2}\left\{-\ln M + \hat{\eta}^2_{\mathrm{S}}(G_2 - G_1^2) + \hat{k}\right\}, \tag{4.48}$$

where

$$\hat{k} = \ln\left(1 + (M-1)e^{\left((0.1\ln 10)^2\hat{\sigma}^2_{\mathrm{S}}(G_{\mathrm{cor}}-1) - \hat{\eta}^2_{\mathrm{S}}(G_2 - G_1^2)\right)}\right). \tag{4.49}$$

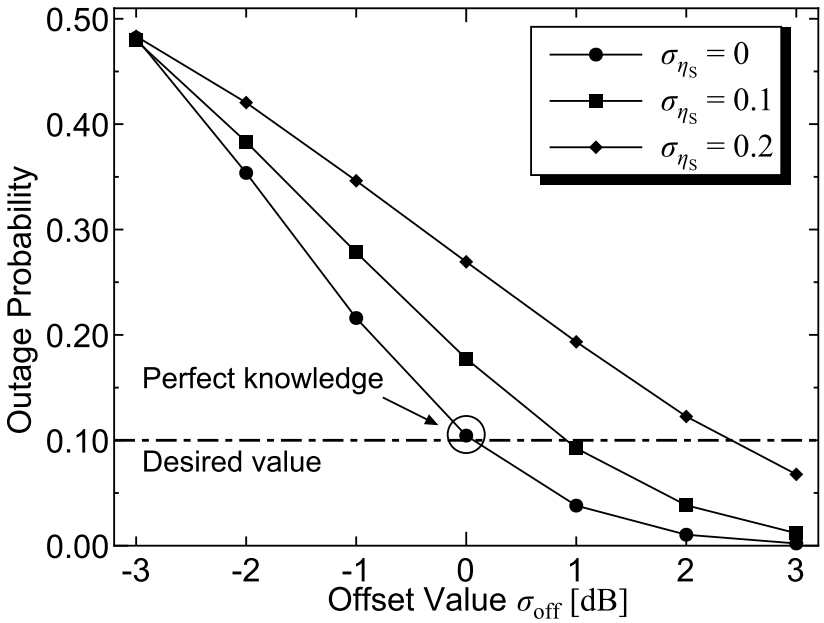

Fig. 4.12 Outage probability with imperfect information of η_S and σ_S, where $N = 50$, $d_{\mathrm{cor,P}} = 20$ [m], $\eta_P = \eta_S = 3.5$, $\sigma_P = \sigma_S = 8.0$, and $R = 50$ [m].

Then, $\bar{I}_{\max}$ can be estimated, as follows:

$$\bar{I}_{\max} \approx \hat{P}(\boldsymbol{x}_0) - \Gamma_{\mathrm{d}} + \sqrt{2(\sigma_k^2 + \hat{\sigma}_{\mathrm{sum}}^2)}\mathrm{erf}^{-1}(2p_{\mathrm{out}} - 1). \tag{4.50}$$

Finally, using Eq. (4.31), we can calculate the maximum allowed transmission power as follows:

$$P_{\mathrm{S,max}} = \bar{I}_{\max} - \left(15\log_{10}M - \frac{1}{0.1\ln 10}\left(\hat{\eta}_S G_1 + \frac{1}{2}\hat{k}\right)\right). \tag{4.51}$$

Figure 4.12 shows the outage probability under the imperfect channel information. We evaluated the dependence property of the offset σ_{off} where $\sigma_{\eta_S} = 0$, 0.1, 0.2. Note that the value of σ_{η_S} considers the results in our previous work [94]. In the figure, the outage probability decreases in proportion to the offset of the standard deviation σ_{err}. This is because the proposed method suppresses the interference power at $\boldsymbol{x}_0$ according to the amplitude of $\hat{\sigma}_S$. Therefore, when $\hat{\sigma}_S > \sigma_S$, the estimated $\bar{I}_{\max}$ is lower than its strict $\bar{I}_{\max}$.

Although the outage probability increases with increasing σ_{η_S}, the harmful interference can be mitigated by overestimating the shadowing standard deviation σ_S. The standard deviation of the shadowing strongly depends on the communication environment, and the value has the range of roughly 4-13 [dB] [4]. By setting $\hat{\sigma}_S$ larger than the empirical (or estimated) value, the proposed method can satisfy the protection criterion (e.g., $\sigma_{\mathrm{off}} > 1$ at $\sigma_{\eta_S} = 0.1$ and $\sigma_{\mathrm{off}} > 2.5$ at $\sigma_{\eta_S} = 0.2$).

4.7 Chapter Summary

In this chapter, for achieving highly efficient spectrum sharing, we have proposed an interference power constraint method using a Kriging-based REM. We first showed that the estimation error of the Kriging-based REM follows the log-normal distribution, and the moments can easily be estimated. The evaluation results demonstrated that the estimated error distribution can be incorporated into the secondary parameter design. Unlike the conventional Kriging-based method, the proposed method can almost achieve the probabilistic interference constraint in the various radio propagation environments. Additionally, the comparison results indicated that the proposed method can increase the secondary transmission power compared with the path loss-based method, even if only a small amount of measurement data is available.

Chapter 5

Database-assisted Radio Propagation Estimation for Wireless Distributed Networks

In previous chapters, we have focused on the radio propagation estimation in primary networks; the knowledge of interference channels were only limited to path loss model and shadowing distribution for simplicity. On the other hand, if we can improve uncertainties of the interference signal, the spectrum sharing efficiency will be improved further. In this chapter, we propose a spectrum database-assisted radio propagation estimation for wireless distributed networks.

5.1 Background

In the dynamic spectrum access, SUs are often assumed as a distributed system. In such wireless distributed networks (WDNs), numberless wireless devices construct *ad-hoc* wireless links that both the transmitter and the receiver exist arbitrary locations, and have to share finite spectrum resources under mutual signal interferences. In the spatial spectrum reuse environment, excess transmission power increases the communication reliability in own link, but decreases the one in other links. On the other hand, insufficient transmission power naturally gets low communication quality in own link. The trade-off requires suitable communication parameter setting based on the proper interference estimation for the highly efficient spectrum use: accurate radio propagation prediction among distributed terminals is a critical issue.

Empirical propagation formula such as Okumura-Hata curve [101][59] can predict rough propagation loss by combining suitable propagation model with knowledges of own communication parameters: frequency, antenna heights, distance, and surrounding obstacle information. However, because empirical models generalize radio propagation environments to typical environments, urban, suburban, and rural, the propagation models cannot include site-specific propagation dispersions [5]. Thus, the propagation model-based link design is unsuitable for the WDN environment where small wireless links exist densely. Besides, path loss parameter correction using measurement values can adjust own path loss formula to the site-specific propagation characteristics [92]. This method unfortunately cannot estimate shadowing fluctuation, therefore, its RMSE remains about 8 dB at best [5]. Ray tracing is a well known method that can estimate the propagation loss with high-accuracy by calculating multiple reflected paths. However, due to requirements of detailed obstacle information and the computational complexity, the method is considered to be an unrealistic technique in WDNs. Measurement-based REM also can achieve highly accurate propagation estimation [72]. Applying the method, however, also be attended with difficulty in that WDNs have infinite positional relationship of terminals: one positional relationship requires one plane of REM with a focus on the transmitter. Taking these problems of conventional methods into account, it is important to discuss a novel radio propagation prediction technique for WDNs from a different perspective.

Incidentally, it is a well known fact that different wireless links have spatial correlation about shadowing effects. Reference [89] empirically showed that the correlation exponentially decreases in proportion as the receiver backs away from the fixed transceiver. Such correlated stochastic process enables to apply spatial interpolation with Kriging interpolation [82]. Several studies have proved the advantage of the technique in wireless networks [72][84]. These existing works mainly focus on the fixed transmitter situation such as TVWS and cellular networks. On the other hand, the propagation loss has similar spatial correlation even if both of the transmitter and the receiver moves [102]. Reference [102] revealed the spatial correlation exponentially decreases in proportion as the summation of respective distances from original and other position of transmitter and receiver increases. Therefore, the Kriging-based method can be applied for the radio propagation estimation in WDN environments by taking the spatial correlation into account.

In this chapter, we propose the novel radio propagation prediction using spectrum database which collects communication results from mobile terminals. In the proposed method, after each signal transmission, the transmitter uploads the signal information: transmission time, power, and location. If the signal was perfectly decoded at the paired receiver, the receiver reports the measured information: received time, signal power, location, and the MAC

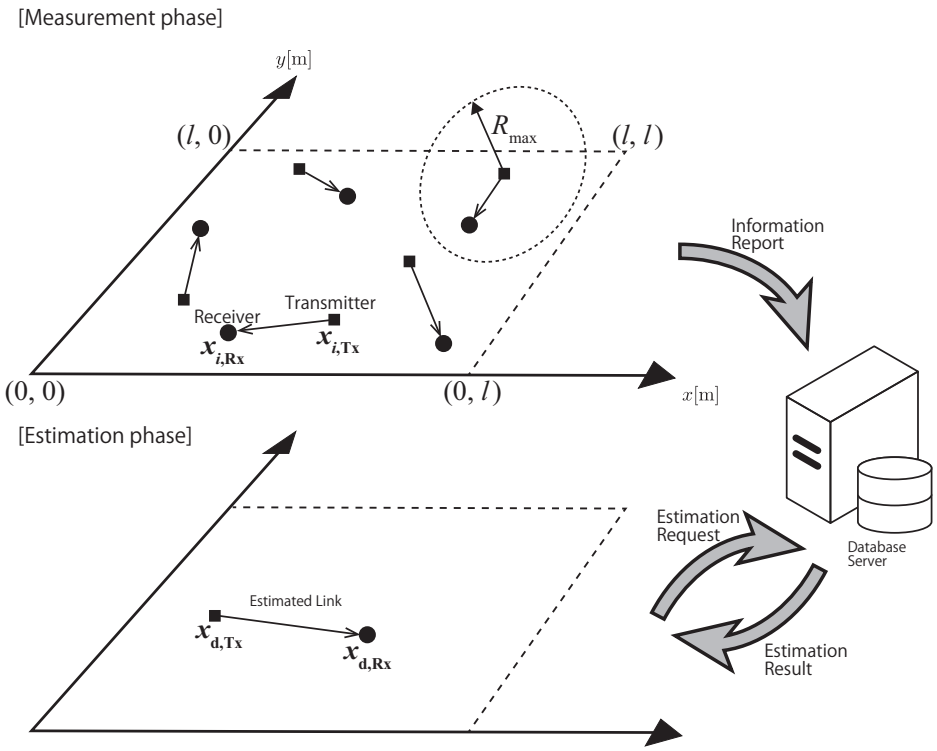

Fig. 5.1 System model.

information of the transmitter. The database server then calculates the radio propagation loss in the positional relationship from the paired report information. After some propagation losses are stored, the propagation loss in a wireless link with arbitrary positional relationship is estimated from the stored results. Through numerical results, it is shown that the proposed method has highly accurate RMSE characteristics compared with the path loss-based estimation method. Furthermore, an important advantage other than the RMSE improvement, the technique can stochastically predict the estimation error, is presented. Because the PDF of estimation error follows log-normal distribution, it can be expected that the proposed technique contributes to set suitable communication parameters by combining with conventional mathematical tools that consider the log-normal propagation distribution.

5.2 System Model

Figure 5.1 shows the system model we treat. We consider WDNs that consist of N Peer-to-Peer (P2P) distributed links. Each transmitter is randomly distributed in a square, l [m] each side. Each receiver exists in a circle of $R_{\max}$ [m] radius centered at the paired transmitter. To store the communication results, all terminals share a same database server. After each signal

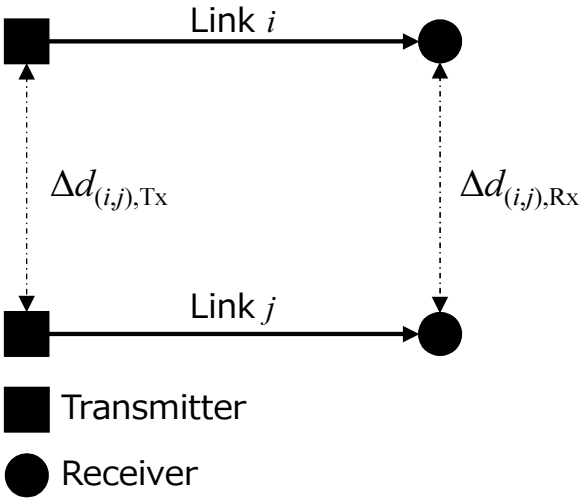

Fig. 5.2 Positional relationship between two communication links.

transmission, the transmitter uploads the signal information: transmission time, power, and location $\boldsymbol{x}_{i,\mathrm{Tx}}(i = 1,2,...,N)$. If the signal was successfully decoded at the paired receiver, the receiver reports the measured information: received time, signal power, location $\boldsymbol{x}_{i,\mathrm{Rx}}$, and the MAC information of the transmitter. The database server calculates the radio propagation loss L_i [dB] between $\boldsymbol{x}_{i,\mathrm{Tx}}$ and $\boldsymbol{x}_{i,\mathrm{Rx}}$ from the paired report information. After N propagation losses are stored, the database calculates the propagation loss L_d between a transmitter at $\boldsymbol{x}_{\mathrm{d,Tx}}$ and the paired receiver at $\boldsymbol{x}_{\mathrm{d,Rx}}$.

In this section, we model the propagation loss L_i as follows.

$$L_i = 10\eta \log_{10} d_i - W_i, \quad (d_i > 1.0) \tag{5.1}$$

where η is the path loss index, and $d_i = \|\boldsymbol{x}_{i,\mathrm{Tx}} - \boldsymbol{x}_{i,\mathrm{Rx}}\|$ [m] is the link distance between $\boldsymbol{x}_{i,\mathrm{Tx}}$ and $\boldsymbol{x}_{i,\mathrm{Rx}}$. W_i [dB] is the log-normal shadowing loss with the standard deviation σ [dB].

Although there is room for a consideration on whether or not it is better to assume such a generalized model rather than a site-specific model as the propagation model of the mobile terminal, some works (e.g., [103]) show that such a generalized model can derive the radio propagation characteristics. Next, the estimated propagation loss L_d is modeled as following equation, as same way as Eq. (5.1).

$$L_\mathrm{d} = 10\eta \log_{10} d_\mathrm{d} - W_\mathrm{d}, \tag{5.2}$$

where W_d [dB] is the shadowing loss and $d_\mathrm{d} = \|\boldsymbol{x}_{\mathrm{d,Tx}} - \boldsymbol{x}_{\mathrm{d,Rx}}\|$ [m] is the link distance. In addition, we particularly assume the spatially correlated shadowing between different wireless links. Let us consider two wireless links, as shown in Fig. 5.2. In this situation, the shadowing

correlation $\rho_{i,j}$ is exponentially decreased as the sum of distances between two transmitters and between two receivers increases [102]:

$$\begin{aligned}\rho_{i,j} &= \frac{\mathrm{E}[W_i W_j]}{\sigma^2} \\ &\approx \exp\left(-\frac{\Delta d_{(i,j),\mathrm{Tx}} + \Delta d_{(i,j),\mathrm{Rx}}}{d_{\mathrm{cor}}}\ln 2\right),\end{aligned} \tag{5.3}$$

where $\Delta d_{(i,j),\mathrm{Tx}} = \|\boldsymbol{x}_{i,\mathrm{Tx}} - \boldsymbol{x}_{j,\mathrm{Tx}}\|$ [m], $\Delta d_{(i,j),\mathrm{Rx}} = \|\boldsymbol{x}_{i,\mathrm{Rx}} - \boldsymbol{x}_{j,\mathrm{Rx}}\|$ [m], and $\mathrm{E}[\cdot]$ is the expected value of the random variable. In addition, d_{cor} [m] is the correlation distance that depends on the building structure around the link. For example, reference [102] reports $d_{\mathrm{cor}} \approx 20$ [m] at 2.4 GHz and 5 GHz in the typical urban area.

5.3 Kriging-based Radio Propagation Prediction

We describe the radio propagation loss estimation method based on the reported results. Using maximum likelihood estimation, the database server preliminarily determines the probabilistic characteristics of the radio propagation: path loss index η, standard deviation σ, and correlation distance d_{cor}. We then exploit Kriging interpolation, a minimum mean squared error method of spatial prediction, to predict the propagation loss L_{d}.

5.3.1 Maximum Likelihood-based Radio Propagation Parameter Estimation

From Eq. (5.3), theoretical semivariogram between links i and j can be written as exponential model:

$$\begin{aligned}\gamma(\Delta d_{i,j}) &= \frac{1}{2}\mathrm{E}\left[\left(W_i - W_j\right)^2\right] \\ &= \alpha_n^2 + \alpha_s^2\left\{1 - \exp\left(-\frac{\Delta d_{i,j}}{\alpha_r}\right)\right\},\end{aligned} \tag{5.4}$$

where $\Delta d_{i,j} \triangleq \Delta d_{(i,j),\mathrm{Tx}} + \Delta d_{(i,j),\mathrm{Rx}}$. Moreover, $\alpha_n^2, \alpha_s^2, \alpha_r$ are *Nugget*, *Sill*, and *Range*, respectively. We define the set of variables $(\alpha_n^2, \alpha_s^2, \alpha_r)$ as a vector $\boldsymbol{\theta}$. As can be seen from the comparison with Eq. (5.3) and Eq. (5.4), $\alpha_n^2 + \alpha_s^2$ and α_r correspond with σ^2 and $d_{\mathrm{cor}}/\ln 2$, respectively. By considering Eq. (5.4), the joint PDF of $(w_1, w_2, ..., w_N)$, the random variable

of W_i, can be written as following multivariate normal distribution,

$$f_{W_i}(w_1, w_2, ..., w_N) = \frac{1}{(2\pi)^{\frac{N}{2}}\sqrt{|\boldsymbol{M}(\boldsymbol{\theta})|}}\exp\left(\frac{1}{2}\boldsymbol{w}^{\mathrm{T}}\boldsymbol{M}(\boldsymbol{\theta})^{-1}\boldsymbol{w}\right). \tag{5.5}$$

Note that $|\boldsymbol{A}|$ is the determinant of the matrix $\boldsymbol{A}$, and $\boldsymbol{A}^{\mathrm{T}}$ is the transposed matrix. In addition, $\boldsymbol{w}$ is a matrix of the random variables,

$$\boldsymbol{w} = \begin{pmatrix} w_1 \\ w_2 \\ \vdots \\ w_N \end{pmatrix} = \begin{pmatrix} 10\eta\log_{10}d_1 - L_1 \\ 10\eta\log_{10}d_2 - L_2 \\ \vdots \\ 10\eta\log_{10}d_N - L_N \end{pmatrix}. \tag{5.6}$$

In addition, the $N \times N$ covariance matrix is written as

$$\boldsymbol{M}(\boldsymbol{\theta}) = \alpha_n^2\boldsymbol{I} + \alpha_s^2\boldsymbol{H}(\alpha_r), \tag{5.7}$$

where $\boldsymbol{I}$ is the identity matrix of size N. $\boldsymbol{H}(\alpha_r)$ is the correlation matrix that consists of

$$H_{i,j} = \exp\left(-\frac{\Delta d_{i,j}}{\alpha_r}\right). \tag{5.8}$$

Next, the log-likelihood function about η and $\boldsymbol{\theta}$ can be written as

$$l(\boldsymbol{w}|\eta, \boldsymbol{\theta}) = -\frac{N}{2}\ln 2\pi - \frac{1}{2}\ln|\boldsymbol{M}(\boldsymbol{\theta})| - \frac{1}{2}\boldsymbol{w}^{\mathrm{T}}\boldsymbol{M}(\boldsymbol{\theta})^{-1}\boldsymbol{w}. \tag{5.9}$$

Finally, the suitable parameters can determined by maximizing Eq. (5.9). Note that we have to sufficiently give care to local solutions when maximizing Eq. (5.9), because the equation is a multi-peak function. To avoid local solutions, referring to [95], we iterate *Nealder-Mead simplex method* [104] with different initial values. Concretely speaking, the maximization of Eq. (5.9) is iterated ten times with different initial values selected according to uniform distribution that has maximum value 1.0 and minimum value 0.0. After that, sub-optimal parameters $\hat{\eta}$ and $\hat{\boldsymbol{\theta}}$ can be determined by taking the maximum log-likelihood value in the results of ten iterations.

5.3.2 Kriging-based Radio Propagation Loss Prediction

After the parameter estimation, *Ordinary Kriging* is applied to predict L_{d}. Kriging interpolation is a minimum mean squared error method of spatial prediction that depends on the

second order properties of the process. The goal is estimating the unknown radio propagation gain at the arbitrary link from measurement datasets. This is reached by assigning weight factor ω_i ($i = 1, \cdots, N$) to each shadowing loss W_i, as follows:

$$\hat{W}_{\mathrm{d}} = \sum_{i=1}^{N} \omega_i W_i, \tag{5.10}$$

where $\hat{W}_{\mathrm{d}}$ is the estimator for W_{d}. Here, shadowing factor W_i is estimated by eliminating the estimated path loss factor from the measurement dataset:

$$W_i \approx 10\hat{\eta}\log_{10} d_i - L_i. \tag{5.11}$$

Ordinary Kriging determines the weights which minimize the variance of the estimation error $\sigma_k^2 = \mathrm{E}[\{\hat{W}_{\mathrm{d}} - W_{\mathrm{d}}\}^2]$ under the following constraint,

$$\sum_{i=1}^{N} \omega_i = 1. \tag{5.12}$$

Using a method of Lagrange multiplier, the objective function $\phi(\omega_i, \mu)$ can be written as

$$\phi(\omega_i, \mu) = \sigma_k^2 - 2\mu\left(\sum_{i=1}^{N} \omega_i - 1\right), \tag{5.13}$$

where μ is Lagrange multiplier. Here, σ_k^2 can be written as following equation,

$$\sigma_k^2 = -\gamma(\Delta d_{\mathrm{d,d}}) - \sum_{i=1}^{N}\sum_{j=1}^{N} \omega_i \omega_j \gamma(\Delta d_{i,j}) + 2\sum_{i=1}^{N} \omega_i \gamma(\Delta d_{i,\mathrm{d}}), \tag{5.14}$$

where the suffix d attached to Δd means the estimated link. From partial derivatives of Eq. (5.14), we can obtain $N+1$ simultaneous equations,

$$\begin{pmatrix} \gamma(\Delta d_{1,1}) & \cdots & \gamma(\Delta d_{1,N}) & 1 \\ \gamma(\Delta d_{2,1}) & \cdots & \gamma(\Delta d_{2,N}) & 1 \\ \vdots & \vdots & \vdots & \vdots \\ \gamma(\Delta d_{N,1}) & \cdots & \gamma(\Delta d_{N,N}) & 1 \\ 1 & \cdots & 1 & 0 \end{pmatrix} \begin{pmatrix} \omega_1 \\ \omega_2 \\ \vdots \\ \omega_N \\ \mu \end{pmatrix} = \begin{pmatrix} \gamma(\Delta d_{1,\mathrm{d}}) \\ \gamma(\Delta d_{2,\mathrm{d}}) \\ \vdots \\ \gamma(\Delta d_{N,\mathrm{d}}) \\ 1 \end{pmatrix}. \tag{5.15}$$

Table 5.1 Simulation parameters.

Standard deviation of shadowing σ [dB]	8.0
Pathloss index η	3.0
Length of simulation area l [m]	50.0
Maximum communication range $R_{\max}$ [m]	50.0
Coordinate $\boldsymbol{x}_{\mathrm{d,Tx}}$	(10 [m], 25 [m])
Coordinate $\boldsymbol{x}_{\mathrm{d,Rx}}$	(40 [m], 25 [m])
Number of trials	10,000

From above simultaneous equations, the weights which minimize σ_k^2 can be derived. Note that the minimized σ_k^2 and σ_k are called *Kriging variance* and *Kriging standard deviation* respectively. Finally, we can derive the estimated $\hat{L}_{\mathrm{d}}$ as,

$$\hat{L}_{\mathrm{d}} = 10\hat{\eta}\log_{10} d_{\mathrm{d}} - \hat{W}_{\mathrm{d}}. \tag{5.16}$$

5.4 Performance Evaluation

In this section, the estimation accuracy with the proposed method is evaluated via Monte Carlo simulation. Simulation parameters are shown in Table 5.1. Here, a trial in the simulation is defined as following procedure:

1. Radio environment is generated.
2. N distributed links report L_i to the database server.
3. The database estimates $\hat{L}_{\mathrm{d}}$ based on the proposed method.
4. The estimation error $L_{\mathrm{d}} - \hat{L}_{\mathrm{d}}$ [dB] is calculated.

After the sufficient trials, estimation accuracy characteristics such as RMSE and the dispersion of pathloss estimation are evaluated.

We confirmed that Eq. (5.15) rarely has no solution due to nearly equal semivariograms in the left member of Eq. (5.15). This problem is caused when the theoretical semivariograms are estimated as $\alpha_s^2\left\{1-\exp\left(-\frac{\Delta d_{i,j}}{\alpha_r}\right)\right\} \approx 0$: $\gamma(\Delta d_{i,j}) \approx \alpha_n^2$. For handling the problem, we neglect *nugget effect* by assuming $\alpha_n^2 = 0$. Because the assumption sets diagonal elements in the left member of Eq. (5.15) as 0, the equation certainly has some sort of solution.

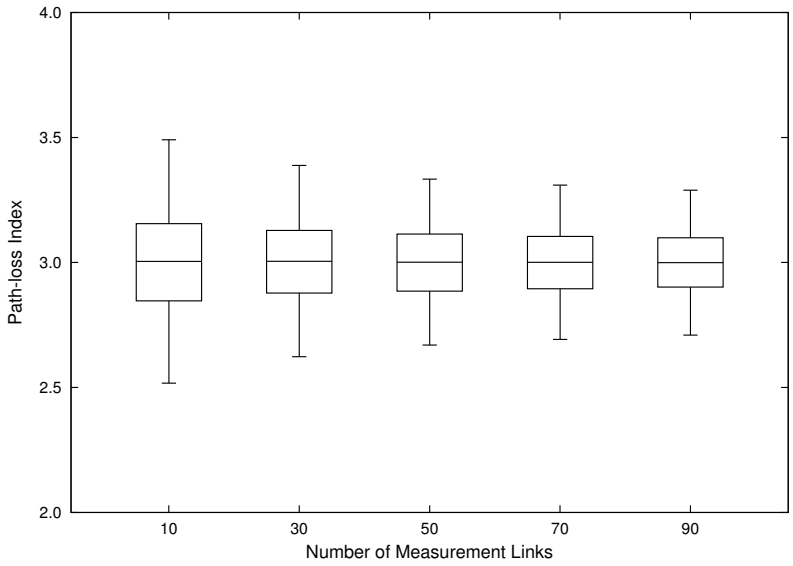

Fig. 5.3 Effect of N on estimation accuracy of path loss index under $d_{\mathrm{cor}} = 20$ [m].

5.4.1 Estimation Accuracy of Path Loss Index η

Figure 5.3 shows the effect of the number of links N on the estimation accuracy of η under $d_{\mathrm{cor}} = 20$ [m]. For confirming the estimation dispersion graphically, this characteristic was evaluated using boxplots. In the boxplots, the bottom and top of the box show the first quartile and the third quartile, respectively. The center line shows the average value. Furthermore, the bottom and top of the whisker are the 2.5 percentile and the 97.5 percentile, respectively: the region among two whisker lines includes 95 % of the estimation results. The figure clarifies the unbiased estimation can be achieved regardless of N. In addition, increasing N reduces the dispersion of $\hat{\eta}$, thus the maximum likelihood technique can accurately estimates the pathloss characteristics with large dataset.

The impact of the correlation distance d_{cor} on the pathloss estimation under $N = 50$ is shown in Fig. 5.4. The result shows that the proposed method can estimate η without the estimation bias in any correlation distance.

5.4.2 Estimation Accuracy of Radio Propagation Loss L_{d}

Next, we evaluated the estimation accuracy of L_{d}. Figure 5.5 shows the effect of N on RMSE [dB] under $d_{\mathrm{cor}} = 20$ [m]. We compared the proposed method with pathloss-based radio environment prediction without Kriging method. Note that the RMSE of the compared method is equal to the shadowing standard deviation σ. The comparison results show the advantage of the proposed method: even if there are only few dataset, the accuracy is higher

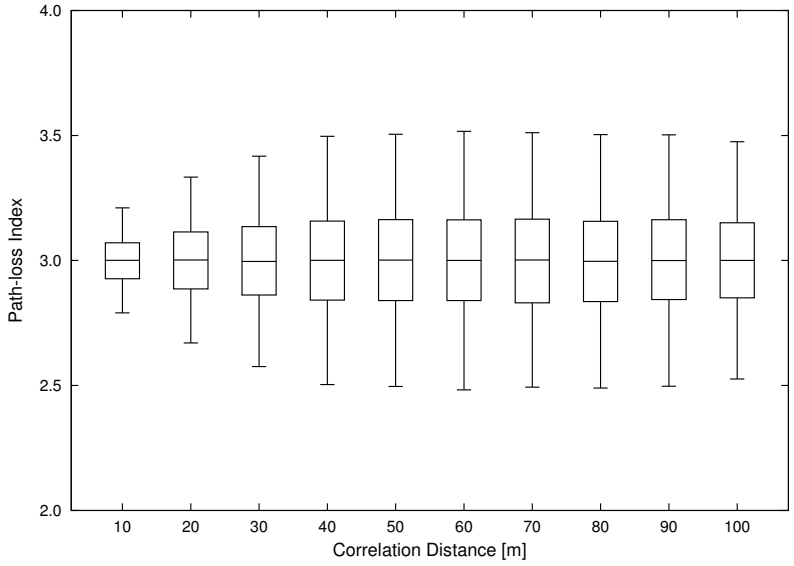

Fig. 5.4 Impact of d_{cor} on estimation accuracy of path loss index under $N = 50$.

than the compared method, and be improved in proportion as N increases. The impact of d_{cor} on L_{d} under $N = 10, 30, 50$ is shown in Fig. 5.6. This result means the link gain can be estimated with high accuracy under the gradual shadowing fluctuation situation. Here, as shown in Fig. 5.4, the accuracy of the pathloss estimation is mostly constant in regions where d_{cor} exceeds 40 [m]. Therefore, the reason why the gradual fluctuation improves the accuracy of L_{d} is that Kriging method can accurately predict the shadowing factor under the long correlation distance environment. This result implies the highly accurate estimation can be achieved if the shadowing fluctuates gradual compared with the measurement area size. We hence can conduct the highly accurate estimation by setting the small measurement area, even if terminals are under the short correlation distance environment.

5.4.3 Probabilistic Error Prediction

We discuss the advantage of the Kriging-based estimation other than the RMSE improvement. As mentioned in Chapter 5, in ordinary Kriging method, the estimation error follows a Gaussian distribution if the datasets fluctuate with a Gaussian process. This behavior can be applied to the typical radio propagation. Figure 5.7 shows three PDFs of the estimation error distribution: $N = 10, 30, 50$. In Fig. 5.7, each curve clearly plots the log-normal distribution and the variance becomes narrow by increasing the number of measurement points N. Correlation and covariance between $\hat{L}_{\mathrm{d}}$ and L_{d} are shown in Fig. 5.8. Because many numerical results in this figure take 0.5 or more, the advantageous region can be achieved realistically. the method proposed in this section can outperform the path loss-based

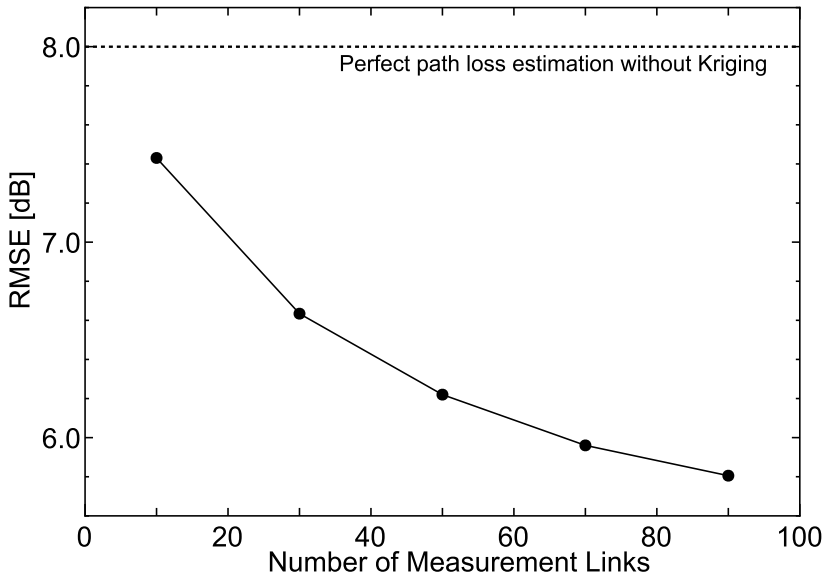

Fig. 5.5 Effect of N on estimation accuracy of L_{d} under $d_{\mathrm{cor}} = 20$ [m].

spectrum database from the view point of the channel capacity (the relationship between the channel capacity and correlation is discussed in Sect. 2.3).

From these figures and Fig. 5.7, we can consider that the PDF of $\hat{L}_{\mathrm{d}}$ and L_{d} follows a bivariate log-normal distribution, as with the Kriging-based REM discussed in Chapter 5. Additionally, if the semivariogram can be estimated perfectly, that means N is enough large, the minimized Kriging standard deviation σ_k approximately equals to the standard deviation of the estimation error. Figure 5.9 indicates $\mathrm{E}[\sigma_k]$ and the error standard deviations under $d_{\mathrm{cor}} = 20$ [m]. In this figure, as the number of measurement points N increases, the Kriging standard deviation converges to the standard deviation of estimation error. Therefore, if the number of measurement points N is enormous, the estimation error nearly follows a log-normal distribution with median value 0 and standard deviation σ_k. Note that Kriging standard deviation σ_k means the standard deviation of the estimation error under the perfect semivariogram estimation. Because Kriging method estimates the semivariogram model from datasets, true estimation error exceeds σ_k. Therefore, the upper bound of $\mathrm{E}[\sigma_k]$ is equal to the standard deviation of estimation error [82].

When the error ϵ is modeled as $L_{\mathrm{d}} = \hat{L}_{\mathrm{d}} + \epsilon$ and $\hat{L}_{\mathrm{d}}$ is given, L_{d} approximately follows the log-normal distribution with mean $\hat{L}_{\mathrm{d}}$ and standard deviation σ_k. We can easily understand that this mathematical structure is equal to the shadowing-fluctuated radio propagation written in Eq. (5.1). Therefore, the proposed method allows to improve the communication efficiency, interference prediction in M2M networks, coverage estimation in HetNets, and

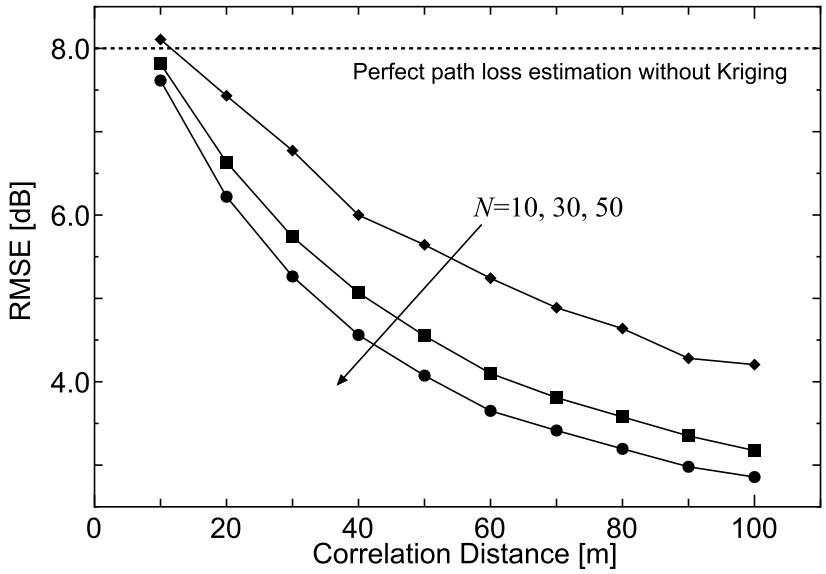

Fig. 5.6 Impact of d_{cor} on estimation accuracy of L_{d}.

suitable rooting in *ad-hoc* networks, using conventional mathematical tools considering the log-normal channel fluctuation.

5.5 Chapter Summary

The geostatistical radio propagation estimation for WDNs have been proposed. Numerical results have shown two advantages of the proposed method: RMSE improvement and probabilistic error prediction. In addition, as can be seen from the analytical results in Sect. 2.3, the Kriging-based radio propagation estimation can dramatically enhance the average transmission power at the SU-Tx.

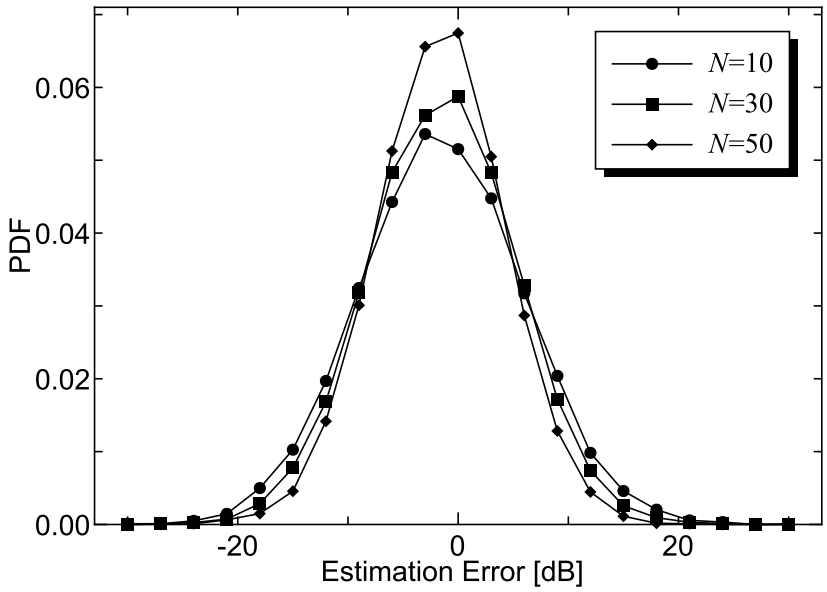

Fig. 5.7 Example of PDF of estimation error ϵ under $d_{\mathrm{cor}} = 20$ [m]. Each curve follows log-normal distribution.

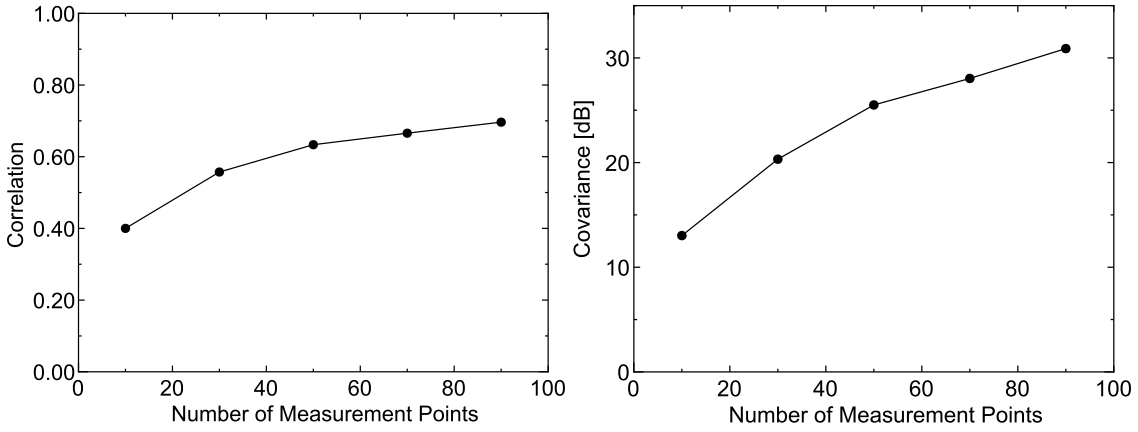

(a) Correlation. (b) Covariance.

Fig. 5.8 Correlation and covariance between $\hat{L}_{\mathrm{d}}$ and L_{d}.

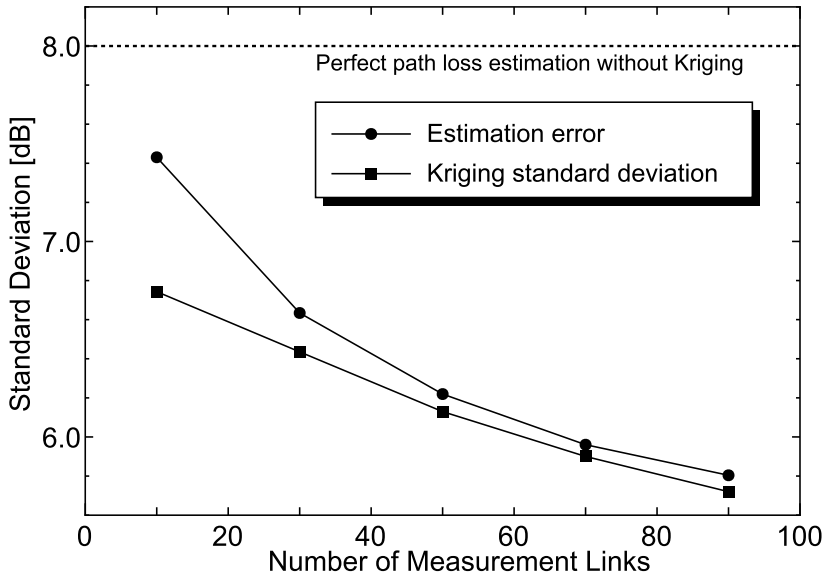

Fig. 5.9 Comparison of error standard deviation and Kriging standard deviation.

Chapter 6

Conclusions and Future Works

This chapter concludes our research works on highly efficient spectrum sharing. First, we summarize the conclusion and contribution of each chapter. After that, the potential future research directions are discussed.

6.1 Conclusions

Motivated by the fact that the efficiency of spectrum sharing strongly depends on the accuracy of radio propagation estimation, we have comprehensively investigated the highly efficient spectrum sharing from the viewpoint of radio propagation estimation. Conclusions and contributions of this thesis are summarized below.

Chapter 1 provided the demands for the spectrum sharing and the motivation for this work. After the brief timeline of this field was given, the outline of this thesis and a list of the contributions were summarized.

Chapter 2 introduced the concept of measurement-based spectrum database that consists of radio environment measurement results from sensors on mobile terminals. After the concept is described, the effect of the proposed database on the spectrum sharing was discussed from the theoretical aspect. We showed that the uncertainties of the radio propagation strongly degrade the average transmission power allowed to the SU. At the same time, it was also shown that the proposed method can improve the spectrum sharing capability.

In Chapter 3, we evaluated the accuracy of measurement-based spectrum database via two one-week measurement campaigns over TV bands. The measurement campaign was conducted in Kumagaya city, Saitama, Japan. The prior measurement datasets were stored in the spectrum database, and the posterior measurement datasets were treated as instantaneous measurement data. From the measurement results, we confirmed that the proposed database dramatically reduces the estimation error of the radio environment information.

In Chapter 4, we proposed the transmission power control method with a measurement-based spectrum database for the secondary networks. The proposed method exploits ordinary Kriging interpolation for the spectrum cartography. According to the predicted distribution of the estimation error, the allowable interference power to the PU is approximately formulated. Numerical results showed that the proposed method can achieve the probabilistic interference constraint asymptotically. Additionally, it was also shown that the proposed method dramatically improves the outage probability of the interference power compared to the conventional Kriging-based method.

Chapter 5 proposed the spectrum database-assisted radio propagation estimation for distributed SUs. The proposed method focuses on the spatial correlation of radio propagation characteristics between different wireless links. Using maximum likelihood-based path loss estimation and Kriging-based shadowing estimation, the radio propagation of the wireless link that has arbitrary location relationship can be predicted. From numerical results, it was shown that the proposed method achieves higher estimation accuracy than conventional path loss-based estimation method.

The methods discussed in this thesis can develop more spatial WSs in existing allocated bandwidth such as TVWS, and can provide these WSs to new wireless systems expected to appear in the future. Additionally, these results will contribute not only to such spectrum sharing but also to improvement of the spectrum management in existing systems. For example, in HetNets, a suitable inter-cell interference management enables transmitters to reuse the frequency efficiently and the user equipment can select the optimum base station. Therefore, this thesis has the possibility to change the way of spectrum in the future. We believe that the results in this thesis will be the cornerstone of contributing to the sustainable development of future wireless communications.

6.2 Future Works

This thesis mainly aims to improve the efficiency of spatial spectrum sharing. On the other hand, there still exist lots of research scopes for future works. At the end of this thesis, we briefly discuss the remaining and potential future works.

Toward Completion of Measurement-based Spectrum Database

In this thesis, we have mainly focused on the spatial spectrum sharing between a fixed primary transmitter and SUs, such as spectrum sharing over TV bands. A major contribution in this paper is the proposal of Kriging-based interference power constraint discussed in Chapter 4. Because the discussions were conducted via numerical simulations, we first need

to experimentally conduct a database-assisted spectrum sharing between a PU and SUs. In addition, in Chapter 4, we put some assumptions: path loss follows an isotropic model in the area, and noise and instantaneous fading do not affect with measurement data. Effects of such assumptions should also be discussed.

Discussions in Chapter 5 also have some important tasks including experimental verification. For example, the system model in Chapter 5 does not consider any effects of PUs. On the other hand, when the proposed method is applied for the radio propagation estimation in secondary networks, the training phase has to consider the interference temperature at PUs. Thus, the procedure of the database construction is an important task. Iteration between the radio environment training and the increase of the transmission power will be an intuitive solution to this problem. Namely, SUs will be able to transmit the signal with a low transmission power, even if the estimated interference characteristics have uncertainty. Because the signal transmission can probe the radio environment and improve the estimation uncertainty, by gradually increasing the transmission power and repeating the training of the radio environment, we will be possible to construct the database while satisfying the interference requirement for PUs.

Three-dimensional Radio Propagation Estimation

Although we have (implicitly) assumed two-dimensional radio environment, the radio propagation characteristics strongly depend on transmitter/receiver heights. Thus, expansion to the three-dimensional radio propagation estimation will be a challenging work.

Statistical Processing in Time Domain

This thesis do not consider time domain activities of the primary systems. On the other hand, communication activities in many existing systems irregularly change over time domain. Thus, statistical analysis in the time domain such as occupancy rate and transition rate will improve the spectrum sharing efficiency.

More Efficient REM Construction

We will be able to construct the REM more efficiently. In Chapters 4 and 5, Kriging interpolation have been applied for the radio propagation estimation. By exploiting the spatial shadowing correlation, Kriging interpolation can obtain the optimal received signal power. Here, some works have demonstrated that shadowing is highly frequency correlated [105]. This fact will enable us to interpolate the received signal power over both frequency and spatial domains.

References

[1] Cisco, "Cisco visual networking index: Global mobile data traffic forecast update, 2016-2021," [Online]. available: https://www.cisco.com/c/en/us/solutions/collateral/service-provider/visual-networking-index-vni/mobile-white-paper-c11-520862.pdf.

[2] NTIA, "US Frequency Allocation Chart," [Online]. available: https://www.ntia.doc.gov/files/ntia/publications/january_2016_spectrum_wall_chart.pdf.

[3] S. Haykin, "Cognitive radio: brain-empowered wireless communications," *IEEE J. Select. Areas in Commun.*, vol. 23, no. 2, pp. 201–220, February 2005.

[4] A. J. Goldsmith, *Wireless Communications*. Cambridge University Press, 2005.

[5] C. Phillips, D. Sicker, and D. Grunwald, "Bounding the error of path loss models," in *Proc. IEEE DySPAN 2011*, May 2011.

[6] R. Y. Mesler, H. Haas, S. Sinanovic, C. W. Ahn, and S. Yun, "Spatial modulation," *IEEE Trans. Veh. Technol.*, vol. 57, no. 4, pp. 2228–2241, July 2008.

[7] M. D. Renzo, H. Haas, A. Ghrayeb, S. Sugiura, and L. Hanzo, "Spatial modulation for generalized MIMO: Challenges, opportunities, and implementation," *Proc. of the IEEE*, vol. 102, no. 1, pp. 56–103, January 2014.

[8] D. Bharadia, E. McMilin, and S. Katti, "Full duplex radios," *SIGCOMM Comput. Commun. Rev.*, vol. 43, no. 4, pp. 375–386, August 2013. [Online]. Available: http://doi.acm.org/10.1145/2534169.2486033

[9] Z. Zhang, K. Long, A. V. Vasilakos, and L. Hanzo, "Full-duplex wireless communications: Challenges, solutions, and future research directions," *Proc. of the IEEE*, vol. 104, no. 7, pp. 1369–1409, July 2016.

[10] Y. Saito, Y. Kishiyama, A. Benjebbour, T. Nakamura, A. Li, and K. Higuchi, "Non-orthogonal multiple access (NOMA) for cellular future radio access," in *Proc. IEEE VTC-Spring 2013*, June 2013.

[11] Z. Ding, Y. Liu, J. Choi, Q. Sun, M. Elkashlan, C. L. I, and H. V. Poor, "Application of Non-Orthogonal Multiple Access in LTE and 5G networks," *IEEE Commun. Mag.*, vol. 55, no. 2, pp. 185–191, February 2017.

[12] E. Paolini, G. Liva, and M. Chiani, "Coded slotted ALOHA: A graph-based method for uncoordinated multiple access," *IEEE Trans. Inf. Theory*, vol. 61, no. 12, pp. 6815–6832, December 2015.

[13] E. Arikan, "Channel polarization: A method for constructing capacity-achieving codes for symmetric binary-input memoryless channels," *IEEE Trans. Inf. Theory*, vol. 55, no. 7, pp. 3051–3073, July 2009.

[14] T. S. Rappaport, S. Sun, R. Mayzus, H. Zhao, Y. Azar, K. Wang, G. N. Wong, J. K. Schulz, M. Samimi, and F. Gutierrez, "Millimeter wave mobile communications for 5G cellular: It will work!" *IEEE Access*, vol. 1, pp. 335–349, 2013.

[15] I. F. Akyildiz, J. M. Jornet, and C. Han, "Terahertz band: New frontier for wireless communications," *Physical Commun. J.*, vol. 20, pp. 16–32, September 2014.

[16] H. Elgala, R. Mesleh, and H. Haas, "Indoor optical wireless communication: potential and state-of-the-art," *IEEE Commun. Mag.*, vol. 49, no. 9, pp. 56–62, September 2011.

[17] K. Harrison, S. M. Mishra, and A. Sahai, "How much white-space capacity is there?" in *Proc. IEEE DySPAN 2010*, 2010.

[18] A. Palaios, J. Riihijärvi, and P. Mähönen, "From Paris to London: Comparative analysis of licensed spectrum use in two European metropolises," in *Proc. IEEE DySPAN 2014*, 2014.

[19] E. Buracchini, "The software radio concept," *IEEE Commun. Mag.*, vol. 38, no. 9, pp. 138–143, September 2000.

[20] J. Mitola, "Software radios: Survey, critical evaluation and future directions," *IEEE Aero. El. Sys. Mag.*, vol. 8, no. 4, pp. 25–36, April 1993.

[21] ——, "The software radio architecture," *IEEE Commun. Mag.*, vol. 33, no. 5, pp. 26–38, May 1995.

[22] ——, "Software radio architecture: a mathematical perspective," *IEEE J. Select. Areas in Commun.*, vol. 17, no. 4, pp. 514–538, April 1999.

[23] A. A. Abidi, "The path to the software-defined radio receiver," *IEEE J. Solid-State Circuits*, vol. 42, no. 5, pp. 954–966, May 2007.

[24] J. Mitola and G. Q. Maquire, "Cognitive radio: Making software radios more personal," *IEEE Pers. Commun.*, vol. 6, no. 4, pp. 13–18, August 1999.

[25] J. Mitola, "Cognitive radio: An integrated agent architecture for software defined radio," *Doctor of Technology, Royal Inst. Technol. (KTH), Stockholm, Sweden*, 2000.

[26] FCC ET Docket, "Spectrum policy task force report," no. 02-135, November 2002.

[27] N. Devroye, P. Mitran, and V. Tarokh, "Achievable rates in cognitive radio channels," *IEEE Trans. Inf. Theory*, vol. 52, no. 5, pp. 1813–1827, May 2006.

[28] M. Gastpar, "On capacity under receive and spatial spectrum-sharing constraints," *IEEE Trans. Inf. Theory*, vol. 53, no. 2, pp. 471–487, February 2007.

[29] A. Ghasemi and E. S. Sousa, "Fundamental limits of spectrum-sharing in fading environments," *IEEE Trans. Wireless Commun.*, vol. 6, no. 2, pp. 649–658, February 2007.

[30] S. A. Jafar and S. Srinivasa, "Capacity limits of cognitive radio with distributed and dynamic spectral activity," *IEEE J. Select. Areas in Commun.*, vol. 25, no. 3, pp. 529–537, April 2007.

[31] S. Srinivasa and S. A. Jafar, "The throughput potential of cognitive radio: A theoretical perspective," *IEEE Commun. Mag.*, vol. 45, no. 5, pp. 73–79, May 2007.

[32] Y. C. Liang, Y. Zeng, E. C. Y. Per, and A. T. Hoang, "Sensing-throughput tradeoff for cognitive radio networks," *IEEE Trans. Wireless Commun.*, vol. 7, no. 4, pp. 1326–1337, April 2008.

[33] R. Zhang, "On peak versus average interference power constraints for protecting primary users in cognitive radio networks," *IEEE Trans. Wireless Commun.*, vol. 8, no. 4, pp. 2112–2120, April 2009.

[34] L. Musavian and S. Aissa, "Fundamental capacity limits of cognitive radio in fading environments with imperfect channel information," *IEEE Trans. Commun.*, vol. 57, no. 11, pp. 3472–3480, November 2009.

[35] H. Suraweera, P. Smith, and M. Shafi, "Capacity limits and performance analysis of cognitive radio with imperfect channel knowledge," *IEEE Trans. Veh. Technol.*, vol. 59, no. 4, pp. 1811–1822, May 2010.

[36] P. Smith, P. Dmochowski, H. Suraweera, and M. Shafi, "The effects of limited channel knowledge on cognitive radio system capacity," *IEEE Trans. Veh. Technol*, vol. 62, no. 2, pp. 927–933, February 2013.

[37] A. J. Goldsmith and P. P. Varaiya, "Capacity of fading channels with channel side information," *IEEE Trans. Inf. Theory*, vol. 43, no. 6, pp. 1986–1992, November 1997.

[38] S. Bhattarai, J. M. J. Park, B. Gao, K. Bian, and W. Lehr, "An overview of dynamic spectrum sharing: Ongoing initiatives, challenges, and a roadmap for future research," *IEEE Trans. Cogn. Commun. Netw.*, vol. 2, no. 2, pp. 110–128, June 2016.

[39] FCC, "Second memorandum opinion and order," September 2010, FCC 08–260.

[40] FCC, "Auction 97: Advanced Wireless Services (AWS-3)," [Online]. available: http://wireless.fcc.gov/auctions/default.htm?job=auction_summary&id=97.

[41] FCC and NTIA, "Coordination procedures in the 1695-1710 mhz and 1755-1780 mhz bands," no. 13-185, July 2014.

[42] FCC, "Report and order and second further notice of proposed rulemaking," no. 12-354, April 2015.

[43] FCC ET Docket, "Notice of proposed rulemaking," no. 13-49, February 2013.

[44] F. WirelessTech, "Verizon, Qualcomm Lobby for LTE-U, Wi-Fi Coexistence Scheme," [Online]. available: http://www.fiercewireless.com/tech/story/verizon-qualcomm-lobby-lte-u-wi-fi-coexistence-scheme/2015-07-2.

[45] C. W. Kim, J. Ryoo, and M. M. Muddhikot, "Design and implementation of an end-to-end architecture for 3.5 GHz shared spectrum," in *Proc. IEEE DySPAN 2015*, September 2015.

[46] M. Mustonen, M. Matinmikko, M. Palola, T. Rautio, and S. Yrjölä, "Analysis of requirements from standardization for Licensed Shared Access (LSA) system implementation," in *Proc. IEEE DySPAN 2015*, September 2015.

[47] M. Palola, M. Höyhtyä, P. Aho, M. Mustonen, T. Kippola, M. Heikkilä, S. Yrjölä, V. Hartikainen, L. Tudose, A. Kivinen, R. Ekman, J. Hallio, J. Paavola, M. Mäkeläinen, and T. Hänninen, "Field trial of the 3.5 GHz citizens broadband radio service governed by a spectrum access system (SAS)," in *Proc. IEEE DySPAN 2017*, March 2017.

[48] F. Paisana, D. Finn, N. Marchetti, and L. DaSilva, "Reduction of radar band exclusion zones through database-aided beamforming," in *Proc. IEEE DySPAN 2015*, September 2015.

[49] M. Grissa, A. A. Yavuz, and B. Hamdaoui, "Location privacy preservation in database-driven wireless cognitive networks through encrypted probabilistic data structures," *IEEE Trans. Cogn. Commun. Netw.*, vol. 3, no. 2, pp. 255–266, June 2017.

[50] N. Rajkarnikar, J. M. Peha, and A. Aguiar, "Location privacy from dummy devices in database-coordinated spectrum sharing," in *Proc. IEEE DySPAN 2017*, March 2017.

[51] H. Cui, J. Li, Z. Li, D. Pan, and Y. He, "Distributed interference-aware cooperative random access in multi-hop wireless networks," *IEEE Access*, vol. 4, pp. 4823–4828, 2016.

[52] S. Y. Lien, K. C. Chen, Y. C. Liang, and Y. Lin, "Cognitive radio resource management for future cellular networks," *IEEE Wireless Commun.*, vol. 21, no. 1, pp. 70–79, Feb. 2014.

[53] A. M. Akhtar, X. Wang, and L. Hanzo, "Synergistic spectrum sharing in 5G HetNets: a harmonized SDN-enabled approach," *IEEE Commun. Mag.*, vol. 54, no. 1, pp. 40–47, Jan. 2016.

[54] K. S. Ali, H. Elsawy, A. Chaaban, and M. S. Alouini, "Non-orthogonal multiple access for large-scale 5G networks: Interference aware design," *IEEE Access*, vol. 5, pp. 21 204–21 216, 2017.

[55] I. Randrianantenaina, H. Dahrouj, H. Elsawy, and M. S. Alouini, "Interference management in full-duplex cellular networks with partial spectrum overlap," *IEEE Access*, vol. 5, pp. 7567–7583, 2017.

[56] G. Caso, L. D. Nardis, and M. G. D. Benedetto, "Toward context-aware dynamic spectrum management for 5G," *IEEE Wireless Commun.*, vol. 24, no. 5, pp. 38–43, October 2017.

[57] A. F. Molisch, L. J. Greenstein, and M. Shafi, "Propagation issues for cognitive radio," *Proc. of the IEEE*, vol. 97, no. 5, pp. 787–804, May 2009.

[58] H. T. Friis, "A note on a simple transmission formula," *Proc. IRE and Waves and Electrons*, May 1946.

[59] Y. Okumura, T. Ohmori, E. Kawano, and K. Fukuda, "Field strength and its variability in VHF and UHF land mobile radio service," *Rev. Electr. Commun. Lab.*, vol. 16, no. 9-10, pp. 825–828, October 1968.

[60] G. Hufford, "The ITS irregular terrain model, version 1.2.2, the algorithm," [Online]. available: https://www.its.bldrdoc.gov/resources/radio-propagation-software/itm/itm.aspx.

[61] D. Cichon and Kürner, "Digital mobile radio towards future generation systems: Cost 231 final report," in *COST European Cooperation in the Field of Scientific and Technical Research - Action 231, Tech. Rep.*, 1993.

[62] T. Rappaport, *Wireless Communications: Principles and Practice*. Prentice Hall, 2002.

[63] ITU-R, "Terrestrial land mobile radiowave propagation in the VHF/UHF bands," 2002.

[64] V. Garg, *Wireless Communications and Networking*. D.Clark, Ed.Morgan Kaufmann, 2007.

[65] T. Yucek and H. Arslan, "A survey of spectrum sensing algorithms for cognitive radio applications," *IEEE Commun. Surveys Tuts.*, vol. 11, no. 1, pp. 116–130, First Quarter 2009.

[66] D. Gurney, G. Buchwald, L. Ecklund, S. Kuffner, and J. Grosspietsch, "Geo-location database techniques for incumbent protection in the TV white space," in *Proc. IEEE DySPAN 2008*, October 2008.

[67] FCC, "Unlicensed operation in the TV broadcast bands, third memorandum opinion and order," *FCC.12-36*, April 2012.

[68] Ofcom, "TV white spaces: Pilot database provider contract," February 2014.

[69] IDA, "Regulatory framework for TV white space operations in the VHF/UHF bands," June 2014.

[70] FCC, "Second memorandum opinion and order in the matter of unlicensed operation in the TV broadcast bands, additional spectrum for unlicensed devices below 900 MHz and in the 3 GHz band," 2010, FCC 10–174.

[71] MIC, "Notice 640 (in japanese)," [Online]. available: http://www.tele.soumu.go.jp/horei/reiki_honbun/a720730001.html.

[72] A. Achtzehn, J. Riihijärvi, and P. Mähönen, "Improving accuracy for TVWS geolocation databases: Results from measurement-driven estimation approaches," in *Proc. IEEE DySPAN 2014*, April 2014.

[73] MIC, "Total results of communication traffic in Japan (May 2017) (in japanese)," [Online]. available: http://www.soumu.go.jp/menu_news/s-news/02kiban04_04000213.html.

[74] H. R. Karimi, "Geolocation databases for white space devices in the UHF TV bands: Specification of maximum permitted emission levels," in *Proc. IEEE DySPAN 2011*, May 2011.

[75] RCC Chugoku Broadcasting Company, "Area kakube (in japanese)," [Online]. available: http://kakube.rcc.ne.jp/.

[76] D. Lopez-Perez, I. Guvenc, G. de la Roche, M. Kountouris, T. Quek, and J. Zhang, "Enhanced intercell interference coordination challenges in heterogeneous networks," *IEEE Wireless Commun.*, vol. 18, no. 3, pp. 22–30, June 2011.

[77] Z. Rezki and M. S. Alouini, "Ergodic capacity of cognitive radio under imperfect channel-state information," *IEEE Trans. Veh. Technol.*, vol. 61, no. 5, pp. 2108–2119, Jun. 2012.

[78] E. Dall'Anese, S. J. Kim, G. B. Giannakis, and S. Pupolin, "Power control for cognitive radio networks under channel uncertainty," *IEEE Trans. Wireless Commun.*, vol. 10, no. 10, pp. 3541–3551, Oct. 2011.

[79] S. Gong, P. Wang, Y. Liu, and W. Zhuang, "Robust power control with distribution uncertainty in cognitive radio networks," *IEEE J. Select. Areas in Commun.*, vol. 31, no. 11, pp. 2397–2408, Nov. 2013.

[80] H. B. Yilmaz, T. Tugcu, F. Alagoz, and S. Bayhan, "Radio environment map as enabler for practical cognitive radio networks," *IEEE Commun. Mag.*, vol. 51, no. 12, pp. 162–169, Dec. 2013.

[81] J. Perez-Romero, A. Zalonis, L. Boukhatem, A. Kliks, K. Koutlia, N. Dimitriou, and R. Kurda, "On the use of radio environment maps for interference management in heterogeneous networks," *IEEE Commun. Mag.*, vol. 53, no. 8, pp. 184–191, August 2015.

[82] N. Cressie, *Statistics for spatial data*. Wiley-Interscience, 1993.

[83] G. Boccolini, G. Hernandez-Penaloza, and B. Beferull-Lozano, "Wireless sensor network for spectrum cartography based on kriging interpolation," in *Proc. IEEE PIMRC 2012*, September 2012.

[84] B. Sayrac, A. Galindo-Serrano, R. J. Jemaa, S. B. and, and P. Mähönen, "Bayesian spatial interpolation as an emerging cognitive radio application for coverage analysis in cellular networks," *Trans. on Emerging Telecommun. Technol.*, vol. 24, no. 7-8, pp. 636–648, October 2013.

[85] B. A. Jayawickrama, E. Dutkiewicz, G. Fang, I. Oppermann, and M. Mueck, "Downlink power allocation algorithm for licence-exempt lte systems using kriging and compressive sensing based spectrum cartography," in *Proc. IEEE GLOBECOM 2013*, Dec. 2013.

[86] E. Dall'Anese, S.-J. Kim, and G. B. Giannakis, "Channel gain map tracking via distributed kriging," *IEEE Trans. Veh. Technol.*, vol. 60, no. 3, pp. 1205–1211, March 2011.

[87] B. L. Mark and A. O. Nasif, "Estimation of maximum interference-free power level for opportunistic spectrum access," *IEEE Trans. Wireless Commun.*, vol. 8, no. 3, pp. 2505–2513, May 2009.

[88] R. M. Vaghefi and R. M. Buehrer, "Received signal strength-based sensor localization in spatially correlated shadowing," in *Proc. IEEE ICASSP 2013*, May 2013.

[89] M. Gudmundson, "Correlation model for shadow fading in mobile radio systems," *Electron. Lett.*, vol. 27, no. 7, pp. 2145–2146, November 1991.

[90] X. Cai and G. B. Giannakis, "A two-dimensional channel simulation model for shadowing processes," *IEEE Trans. Veh. Technol.*, vol. 52, no. 6, pp. 1558–1567, Nov. 2003.

[91] K. Sato and T. Fujii, "Average interference power constraint with measurement-based spectrum database," in *Proc. IEEE WCNC 2015 International Workshop on Smart Spectrum*, March 2015.

[92] C. Phillips, D. Sicker, and D. Grunwald, "A survey of wireless path loss prediction and coverage mapping methods," *IEEE Commun. Surveys Tuts.*, vol. 15, no. 1, pp. 255–270, May 2013.

[93] A. Achtzehn, J. Riihijärvi, and P. Mähönen, "Error distribution in maximum likelihood estimation of radio propagation model parameters," in *Proc. IEEE SECON 2012*, June 2012.

[94] K. Sato, K. Inage, and T. Fujii, "Spectrum database-assisted radio propagation prediction for wireless distributed networks: a geostatistical approach," in *Proc. IEEE PIMRC 2016*, Sept 2016.

[95] A. E. Gelfand, P. Diggle, P. Guttorp, and M. Fuentes, *Handbook of Spatial Statistics*. CRC Press, 2010.

[96] R. S. de Souza and R. D. Lins, "A new propagation model for 2.4 GHz wireless LAN," in *Proc. APCC 2008*, Oct 2008.

[97] N. Cressie, "Spatial prediction and ordinary kriging," *Mathematical Geology*, vol. 20, no. 4, pp. 405–421, May 1988.

[98] S. S. Szyszkowicz and H. Yanikomeroglu, "Analysis of interference from large clusters as modeled by the sum of many correlated lognormals," in *Proc. IEEE WCNC 2008*, March 2008.

[99] ——, "A simple approximation of the aggregate interference from a cluster of many interferers with correlated shadowing," *IEEE Trans. Wireless Commun.*, vol. 13, no. 8, pp. 4415–4423, August 2014.

[100] D. den Herrtog, J. Kleijnen, and A. Siem, "The correct kriging variance estimated by bootstrapping," *Journal of the Operational Research Society*, vol. 54, no. 4, pp. 400–409, April 2006.

[101] M. Hata, "Empirical formula for propagation loss in land mobile radio services," *IEEE Trans. Veh. Technol.*, vol. 29, no. 3, pp. 317–325, August 1980.

[102] Z. Wang, E. K. Tameh, and A. R. Nix, "Joint shadowing process in urban peer-to-peer radio channels," *IEEE Trans. Veh. Technol.*, vol. 57, no. 1, pp. 52–64, January 2008.

[103] N. Karedal, and L. Czink, A. Paier, F. Tufvesson, and A. Molisch, "Path loss modeling for vehicle-to-vehicle communications," *IEEE Trans. Veh. Technol.*, vol. 60, no. 1, pp. 323–328, January 2011.

[104] J. A. Nelder and R. Mead, "A simplex method for function minimization," *Comput. J.*, vol. 7, pp. 308–313, 1965.

[105] E. Perahia and D. C. Cox, "Shadow fading correlation between uplink and downlink," in *Proc. IEEE VTC-Spring 2001*, May 2001.

Appendix A

Parametric Bootstrap Method

We summarize the parametric bootstrap-based Kriging variance estimation proposed in [100]. The bootstrap method is a Monte Carlo method that estimates properties of the estimator based on the approximated distribution of samples. According to whether or not we have the knowledge of the distribution shape of samples, the approach can be categorized into two methods: parametric and nonparametric bootstrap methods. In our system model, the parametric bootstrap method can be implemented with following steps:

1. σ_{P}, η_{P}, and $d_{\mathrm{cor,P}}$ are estimated from the measurement dataset $\boldsymbol{y} = (P(\boldsymbol{x}_1), P(\boldsymbol{x}_2), ..., P(\boldsymbol{x}_N))$. This can be achieved by maximizing Eq. (4.13). Each estimated value is defined as $\hat{\sigma}_{\mathrm{P}}$, $\hat{\eta_{\mathrm{P}}}$, and $\hat{d}_{\mathrm{cor,P}}$, respectively.

2. We assume that the received signal power from the PU follows the multivariate log-normal distribution with P_{Tx}, $\hat{\sigma}_{\mathrm{P}}$, $\hat{\eta_{\mathrm{P}}}$, and $\hat{d}_{\mathrm{cor,P}}$. The assumed received signal power is defined as $P^*_b(\boldsymbol{x})$.

3. The received signal power at $\boldsymbol{x}_0$ and $\{\boldsymbol{x}_i | i = 1, 2, 3, ..., N\}$ is generated according to the assumed distribution.

4. $P^*_b(\boldsymbol{x}_0)$ is estimated using the ordinary Kriging and the dataset $\{P^*_{b,i}(\boldsymbol{x}) | i = 1, 2, ..., N\}$. The estimated received signal power is defined as $\hat{P}^*_b(\boldsymbol{x}_0)$.

5. Step 3 and 4 are repeated B times.

6. The RMSE is evaluated with the following equation:

$$RMSE(P^*(\boldsymbol{x}_0)) = \sqrt{\frac{1}{B}\sum_{b=1}^{B}\left(P^*_b(\boldsymbol{x}_0) - \hat{P}^*_b(\boldsymbol{x}_0)\right)^2}.$$

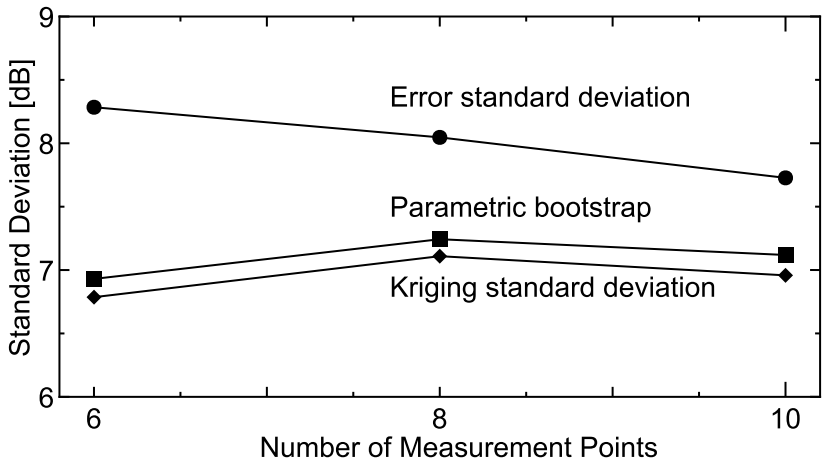

Fig. A.1 Standard deviation with parametric bootstrap method where $B = 1000$. Other parameters follow Table 4.1.

7. The estimated RMSE is treated as the Kriging standard deviation, σ_k.

Figure A.1 shows the standard deviation prediction characteristics of the parametric bootstrap. Curves of the parametric bootstrap and Kriging standard deviation plot the expected value of the results obtained from the Monte Carlo simulations. Using the procedure, we can improve the gap between the error standard deviation and σ_k.

Publications

List of Publications Directly Related to The Dissertation

Journal Papers

1. Koya Sato and Takeo Fujii, “Kriging-based interference power constraint: Integrated design of the radio environment map and transmission power ,” *IEEE Trans. Cogn. Commun. Netw.*, vol.3, no.1, pp.13-25, March 2017.

2. Koya Sato, Masayuki Kitamura, Kei Inage, and Takeo Fujii, “Measurement-based spectrum database for flexible spectrum management, ” *IEICE Trans. Commun.*, vol.E98-B, no.10, pp.2004-2013, October 2015.

Refereed International Conference Papers

1. Koya Sato, Kei Inage, and Takeo Fujii, “Spectrum database-assisted radio propagation prediction for wireless distributed networks: A geostatistical approach, ” in *Proc. IEEE PIMRC 2016*, September 2016.

List of Referenced Publications

Journal Papers

1. Koya Sato, Kei Inage, and Takeo Fujii, “Modeling the Kriging-aided spectrum sharing over log-normal channels, ” *IEEE Wireless Commun. Lett.* (to be submitted).

2. Keita Katagiri, Koya Sato, and Takeo Fujii, “Crowdsourcing-assisted radio environment database for V2V communication, ” submitted to *Sensors* (major revision).

3. Rei Hasegawa, Keita Katagiri, Koya Sato, and Takeo Fujii, "Low storage, but highly accurate measurement-based spectrum database via mesh clustering, " *IEICE Trans. Commun.* (in press).

4. Koya Sato, Kei Inage, and Takeo Fujii, "Frequency correlation of shadowing over TV bands in suburban area, " *Electron. Lett.*, vol.54, no.1, pp.6-8, January 2018.

5. Cong-Hoang Diem, Koya Sato, and Takeo Fujii, "Cooperative distributed STBC transmission scheme for multi-hop V2V communications, " *IEICE Trans. Fundamentals*, vol.E99-A, no.1, pp.252-262, January 2016.

Refereed International Conference Papers

1. Tatsuya Ute, Yuta Watanabe, Koya Sato, Takeo Fujii, Takayuki Shimizu, and Onur Altintas, "Multi-antenna successive interference cancellation to improve reliability of V2V communication, " in *Proc. IEEE VNC 2017*, November 2017.

2. Koya Sato, Kei Inage, and Takeo Fujii, "Compensation of survivorship bias in path loss modeling, " in *Proc. IEEE PIMRC 2017*, October 2017.

3. Keita Katagiri, Koya Sato, and Takeo Fujii, "Crowdsourcing-assisted radio environment maps for V2V communication systems, " in *Proc. IEEE VTC 2017-Fall*, September 2017.

4. Koya Sato and Takeo Fujii, "Radio environment aware computation offloading with multiple mobile edge computing servers, " in *Proc. IEEE WCNC 2017 International Workshop on Smart Spectrum (IWSS)*, March 2017.

5. Daichi Ishikawa, Koya Sato, Takeo Fujii, Matthias Wilhelm, Haris Kremo and Onur Altintas, "Location-based distributed channel assignment for communications among autonomous vehicles, " in *Proc. IEEE VNC 2015*, December 2015.

6. Koya Sato and Takeo Fujii, "Kriging-based interference power constraint for spectrum sharing based on radio environment map, " in *Proc. IEEE GLOBECOM Workshop on Emerging Technologies for 5G Wireless Cellular Networks (ET5G)*, December 2015.

7. Hao Wang, Koya Sato, and Takeo Fujii, "Received power detection under multiple ON/OFF environment for registering radio environment database, " in *Proc. ICTC 2015*, October 2015.

8. Koji Ichikawa, Hao Wang, Koya Sato, and Takeo Fujii, “Height power estimation with radio environment database in urban area, ” in *Proc. ICUFN 2015*, July 2015.

9. Koya Sato and Takeo Fujii, “Average interference power constraint with measurement-based spectrum database, ” in *Proc. IEEE WCNC 2015 International Workshop on Smart Spectrum (IWSS)*, March 2015.

10. Koya Sato, Takashi Kosugi, Masayuki Kitamura, and Takeo Fujii, “Demo: A field test of measurement-based spectrum database using probing vehicles, ” in *Proc. IEEE VNC 2014*, December 2014.

11. Shunsuke Takagi, Shunta Sakai, Koya Sato, and Takeo Fujii, “Spectrum shared wireless sensor networks based on radio environment database, ” in *Proc. SDR-WInnComm-Europe 2014*, November 2014.

12. Koya Sato, Kei Inage, and Takeo Fujii, “Parameter estimation method of primary user using measurement-based spectrum database, ” in *Proc. IEEE CCNC 2014*, January 2014.

Domestic Conference Papers (in Japanese)

1. Keita Katagiri, Koya Sato, and Takeo Fujii, “Highly accurate prediction of signal variation distribution using surrounding vehicles information, ” in *IEICE Tech. Rep.*, SR2017-104, January 2018.

2. Miho Itoh, Keita Onose, Koya Sato, Kei Inage, and Takeo Fujii, “A calibration method for crowdsensing based radio environment database, ” in *IEICE Tech. Rep.*, SR2017-103, January 2018.

3. Keita Onose, Koya Sato, Kei Inage, and Takeo Fujii, “Experimental verification of frequency-correlation for radio environment recognition using crowd sensing, ” in *IEICE Tech. Rep.*, SR2017-74, October 2017.

4. Tatsuya Ute, Yuta Watanabe, Koya Sato, Takeo Fujii, Takayuki Shimizu, and Onur Altintas, “Multi-antenna successive interference cancellation to improve reliability of V2V communications, ” in *IEICE Tech. Rep.*, SR2017-58, July 2017.

5. Kei Inage, Koya Sato, and Takeo Fujii, “Accuracy improvement of measurement-based spectrum database using self-organizing maps, ” in *IEICE Tech. Rep.*, SR2017-1, May 2017.

6. Keita Katagiri, Koya Sato, and Takeo Fujii, "[Technology exhibit] Construction of radio environment maps for improving communication reliability of cooperative automated vehicles, " in *IEICE Tech. Rep.*, SR2017-13, May 2017.

7. Keita Onose, Koya Sato, Kei Inage, and Takeo Fujii, "Experimental verification of frequency-correlated shadowing in indoor wireless LAN environment, " in *Proc. IEICE Gen. Conf. '17*, B-17-2, March 2017.

8. Koya Sato and Takeo Fujii, "A radio environment aware computation offloading for mobile edge computing, " in *IEICE Tech. Rep.*, SR2016-89, January 2017.

9. Koya Sato, Kei Inage, and Takeo Fujii, "Impact of spectrum database-assisted any-to-any radio propagation estimation on multihop routing, " in *IEICE Tech. Rep.*, SR2016-27, May 2016.

10. Koya Sato and Takeo Fujii, "Frequency correlation of received signal power over TV bands, " in *Proc. IEICE Gen. Conf. '16*, B-17-28, March 2016.

11. Bat-Ulzii Tsend-Ochir, Koya Sato, Takeo Fujii, and Kohei Mizuno, "An efficient data gathering method for wireless sensor network using multilayer priority buffers, " in *Proc. IEICE Gen. Conf. '16*, B-17-36, March 2016.

12. Hao Wang, Koya Sato, and Takeo Fujii, "Accuracy improvement for spectrum database considering primary signal in time domain under fading environment, " in *IEICE Tech. Rep.*, SR2015-99, March 2016.

13. Koya Sato, Kei Inage, and Takeo Fujii, "A spectrum database-assisted geostatistical radio propagation estimation for wireless distributed networks, " in *IEICE Tech. Rep.*, SR2015-98, March 2016.

14. Daichi Ishikawa, Koya Sato, Takeo Fujii, Matthias Wilhelm, Haris Kremo, and Onur Altintas, "Study of channel resource assignment method based on location for automated vehicle communications," in *Proc. ITS Symposium '15*, 1-2A-08, December 2015.

15. Koya Sato and Takeo Fujii, "Maximum likelihood-based transmission power adaptation for spectrum sharing, " in *Proc. IEICE Society Conf. '15*, B-17-5, March 2016.

16. Cong-Hoang Diem, Koya Sato, and Takeo Fujii, "A highly efficient transmission scheme for multi-hop V2V communications on highway, " in *IEICE Tech. Rep.*, SR2015-2, July 2015.

17. Koji Ichikawa, Hao Wang, Koya Sato, and Takeo Fujii, “Height power estimation for DTV based on measurements in urban environment, ” in *IEICE Tech. Rep.*, SR2015-2, May 2015.

18. Koya Sato and Takeo Fujii, “Probabilistic interference constraint using a radio environment map based on Kriging interpolation, ” in *IEICE Tech. Rep.*, SR2014-95, January 2015.

19. Koya Sato, Takashi Kosugi, Masayuki Kitamura, Yuya Ohue, and Takeo Fujii, “[Demo] Field tests of measurement-based spectrum database over TV bands, ” in *IEICE Tech. Rep.*, SR2014-91, October 2014.

20. Shunsuke Takagi, Shunta Sakai, Koya Sato, and Takeo Fujii, “Spectrum sharing using channel selection considering mutual interference supported by radio environment database,” in *Proc. IEICE Society Conf.'14*, B-17-19, September 2014.

21. Koya Sato and Takeo Fujii, “[Poster presentation] An interference constraint method using measurement-based radio environment database, ” in *IEICE Tech. Rep.*, SR2014-36, July 2014.

22. Koya Sato, Yuya Ohue, Masayuki Kitamura, and Takeo Fujii, “[Technology exhibit] Advanced spectrum database with probing vehicles, ” in *IEICE Tech. Rep.*, SR2014-7, May 2014.

23. Koya Sato, Kei Inage, and Takeo Fujii, “Primary user's parameter estimation method using measurement-based spectrum database, ” in *IEICE Tech. Rep.*, SR2013-76, January 2014.

24. Koya Sato, Kei Inage, and Takeo Fujii, “Impact of correlated shadowing for radio environment estimation in outdoor environment, ” in *Proc. IEICE Society Conf. '13*, BS-8-3, September 2013.